Deciphering the impact of macroautophagy perturbation by influenza A virus on virus replication and host cell response to infection

Brieuc Pierre Francois Pérot

Université Pierre et Marie Curie

École doctorale Physiologie et Physiopathologie (ED 394)

Immunobiologie des Cellules Dendritiques (Unité Mixte Pasteur/Inserm U1223)

Étude de l'impact des perturbations de la macroautophagie induite par le virus de la grippe A sur sa réplication et sur la réponse cellulaire à l'infection

par Brieuc Pérot

Thèse de doctorat d'Immunologie

dirigée par Matthew L. Albert, MD, PhD et
co-supervisée par Molly A. Ingersoll, PhD

présentée et soutenue publiquement le 28 septembre 2016

devant un jury composé de :

Béhazine COMBADIERE, PhD	Présidente
Marlène DREUX, PhD	Rapportrice
Nicolas GLAICHENHAUS, PhD	Rapporteur
Arnaud MORIS, PhD	Examinateur
Jeremy S. ROSSMAN, PhD	Examinateur
Matthew L. ALBERT, MD, PhD	Directeur de thèse
Molly A. INGERSOLL, PhD	Co-directrice de thèse

Université Pierre et Marie Curie

École doctorale Physiologie et Physiopathologie (ED 394)

Laboratory of Dendritic Cell Biology (Mixed Pasteur/Inserm U1223 unit)

Deciphering the impact of macroautophagy perturbation by influenza A virus on virus replication and host cell response to infection

by Brieuc Pérot

Doctoral thesis in Immunology

directed by Matthew L. Albert and co-supervised by Molly A. Ingersoll, PhD

defended publically on September 28th 2016

in front of a jury composed of:

Béhazine COMBADIERE, PhD	President
Marlène DREUX, PhD	Reporter
Nicolas GLAICHENHAUS, PhD	Reporter
Arnaud MORIS, PhD	Reviewer
Jeremy S. ROSSMAN, PhD	Reviewer
Matthew L. ALBERT, MD, PhD	Thesis Director
Molly A. INGERSOLL, PhD	Thesis Co-Director

TABLE OF CONTENTS

ABSTRACT

Influenza A virus (IAV) is an *Orthomixoviridae* virus family member responsible for yearly epidemics and sporadic pandemics, which makes it a major public health issue. The symptom severity of influenza, the disease caused by this virus, ranges from mild to deadly. A key element that impacts both viral fitness and systemic and local symptoms is the innate immune response to infection. It is believed that the robust cytokine release in the context of influenza is the primary driver of symptoms. Understanding the mechanism by which the inflammatory response is mounted and controlled is key to manage the disease. IAV perturbs a variety of metabolic pathways in the cells it infects, including macroautophagy. Macroautophagy, hereafter referred to as autophagy, is a catabolic pathway that allows bulk degradation of cytoplasmic components such as organelles and protein aggregates. Autophagy is active in all nucleated cells to maintain homeostasis. In stress condition, such as starvation or hypoxia, however, autophagic activity can be increased, thereby acting as a pro-survival mechanism. A variety of viruses perturb autophagy, either inducing it or preventing its occurrence. IAV has been described to both induce autophagy and block its completion mainly through its matrix protein 2 (M2). However, the impact of such perturbation on viral replication and host cell response to infection is still unknown. Commonly used techniques to study autophagy perturb key metabolic processes, thereby limiting our capacity to understand the effect of autophagy and its perturbation by IAV. In my thesis work, I developed cellular models in which autophagy capacity can be specifically restored in cell lines that are otherwise autophagy-incompetent. Using these models, I showed that autophagy does not impact IAV infection and replication but inhibits interferon-β induction at early stages post infection, leading to dampened induction of interferon-stimulated genes. Since M2 is the master regulator of autophagy by IAV, I also generated cell lines in which M2 can be stabilized. Using these models and mutant viruses devoid of M2, evidence suggests that M2 does not prevent autophagy completion by itself but only in the context of IAV in a caspase-activation dependent fashion. In summary, my thesis work, using these novel autophagy models, revealed that early autophagy induction post-IAV infection inhibits IFN-β, leading to a global decrease in interferon stimulated gene expression. Indeed, sustained autophagy perturbation through M2 may allow IAV to limit the IFN-β response throughout its life cycle. Preventing M2-mediated autophagy perturbation may allow us to develop new antiviral strategies as well as new live attenuated influenza virus vaccines with boosted inflammation-induction capacity.

RÉSUMÉ

Le virus influenza A (VIA), qui appartient à la famille des *Orthomixoviridae*, est responsable d'épidémies annuelles et de pandémies sporadiques, ce qui en fait un problème majeur de santé publique. La sévérité des symptômes de la grippe, la maladie causée par cet agent infectieux, est variable et il peut être mortel. Un élément clef, impactant à la fois la réplication du virus et les symptômes de l'hôte, est la réponse immunitaire innée. La forte sécrétion cytokinique et l'inflammation associée impactent fortement les symptômes des patients. La compréhension des mécanismes entrainant la mise en place et l'orchestration de cette forte inflammation est importante pour contrôler cette maladie. Le VIA perturbe les voies métaboliques des cellules infectées, notamment la macroautophagie. La macroautophagie, par la suite appelée simplement autophagie, est une voie du catabolisme cellulaire permettant la dégradation d'éléments cytoplasmiques tels que les organites et les agrégats protéiques. L'autophagie est constitutive dans les cellules nucléées et participe au maintien de l'homéostasie cellulaire. En réponse à un stress cellulaire, comme par exemple le manque en nutriments ou en dioxygène, l'autophagie peut être stimulée et agit alors comme un mécanisme de survie. Un grand nombre de virus perturbe l'autophagie, soit en la stimulant, soit en l'inhibant. Le VIA induit l'autophagie mais inhibe sa phase finale, un mécanisme impliquant sa protéine de matrice 2 (M2). Cependant, les impacts de cette perturbation de l'autophagie sur la réplication virale et sur la réponse de la cellule hôte à l'infection sont encore peu compris. Les techniques communément utilisées pour étudier l'autophagie perturbent d'autres processus métaboliques cellulaires, ce qui limite notre capacité à comprendre les effets liés à la perturbation de l'autophagie en elle-même. Au cours de ma thèse, j'ai développé des modèles cellulaires dans lesquels la capacité d'autophagie peut être spécifiquement restaurée dans des lignées cellulaires autrement incapables d'autophagie. L'utilisation de ces modèles m'a permis de montrer que l'autophagie ne change ni l'infectiosité du virus ni si capacité de réplication intracellulaire mais inhibe l'induction de l'interféron-β et des gènes induits par celui-ci. L'utilisation d'autres modèles que j'ai générés, m'a permis de mettre en évidence que M2 n'inhibe la phase finale de l'autophagie que dans le cadre de l'infection et de l'activation de l'apoptose. Une meilleure compréhension des perturbations de l'autophagie par M2 pourrait permettre d'introduire de nouvelles stratégies de développement de molécules antivirales et de nouveau virus atténués induisant une plus forte réponse immunitaire.

LIST OF FIGURES

LIST OF TABLES

ACKNOWLEDGMENTS

Thank you Matthew Albert for having welcomed me in your laboratory and providing me with a great environment for my thesis. The time we met in Boston when I was doing my master's internship seems very far now. I remember being amazed by your excitement and the amount of ideas and possible projects that I could do in your laboratory. Being in your laboratory for all these years made me grow as a scientist and I cannot thank you enough for all the things that you taught me.

Molly Ingersoll, I would like to thank you for your nice co-supervision and being there on a day to day basis for all the questions I had and for having guided me especially in the last part of the PhD. You were great (and still are) to interact with and I admire your positivity and energy. I learnt a lot from you during all these years.

Thank you Jeremy Rossman for helping me so much with great scientific ideas, guidance for virology questions and protocols. For being so friendly and having welcomed me in your laboratory during my PhD.

Thank you Nader, for all your contributions and nice ideas for my project. I look up to you a lot. You are one of the brightest people I know, a living PubMed with great ideas and a contagious excitement for science in general. You are also a dear friend and I feel very lucky to have met you.

Thank you J Boussier, for all the things you have taught me. I have learnt so much about statistics and data analysis in biology with you. Discussing my project with you was also very helpful and your advice was very valuable. You also taught me so much about English writing and I know it will be precious knowledge for the future. Thanks for all the edits you made on both the thesis and the paper manuscript. Thank you most importantly for being such a good friend. Having you by my side during my PhD felt great!

Thank you Clémence Hollande for your precious scientific feedback and all the fun we had during the PhD. I am impressed by your data and I am positive you will do a brilliant PhD and career. Being around you for the past few years felt really great.

Thanks Rosa Barreira da Silva, Tracy Canton, Bilana Zafirova for all the nice scientific interaction and all the fun we had.

Thank you Basma Bahsoun for having welcomed me in your laboratory, teaching me new protocols and most importantly for being so friendly. Thanks for all the tips during my stay in England, the day we went to the Airshow and had nice discussion while watching the planes remains a great memory for me.

To all ICD members that I had the chance to work / interact with: thank you. This past few years were great and you are a major cause for that. Interacting with you was enriching scientifically and the nice atmosphere in the laboratory made it a great place to work.

Thank you to the Centre d'Immunologie humaine, for providing such a nice environment to work and great technologies. Thank you in particular to Milena Hasan, Valentina Libri and Bruno Charbit.

I also thank my friends outside the laboratory and in particular my dear friends Stephane Arnoux, Hélène Thomas, Caroline Le Quellec, Julien Lizé, Antoine Hochet, Emma Le Guéziec, Guillaume Gouerou, Marie Monteil and Arnaud Pearl. Being around you was really great although I would have liked to be more available.

To my mother, siblings, grandparents and the rest of my family, thank you. Thank you first for having accepted the fact that I was not as available as I wanted to. Thank you for your support, your love and generosity.

A special thank to the members of the jury for their time and interest. To Marlène Dreux and Nicolas Glaichenhaus for their critical reading of the manuscript. Arnaud Moris and Jeremy Rossman for accepting to examine my manuscript and to Behazine Combadière for having accepted to be the president of my jury.

ABBREVIATION LIST

(-)vRNA	negative sense viral RNA
5'm7G	N7-methylated guanosine
APAF-1	apoptosis protease-activating factor 1
Atg	autophagy-related
BDI	bright detail intensity
CTL	cytotoxic T lymphocyte
CQ	chloroquine
DAMP	damage-associated molecular pattern
DC	dendritic cell
DD	destabilization domain
dsRNA	double-stranded RNA
FKBP12	FK506/Rapamycin binding protein 12
GSEA	gene set enrichment analysis
HA	hemagglutinin
HCV	hepatitis C virus
hPAF1C	human PAF1 transcription elongation factor
HSP	heat-shock protein
IAV	influenza A virus
IFN	interferon
IFNAR	interferon-α/β receptor
IL	interleukin
IRF	interferon regulatory factor
ISG	interferon-stimulated gene
KO	knock-out
LC3	microtubule-associated protein 1 light chain-3
LIR	LC3-interacting region
M1	IAV matrix protein 1
M2	IAV matrix protein 2
MAVS	mitochondrial antiviral signaling protein

MDA5	melanoma-differentiation-associated gene 5
MEF	mouse embryonic fibroblasts
MOI	multiplicity of infection
mTOR	mammalian target of rapamycin
mTORC	mTOR complex
NA	IAV neuraminidase
NEMO	NF-κB essential modulator
NEP	IAV nuclear export protein, also known as NS2
NF-κB	nuclear factor-kappaB
NLRP	NOD-like receptor (NLR) family, pyrin domain–containing protein
NP	IAV nucleoprotein
NS1	IAV non-structural protein 1
NS2	IAV non-structural protein 2, also known as NEP
OAS	2-5 oligoadenylate synthetase
PA	IAV polymerase subunit A
PAMP	pathogen-associated molecular pattern
PACT	PKR activator
PE	phosphatidylethanolamine
PB1	IAV polymerase subunit B1
PB2	IAV polymerase subunit B2
PC	principal component
pDC	plasmacytoid DC
PI3K-III	class III phosphatidylinositol 3-kinase
PKR	double-stranded RNA-dependent protein kinase
PRR	pattern recognition receptor
PR8	A/PR/8/1934 (H1N1)
qPCR	quantitative PCR
RIG-I	retinoic acid-induced gene 1
ROS	reactive oxygen species
RT	reverse transcription
SA	sialic acid
siRNA	small interfering RNA

SOCS3	suppressor of cytokine signaling-3
ssRNA	single stranded RNA
TLR	Toll-like receptor
TOLLIP	Toll-interacting protein
TRIM 25	tripartite motif Containing 25
UVRAG	UV radiation resistance-associated gene
vRNA	viral RNA
vRNP	viral ribonucleoprotein
VSV	vesicular stomatitis virus
WT	wildtype

INTRODUCTION

Viruses are intracellular parasites that hijack cellular machineries to multiply. They can infect a range of cells, from archaea and bacteria to mammalian cells[1,2]. Along the long history of coexistence of cells with these parasites, higher eukaryotes have evolved immune systems that allow them to cope with these parasites by either killing or tolerating them[3]. The immune system can be divided into two heavily interconnected parts: the innate and the adaptive immune systems. Components of the innate immune system can recognize key features shared by viruses (or other microorganisms), or associated changes in the cellular microenvironments through molecular sensors[4]. These sensors, when activated, trigger the activation of anti-viral transcriptional and other phenotypic programs allowing the organism to quickly and potently respond to infection. This first line of response is referred to as the inflammatory response and allows, through inflammation, the containment of the infection or its complete clearance, while the adaptive immune response is mounted. Inflammation encompasses several phenomena such as (a) increased blood flow to the site of infection, (b) pro-inflammatory cytokine secretion, which induces the recruitment of innate immune cells (e.g. neutrophils, natural killers, macrophages, dendritic cells and monocytes) to the site of infection, and (c) programed cell death, by which a cell kills itself before it starts producing viruses[5,6]. Type I interferons (IFNs) are cytokines that allow uninfected cells to enter an anti-viral mode and to participate in controlling infection[7]. Recruited innate immune cells help clear the infection through killing of virus-infected cells and maintenance of an anti-viral microenvironment. Dendritic cells (DCs) are key cells that bridge the innate and adaptive immune response[8]. They engulf viruses or dying virus-infected cells while maturing, and subsequently migrate to the draining lymph node. Maturation of DCs is primed by the detection of pathogen/damage-associated molecular patterns (PAMPs/DAMPs) by pattern recognition receptors (PRRs). While maturing, DCs engulf viral antigens, which are then presented to $CD4^+$ or $CD8^+$ T cells bearing the receptor that recognizes the specific processed antigen[8]. Activated virus-specific T lymphocytes, key effectors of the adaptive immune system, then migrate to the site of infection (following the inflammatory cytokine gradient permitted by the innate immune response) where they fight the virus through maintenance of inflammatory environment and killing of virus-infected cells[9]. Adaptive immunity also relies on the activation of B cells by DCs, which allows the production of virus-specific antibodies[10].

The infected cell itself plays a key role in initiating the immune response. It can sense the infection through PRRs, which allows the signaling of the infection to other cells—

thereby attracting immune cell—and may prime their self-killing. Conversely, viruses have evolved strategies to prevent their detection and/or the anti-viral events that follow[11]. Viruses also richly interfere with the cellular metabolism to hijack it while cells tune both anabolism and catabolism to fight the virus[12,13]. A key pathway that is both induced by cells during many viral infections and hijacked by many viruses is macroautophagy, hereafter referred to as autophagy[14]. Autophagy, as a stress-induced pathway, was foreseen by several investigators, including Matthew Albert, as a mechanism that could interact with viral sensing or early anti-viral actions taken by dying virus-infected cells. Namely, the hypothesis was that autophagy itself, having co-evolved in eukaryotes for 2.5 billion years as a stress pathway along viral infection[15], may have itself become a danger-associated signal that might crosstalk with PRR signaling in the infected cell. In line with this idea, many evolutionarily distant viruses have evolved mechanisms that perturb autophagy, reveal it as a key viral fitness-impacting pathway[14].

The Albert lab has long been interested in influenza A virus (IAV), firstly as a model through which they showed for the first time that DCs can present antigen from engulfed dying infected cells, thereby priming IAV-specific $CD8^+$ T cells[16,17]. In Matthew Albert's words, "death is not an endpoint, but the beginning of an immune response" we could add that the degree of cell stress when it dies may also impact how DCs prime the immune response. Hence, one of the starting focuses of his team is the study of the impact of stress and death programs on the cross-priming of $CD8^+$ T cells. In this context, the Albert laboratory demonstrated that autophagy in dying IAV-infected cells stimulates cross-priming of IAV-specific $CD8^+$ T cells through stimulation of pro–cross-priming type I IFN production by the engulfing DCs[18].

The aim of the present study was to better understand how autophagy is perturbed in IAV-infected cells. I also wanted to investigate the impact of such perturbations on IAV replication and on the innate immune response of cells using models where autophagy could be experimentally controlled. In this introduction, I review, in detail, the biology of IAV as well as its pathology and epidemiology. I describe known mechanisms by which IAV infection is sensed by the host and escape pathways evolved by IAV. I will then describe the autophagy pathway, addressing key molecular events permitting this catabolic pathway and its regulation. The literature is filled with examples of how autophagy crosstalks with immune pathways in the context of viral infection; this will be addressed in the following section. I will then explain how IAV has been described to manipulate autophagy with conflicting

results, and to what extent the impact of such perturbation on host cell response to infection remains unclear. I believe that commonly used techniques to study autophagy present important caveats and are likely to cause artifactual phenotypes, which may explain conflicting results observed in the literature. This will be described in a last section that highlights the need for the development of new biotechnological tools to study autophagy that allow greater insight into the impact of its perturbation on host response to IAV.

1. Influenza epidemiology and pathology

IAV, which belongs to the *Orthomyxoviridae* virus family, is a negative sense single stranded RNA virus that is responsible for a condition referred to as influenza. Influenza outbreaks come as yearly epidemics and sporadic pandemic that can cause severe morbidity and mortality rates. Worldwide, 3 to 5 million severe influenza cases are reported yearly with lethal cases ranging from 250,000 and 500,000 (World health organization). However, highly lethal and remarkably contagious pandemic strain sporadically appear as the devastating 1918 one, which killed up to 50 million people in the first 25 weeks and is believed to have infected one third of the world population[19]. Devastating pandemic outbreaks continue to emerge regularly (3 in the last 10 years) and future ones are expected, with a fear of a highly devastating one. A better understanding of IAV biology and the host response it triggers therefore remains crucial in order to ameliorate vaccine strategies and alleviate symptoms[20].

Influenza induced by IAV causes symptoms that can differ in type and severity depending on the viral strain and the host. These symptoms include inflammation of the respiratory tree and the trachea, high fever, rhinitis, cough, headache, myalgia, weakness, fatigue, malaise and most commonly recess after 7 to 10 days[21]. Although inflammation allows control of the infection[11], symptom severity and lethality have been linked to poorly-controlled inflammatory response leading to hypercytokinemia[21,22]. Being involved in eliminating IAV as well killing hosts, understanding the innate immune response to IAV is key to fight influenza.

2. IAV biology

IAV genome is segmented and consists of 8 segments of single stranded negative sense viral RNA ((–)vRNA), each coding one or more proteins, tightly coiled around nucleoproteins (NPs), together forming viral ribonucleoproteins (vRNPs). vRNPs have polymerase complexes formed of 3 subunits (PA, PB1 and PB2) at their 5' ends[23]. The virions are

enveloped and can be spherical (100 nm in diameters) or filamentous (100 nm by 20 µm)[24]. The virions are coated by hemagglutinin (HA) and neuraminidase (NA) proteins, which are transmembrane proteins facing the external part of the virion (Figure 1). The subtype of HA and NA typically allows classification of pandemic and epidemic IAV strains (e.g. H5N1, H7N9). 18 HA and 11 NA subtypes have been documented[25]. Matrix protein 1 (M1) coats the inner part of the virion, whereas M2 forms transmembrane homotetramers. NA, NP, HA, polymerase subunit B1 (PB1), PB2 and PA are all expressed from their corresponding genomic segments, whereas M1 and M2 come from alternative splicing of the M segment. PB1 segment also generates the nonstructural protein N40 and PB1-F2, which is made from an alternative open reading frame from PB1, in some viral strains. NS segment generates proteins from alternative splicing, namely non-structural protein 1 (NS1) and nuclear export protein (NEP, also known as NS2)[23].

HA, which is cleaved by host enzymes during infection[26], interacts with sialic acids at the host cell surface, which is followed by viral entry through clathrin-mediated endocytosis (for spherical viruses) or macropinocytosis (for filamentous viruses)[24]. Acidification of endosomes leads to the opening of M2 ion channel, in turn leading to the acidification of the inside space of the virion[23,27]. Acidification of the virion triggers cleaved HA complex transconformational changes, which induce virion and endosomal membrane fusion, resulting in the release of vRNPs in the host cell cytosol[23,27]. Following shuttling of vRNPs to the nucleus, the RNA-dependent RNA polymerase generates viral mRNAs through primary transcription. After nuclear export and cytosolic translation, viral proteins are transported to the plasma membrane (HA, NA and M2) or to the nucleus (PB1, PB2, PA, NP, M1, NEP). In the nucleus, 3 types of positive-sense RNAs (+RNAs) are produced through the polymerase complex[22]:

- complementary (+)vRNAs, which serve as templates to generate more (–)vRNAs
- negative-sense small viral RNAs, believed to regulate the switch between transcription and replication
- viral messenger RNAs, which are exported to the cytoplasm for translation of viral proteins (secondary translation).

Generated (–)vRNAs form, along with NP and the polymerase subunits PA, PB1 and PB2 progeny vRNPs that leave the nucleus via the help of NEP and M1. Trafficking to the plasma membrane then occurs through Rab11 vesicles and packaging and budding take place at the

plasma membrane[22]. M2 is involved in scission of budding viruses[28] and NA prevents aggregation of newly produced virions through enzymatic cleavage of sialic acids[29]. During replication, IAV also generates non structural protein 1 (NS1) and PB1-F2 that modulate host immune cell response. Their activity will be further addressed in a following section.

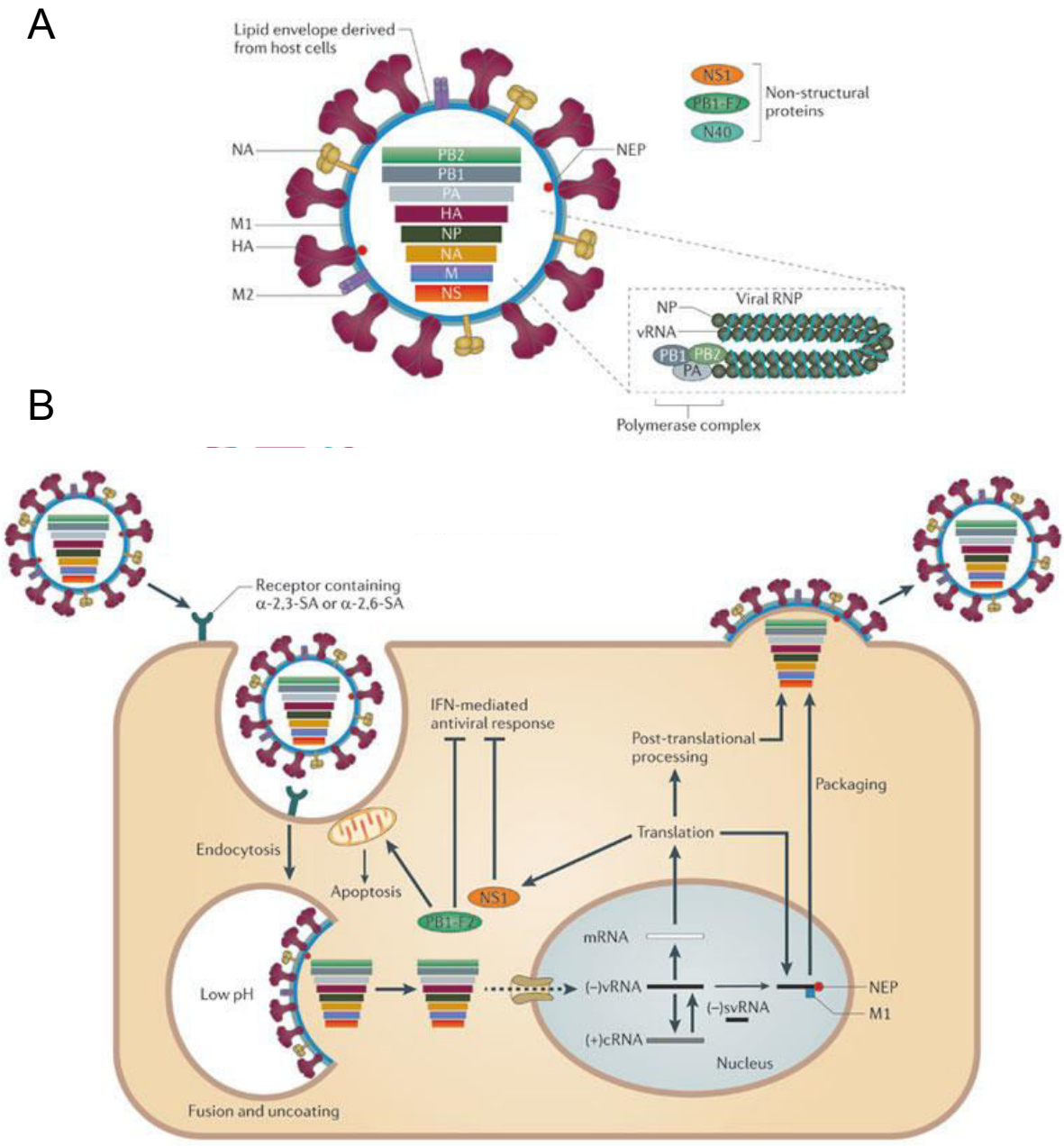

Figure 1: IAV virion and life cycle.
(**A**) IAV virion with key elements are represented; colored rectangles at the center of the virion represent the 8 different viral ribonucleoproteins (vRNPs). (**B**) Representation of IAV life cycle. After attachment of the virion to cell membrane sialic acids (SA), the virus is endocytosed. Following a drop in pH, the virion envelop fuses with the endosomal membrane,

which results in viral vRNP release in the cystosol, followed by shuttling to the nucleus. Transcription of messenger RNA occurs along with viral RNA replication, and viral protein translation occurs in the cytosol. Newly generated viral vRNPs exit the nucleus along with NEP and M1. Packaging and budding of new viral particles occur at the cell membrane. Adapted from Ref. 30.

Importantly, segmentation of the viral genome is associated with the capacity of IAV to allow the reassortment of genomic fragments between viruses in cells co-infected by more than one virion[31]. This process is sometimes referred to as antigenic shift, as opposed to antigenic drift, which is the result of mutation accumulation throughout IAV life cycles. Antigenic shift through reassortment is believed to allow chimeric viruses emergence, in turn promoting viral evolution, immune escape and allowing cross-species infection that facilitate the emergence of pandemic outbreaks[31].

Interestingly, Jonathan Yewdell's group showed that most IAV-infected cells fail to express at least one IAV protein when infected *in vitro* with low multiplicity of infection (MOI)[32]. This was proposed by the group as being a result of segmentation. Indeed, this phenotype may be explained by failure of certain segments to traffic to the nucleus of the infected cells.

As mentioned above, viral fitness and host symptom severity are impacted by the inflammatory response to IAV. It also helps orchestrate the adaptive immune response to IAV, which is important for protective immunity—for instance in the context of vaccination—and for viral clearance after infection has occurred (facilitated by $CD8^+$ T cell-mediated immunity)[11]. As such, the early inflammatory response, which debuts in the infected cells themselves, is key and relays on the host PRRs.

3. IAV type I interferon and inflammatory cytokine induction: known regulators and mechanisms of viral interference

3.1. Innate sensing of IAV by host cells and type I IFN induction mechanisms

The innate immune system can detect IAV presence through PRRs, which sense PAMPs. In the case of IAV, viral presence can be detected by membrane-bound Toll-like receptors (TLRs) or by cytosolic retinoic acid-inducible gene I (RIG-I) and NOD-like receptor (NLR) family, pyrin domain–containing protein 3 (NLRP3). Notably, IAV has evolved mechanisms to prevent its detection by certain of these PRRs.

3.1.1. TLR-mediated IAV recognition

TLR3 expressed in macrophages and respiratory epithelial cells is believed to allow sensing of double-stranded RNA (dsRNA) structures that originate from engulfed dying IAV-infected cells[33]. This induces the activation of two transcription factors, phosphorylated interferon regulatory factor 3 (IRF3) and nuclear factor-kappaB (NF-κB), which in turn stimulate the transcription of type I IFNs and pro-inflammatory cytokines[34]. (**Figure 2A**).

TLR7 is expressed by plasmacytoid dendritic cells (pDCs) and allows the sensing of single stranded RNA (ssRNA) present in endocytosed virions after their acid condition denaturation. Importantly, TLR7-mediated IAV recognition does not require IAV replication[35]. This triggers the activation of IRF7 and NF-κB that in turn induce type I IFN and other cytokines expression[36] (**Figure 2B**).

Type I IFN induces the expression of interferon-stimulated genes (ISGs), many of which have anti-viral properties[7].

3.1.2. RIG-I–mediated IAV recognition

Unlike the TLR-mediated sensing described in the previous section, RIG-I–mediated IAV sensing solely occurs in infected cells. RIG-I pathway is activated by 5'-triphosphate ssRNAs in base paired conformation that are sensed after delivery of vRNPs in the cytoplasm during entry and produced by infected cells at later stages (release of newly produced vRNA)[37,38,39-41]. RIG-I signals through mitochondrial antiviral signaling protein (MAVS, also known as CARDIF or IPS-1), located on mitochondrial membranes, that activates NF-κB and IRF3 signaling, thereby inducing the expression of type I IFNs and pro-inflammatory cytokines by infected cells[42] (**Figure 2C**).

3.1.3. NLRP3-mediated IAV recognition

Unlike other previously mentioned PRRs, NLRP3 is activated upon IAV-mediated cellular homeostasis rupture in the infected cells. NLRPs form multiproteic inflammasomes, which are key mediator of inflammation[43]. These inflammasomes are composed of NLRPs, the adaptor protein Apoptosis-associated speck-like protein containing a CARD (ASC) and pro-caspase 1. Their activation leads to the autocatalytic cleavage of pro-caspase 1 into caspase 1. Caspase 1 then cleaves pro–interleukin-1β (IL-1β) and pro–IL-18 into IL-1β and IL-18 respectively, which are then secreted as mediators of inflammation[43]. Furthermore, inflammasome activation can induce pyroptosis, a form of programed cell death in infected

cells[44]. NLRP3 is expressed in dendritic cells, monocytes, macrophages, neutrophils and bronchial epithelial cells[38]. NLRP3 activation requires two consecutive events. In the first one, typically referred to as signal 1, TLR, IL-1 receptor or tumor necrosis factor receptor signaling—directly or indirectly induced by PAMPs—induces the expression of NLRP3, pro–IL-1β and pro–IL-18. Signal 2 can be made of a broad range of events that are mainly linked to perturbation of homeostasis (e.g. calcium flux, potassium efflux, elevated reactive oxygen species (ROS)) or signs of cellular damage (e.g. leakage of mitochondria or lysosome)[45,46]. Signal 2 induces the formation of NLRP3 inflammasome.

Commensal bacteria presence acts as a signal 1 for at least some cell types at steady state and TLR7 and RIG-I stimulation by IAV can act as further signal 1 mediators in infected cells[38]. In the context of IAV, two signal 2s have been described. The first one consists of M2-mediated proton flux induction between the cytoplasm and the *trans*-Golgi[47]. The second described IAV-induced NLRP3 signal 2 is the presence in the lysosome of high molecular weight aggregates of PB1-F2 presumably post engulfment of PB1-F2 fibril-containing dying IAV-infected cells[48] (**Figure 2C**).

Altogether, the different host IAV sensing modalities, as the first line of defense of the organism, can impact viral fitness (for example through anti-viral interferon-stimulated gene expression) and are also key to orchestrate the forthcoming anti-viral adaptive immune response. As an illustration of the importance of IAV molecular detection by host cells, this virus has evolved a variety of strategies that inhibits its sensing.

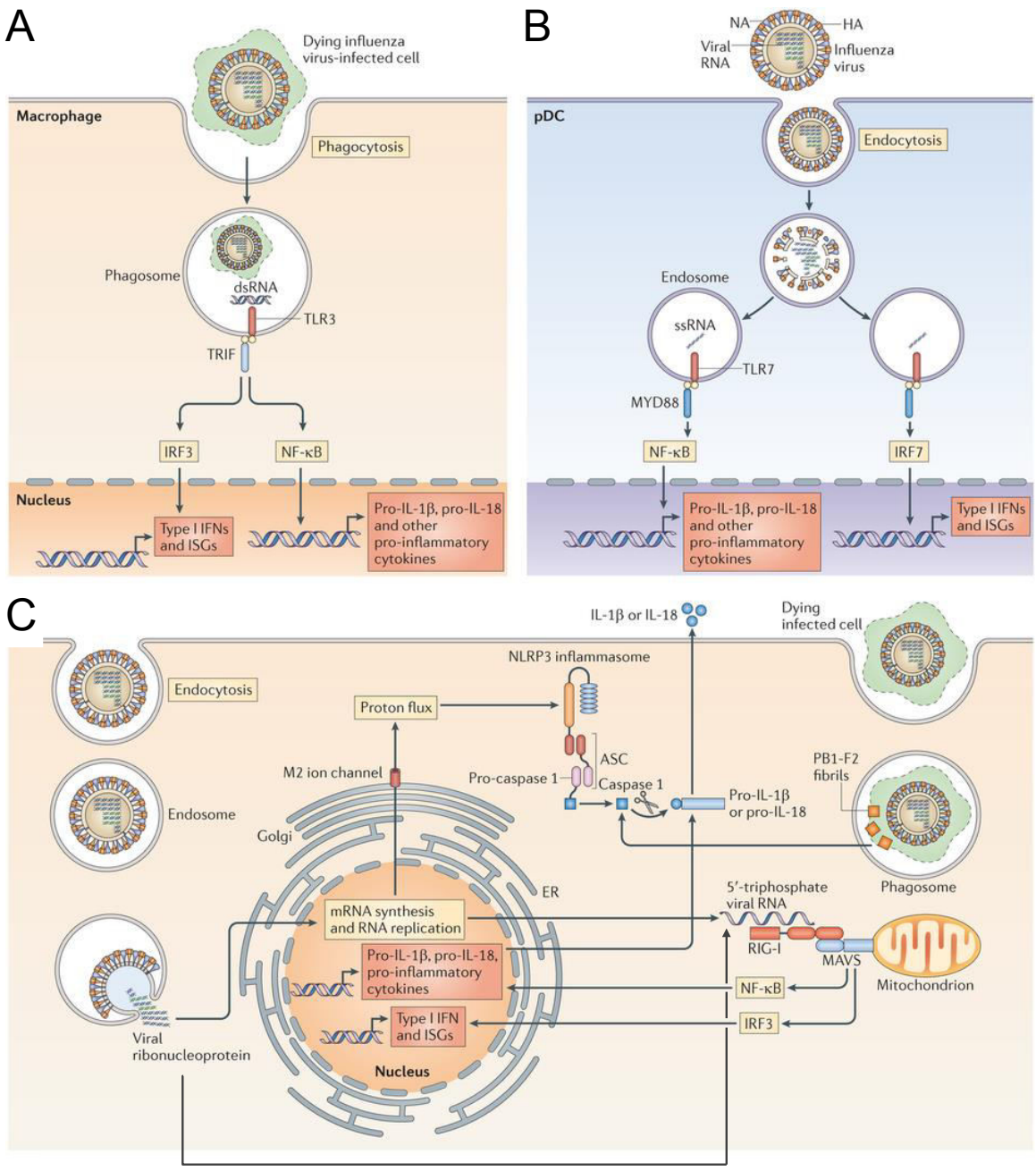

Figure 2: IAV sensing by pattern recognition receptors and associated signaling.
(**A**) Dying IAV-infected cells may be engulfed by macrophages or DCs which can stimulate TLR3 in phagosomes through dsRNA or dsRNA-like elements and downstream activation of IRF3 and NF-κB mediated by TRIF. (**B**) pDCs express TLR7 in endosomes, which can be stimulated by endocytosed virions and activate NF-κB or IRF7 (in distinct endosomes). (**A**, **B**) Activated IRF3 and IRF7 allow expression of type I IFNs while NF-κB stimulates transcription of pro-inflammatory cytokines. (**C**) In infected cells, newly produced 5'-triphophate viral RNA and incoming viral ribonucleoparticles activate RIG-I, which induces NF-κB and IRF3 via MAVS on mitochondria. This results in expression of type I IFN, inflammatory cytokines, pro–IL-1β and pro–IL-18 (signal 1). NLRP3 inflammasome activation occurs following M2-mediated proton flux toward the cytosol or by PB1-F2 fibrils acquired from engulfed IAV-infected cells. Adapted from Ref. 38.

3.2. Known IAV anti-interferon-stimulated genes and inflammation induction strategies

3.2.1. Hiding PAMPs

As opposed to many RNA viruses, IAV has an atypical life cycle as its replication occurs in the nucleus of the host cell. Since RIG-I is present in the cytosol, authors have suggested that replication in the nucleus has been selected for as a means of preventing sensing of viral RNA[49]. Nuclear replication might benefit segmented viruses the most since segmentation may increase the amount of PRR agonists present in cells. Indeed, eight segments entering the host cell result in eight 5'triphosphate RNAs (RIG-I agonists) as opposed to, for instance, viruses like vesicular stomatitis virus (VSV), a negative sense non-segmented RNA virus, which have one RIG-I agonist per virion[50].

However, vRNPs have to be shuttled through the cytoplasm to and from the nucleus after entry and before budding, respectively. These two steps are therefore believed to be the ones where RIG-I is activated by IAV RNA[49]. Interestingly, one polymerase complex is associated with each vRNPs and is located in close proximity to the two RNA termini, which, through base pairing, form a double-stranded like structure[23]. This 5'triphosphated dsRNA-like structure acts as IAV RIG-I agonist, and the polymerase complex has been showed to prevent RIG-I access to these[51,37,52]. Polymerase complex therefore acts as a shield that prevents IAV PAMP detection[53,54].

In addition to the shielding of PAMPs from detection by RIG-I, IAV has active mechanisms that limit its sensing and downstream signaling.

3.2.2. NS1 prevents sensing of IAV RNA

NS1 is a key viral multifunctional anti–innate immune sensing and signaling IAV factor[11]. First of all, NS1 has been shown to possess direct RNA binding properties, which limits IFN-β induction[53,54,55].

NS1 also interferes with E3 ubiquitin ligases involved in RIG-I K63 polyubiquitination[49]. These ubiquitination events, mediated by tripartite motif Containing 25 (TRIM25) and RIPLET induce the tetramerization of RIG-I, which is the active form of this protein. NS1 is able to prevent both TRIM25 and RIPLET-mediated RIG-I activation[56,57](**Figure 3**).

Double-stranded RNA-dependent protein kinase (PKR) activator (PACT), a key co-factor in the activation of RIG-I by its agonists is also inhibited by NS1 through direct interaction[58].

3.2.3. PB1-F2 prevents MAVS signaling

PB1-F2 is a protein translated from PB1 RNA that originates from an alternative open reading frame[59]. In the course of infection, PB1-F2 translocates to the mitochondrial inner membrane, which attenuates its transmembrane potential. In turn, this change in potential accelerates mitochondrial fragmentation, which suppresses RIG-I signaling, presumably through decrease in MAVS, which is docked on mitochondria[60]. Direct interaction of PB1-F2 with MAVS has also been shown to prevent signaling[61](**Figure 3**).

3.2.4. Inhibition of host cell gene expression by IAV proteins

IAV infection leads to limitation of host gene expression through different proteins (**Figure 3**).

NS1, via interaction with the cleavage and polyadenylation–specific factor, interferes with the 3'polyadenylation of newly synthesized host pre-mRNA. This specifically inhibits the nuclear export of cellular but not viral mRNA[62]. Eukaryotic mRNA harbors an N7-methylated guanosine (5'-m7G) linked to the first 5' nucleotide of the RNA molecule[63]. This RNA post transcriptional modification is involved in pre-mRNA processing, nuclear export and mRNA translation. IAV mRNAs harbor 5'-m7G caps that are acquires through cap-snatching, a mechanism involving IAV polymerase complex[11]. In this process, PB2 mediates binding to 5'-m7G caps of host mRNA and the PA subunit harbors the endonuclease activity that allows the cutting of host mRNA 10 to 13 nucleotides downstream of the 5' terminus[64]. Since both interference with polyadenylation and cap snatching prevent the maturation of host newly synthesized pre-mRNAs, these pathways impact primarily host mRNAs that have a high turnover rate or are newly synthesized (e.g. type I IFN and other pro-inflammatory cytokines)[11].

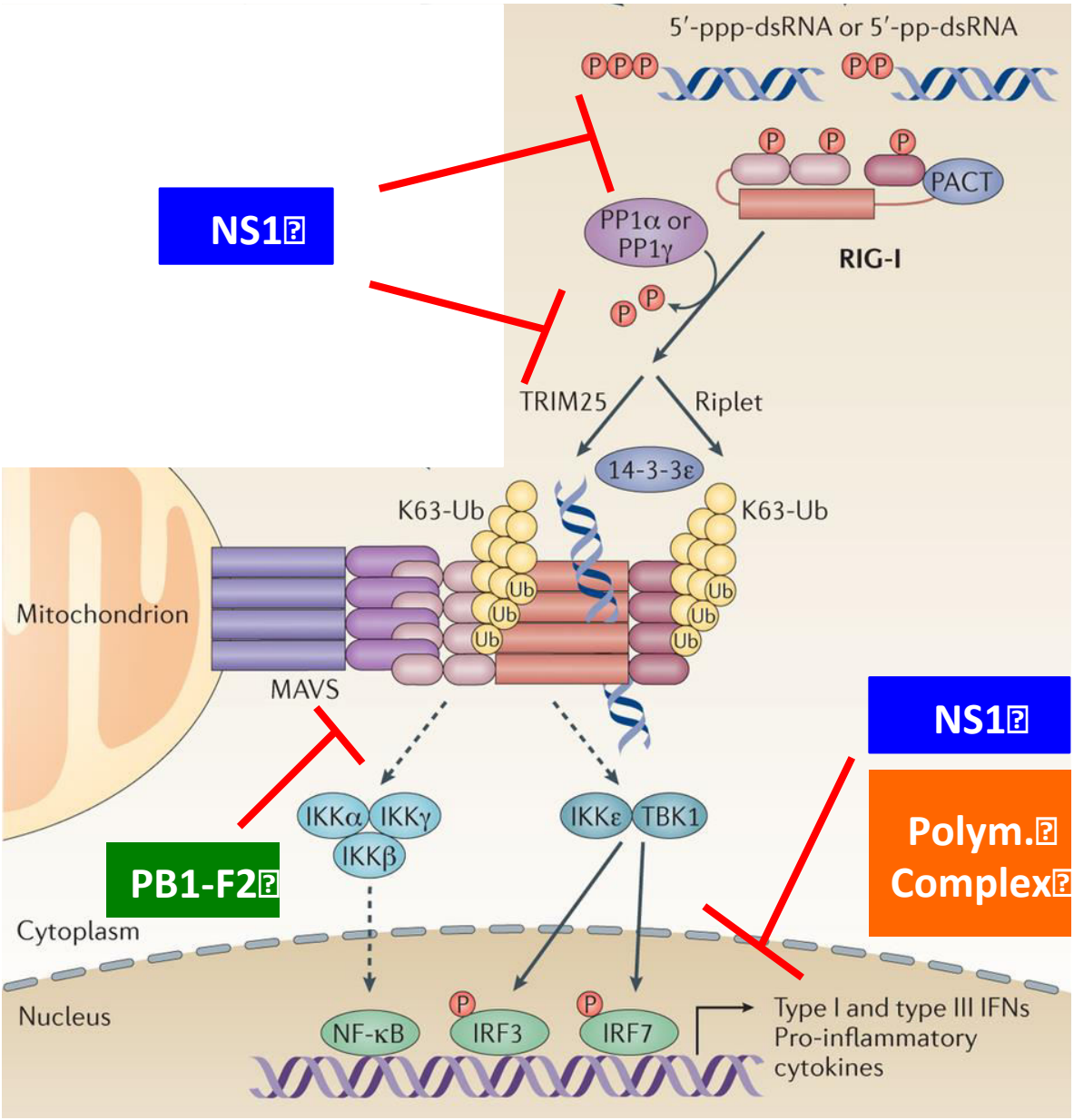

Figure 3: Targeting of RIG-I signaling by IAV proteins.
NS1 can prevent RIG-I activation through targeting of PACT, TRIM25 and RIPLET, which are all important co-factor involved in RIG-I activation. PB1-F2 also inhibits RIG-I signaling through direct interaction with MAVS and mitochondrial disruption. Both NS1 and IAV polymerase complex possess anti-host mRNA maturation properties, which are believed to limit the expression of RIG-I signaling-mediated inflammatory cytokines. Adapted from Ref. 49. Polym. stands for polymerase.

3.2.5 Histone mimicry by NS1

The NS1 protein of IAV A/Wyoming/3/2003 (H3N2 strain) possesses a histone-like sequence that interferes with the epigenome of infected cells through interaction with human PAF1 transcription elongation factor (hPAF1C)[65]. hPAF1C was shown to mediate transcription of

numerous antiviral genes and NS1 prevents, via its histone-like domain, hPAF1C-mediated transcriptional elongation[65].

3.2.6. Mechanisms limiting type I IFN effector function

IAV has been shown to limit type I IFN effector function. Indeed, suppressor of cytokine signaling-3 (SOCS3) is induced by IAV in an NF-κB–dependent manner[66]. The induction of SOCS-3 leads to decreased STAT1 phosphorylation, an event required for type I IFN signal transduction, and limits ISG expression.

NS1 also exerts an inhibitory effect on viral restriction factors induced by type I IFN. PKR is a protein, induced by type I IFN, which harbors anti-viral properties partially due to its anti-translation activity[67]. NS1 has been shown to inhibit PKR through direct interaction[68,69].

2-5 oligoadenylate synthetase (OAS) is an ISG that activates RNase L when it is itself activated by dsRNA in infected cells. In its active form, RNase L degrades cellular and viral RNA, in turn restricting viral infection[70]. NS1 protein dsRNA binding domain has been proposed to sequester dsRNA away from OAS, thereby limiting its anti-viral function[71]. Interestingly, NS1-mediated prevention of RNase L activation has also been hypothesized to limit IFN-β expression as RNase L is involved in increasing the expression of this cytokine in the context of viral infection in some cell types[72,73].

3.2.7. Hijacking cell death

Programed cell death is an innate immune response event that is able to restrict viral replication[74]. Conversely, many viruses have evolved strategies to evade cell death occurrence in the cell that they infect[75].

It is generally believed that IAV inhibits apoptosis at early timepoints post infection, which allows early replication[76,77]. At later stages of infection however, apoptosis is thought to exert a pro-viral replication role, presumably allowing virus elements (vRNPs) to escape the cellular nucleus[78,79].

NS1 protein induces anti-apoptotic signaling[80] and also limits IAV-induced IFN-mediated apoptosis[81]. Furthermore, NS1 from the circulating highly pathogenic H5N1 IAV directly interacts with SCRIBBLE, a pro-apoptotic protein, thereby limiting its activity and exerting an anti-apoptotic function[82].

At early stages post infection, heat-shock protein 70 (HSP70) is induced and limits apoptosis through interaction with apoptosis protease-activating factor 1 (APAF-1) a key component the apoptosome[83]. At later stages of infection however, M1, through binding to HSP70, limits this interaction and exerts a pro-apoptotic role[83]. NP was also showed to stimulate cell death by apoptosis via suppression of the expression of the antiapoptotic protein API5[76]. Another way by which NP induces apoptosis is through diminution of RING finger protein 43 expression, which increases p53 stability through prevention of its polyubiquitination and stimulates p53-mediated apoptosis[84]. NP also stimulates apoptosis through direct interaction with the anti-apoptotic clusterin protein[85]. PB1-F2 also promotes apoptosis through promotion of mitochondrial permeabilization mediated by its interaction with the adenine nucleotide translocator of the inner membrane of mitochondria and with the voltage-dependent anion channel 1 of the mitochondrial outer membrane[86]. NS1 also harbors pro-apoptotic properties. Indeed, NS1 binding to HSP90 has been shown to augment APAF-1 binding to cytochrome c while limiting its binding to HSP90, thereby facilitating IAV-induced apoptosis[87]. Finally, Gannage and colleagues showed that M2 induces apoptosis in a presumably autophagy-dependent manner[88].

IAV not only perturbs PRR signaling in infected cells but also their metabolic activities such as autophagy.

5. The autophagy pathway

Autophagy is a catabolic and recycling pathway conserved among eukaryotic organisms[89]. Autophagic flux occurs in cells as a homeostatic process that aids in the degradation of aged and potentially harmful or damaged organelles. It also plays a role in the recycling of cellular nutrients for energy conservation[90]. Autophagic activity may be induced by various stress conditions such as starvation, absence of growth factors, or endoplasmic reticulum (ER) stress [91,92,93]. The mammalian target of rapamycin (mTOR) complex I (mTORC1) is a key signal integrator involved in keeping autophagy in check when stimulated (e.g. by ATP, oxygen, amino acids, by growth factor presence on surface receptors). Finally, microbial infection can promote or limit autophagy through multiple mechanisms[94,14].

The autophagic pathway is divided into three phases[95] (**Figure 4**): the initiation phase, which induces the budding of a cysternal membrane structure, termed a phagophore; the elongation phase, during which the double-membraned autophagosome sequesters cytosolic proteins or organelles; and the maturation phase, consisting in the fusion between the

autophagosome and lysosomes, facilitating degradation of the autophagosomal contents. Molecular events leading to autophagy involve approximately 30 autophagy-related (Atg) proteins, which were originally identified in yeast and subsequently found to have mammalian orthologs[96,97]. The initiation phase begins with the activation of the class III phosphatidylinositol 3-kinase (PI3K-III) complex, containing Beclin1 protein[98]. Stimulation of this complex generates phosphatidylinositol-3-phosphate, which, in turn, leads to the nucleation of the phagophore[98]. The origin of the phagophore membrane is subject to debate with studies indicating that it can arise from ER, mitochondria, golgi, or the plasma membrane[99]. The elongation phase involves two ubiquitin-like conjugation systems[98]. In the first, ATG7 (E1 ubiquitin-like activating enzyme) and ATG10 (E2 ubiquitin-like conjugating enzyme) mediate the covalent association of ATG5 and ATG12. The ATG5–ATG12 complex then associates with ATG16L1, tethering the complex to the outer membrane of the phagophore. In the second conjugation system, ATG7 and ATG3 (an alternative E2 ubiquitin-like conjugating enzyme) mediate the conjugation of phosphatidylethanolamine (PE) to microtubule-associated protein 1 light chain-3 (LC3). The PE-conjugated form of LC3, referred to as LC3-II, is present on both the inner and outer membranes of autophagosomes. At the end of the elongation step, the phagophore surrounds targeted elements, resulting in their isolation within the newly formed autophagosome[98]. During the final phase, autophagosomes mature by fusing with lysosomes, either directly or after intermediary fusion with late endosomes[98]. Formation of this structure, referred to as an autolysosome, requires a complex containing Beclin1, UV radiation resistance-associated gene (UVRAG) and PI3K-III, as well as the recruitment of the small GTPase Rab7[100]. Although autophagy provides a mechanism for non-specific bulk degradation, additional, specific roles have been uncovered. Interestingly, mechanisms have evolved that support targeting of protein aggregates, intermediates of cell stress, organelles, and in some instances, intracellular microorganisms to the autophagy pathway[101]. Autophagy receptors are proteins that interact with cellular elements targeted for degradation and with elements on autophagophore membrane, thereby allowing their specific degradation[101]. More than two dozen autophagy receptors have been identified in mammalian cells, the best studied of which is p62 that possess a LC3-interacting region (LIR) and also interacts with ubiquitinated elements targeting them for degradation[101,102].

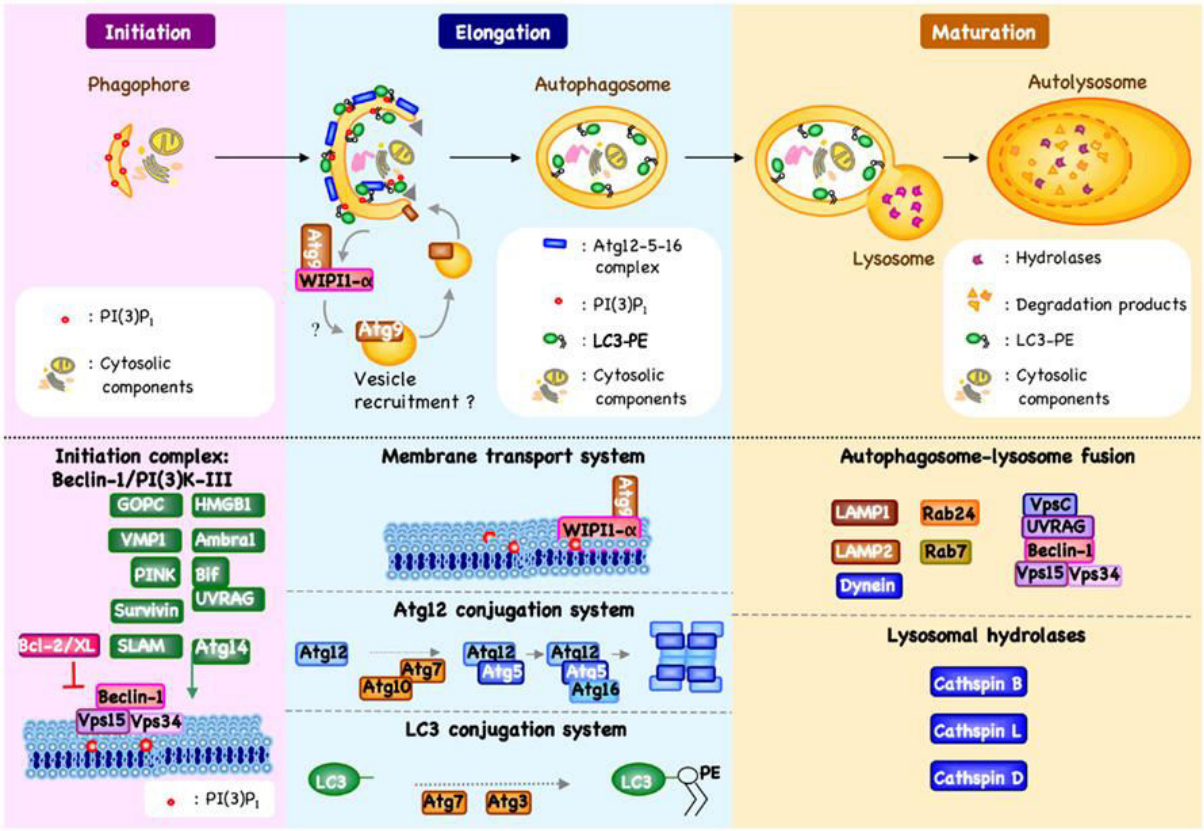

Figure 4: The autophagy pathway.
Beclin-1/PI3K-III complex activation, which is regulated by different pathways, induces the formation of phosphatidylinositol 3-phosphate [PI(3)P1] and the nucleation of autophagic vesicles, characterized by a double-membrane, and called autophagosomes. Two ubiquitin-like conjugation systems permit autophagosome membrane elongation. In the first one, ATG12 is conjugated to ATG5; ATG5–ATG12 then forms a complex with ATG16L1, which decorates the outer membrane of the phagophore (croissant shape growing membrane structure). LC3 conjugation to phosphatidylethanolamine (PE) constitutes the second ubiquitin-like system, present at the outer and inner autophagosomal membrane. Unlike the ATG12–ATG5-ATG16L1 complex, which is recycled by the protease ATG4, the LC3-PE complex (referred to as LC3-II) remains associated with the inner membrane of autophagosomes. Autophagosome maturation is characterized by the formation of an autolysosome, the product of fusion with the lysosome. Adapted from Ref. 98.

6. Direct impacts of autophagy on viral infection

As a key cellular catabolic process that crosstalks with PRR signaling and cell death (all being part of the innate anti-viral immune response), autophagy exerts both direct and indirect effects on viral fitness in infected cells.

6.1. Virophagy, direct targeting of microorganisms for degradation

Xenophagy, the process of autophagy-mediated degradation of microorganisms, is well documented for invasive bacteria, but also targets viral components for lysosomal degradation and is referred to as virophagy[103]. Indeed, Beth Levine's group described that infection with Sindbis virus, a positive stranded RNA virus, induces autophagy in neurons which leads to p62 and autophagy–mediated clearance of Sindbis virus capsid proteins *in vitro* [104]. *In vivo*, inactivation of autophagy in Sindbis virus-infected neurons leads to neuronal cell death associated with accumulation of p62 and Sindbis virus nucleocapsid. Their findings suggest that autophagy can act as a catabolic pathway that prevents toxic viral protein accumulation in host cells. Virophagy has also been described for herpes simplex virus type 1virions that are degraded through PKR-induced autophagy[105].

6.2. Pro-viral effects of the autophagy machinery

Autophagy has been shown to facilitate viral replication in host cells for different viruses. For instance, hepatitis C virus (HCV) replication initiation has been shown to depend on autophagy[106]. Studies suggest that autophagosome-like structures that are induced by HCV serve as platforms for viral replication[107,108]. The Hanada group also highlighted that autophagy acts at the stage of production of infectious HCV particles at later times of HCV life cycle[109]. Other RNA viruses, such as rotaviruses and polioviruses, are believed to use the autophagy machinery and/or autophagosome-like structures for their cytosolic replication[110].

Virus particle assembly and egress are also impacted by autophagy machinery. For example, efficient envelopment of hepatitis B virus was shown to rely on autophagy[111]. Autophagy machinery has also been proposed to allow unconventional secretion of poliovirus particles allowing nonlytic intercellular spread of cytoplasmic viral particles[112].

As a recycling process, autophagy renders nutrients available, which can support viral replication. Indeed, Dengue virus-induced autophagy leads to lipid droplet degradation. By delivering lipids to lysosomal degradation, autophagy release of free fatty acids that simulate mitochondrial β–oxidation and ATP generation. This autophagy-mediated ATP enrichment is thought to benefit viral replication in host cells[113].

7. Autophagy crosstalks with type I IFN and other pro-inflammatory cytokine induction during viral infection

Sensing of viral PAMPs through PRRs, signal transduction and induction of transcriptional programs leading to acquisition of antiviral state in infected and bystander cells and secretion of anti-viral cytokines are key to elicit anti-viral immunity[114]. Key PRRs that sense viral PAMPs are the membrane-bound TLRs, the cytoplasmic RIG-I–like receptors (RLRs), and inflammasomes, among which the best described is the NLRP3 inflammasome. As mentioned previously, key transcriptional programs involved in these 3 types of virus sensing pathways are NF-κB, phosphorylated IRF3 and phosphorylated IRF7.

7.1. Autophagy as an anti-type I IFN induction mechanism

As one could expect given their key role in initiating anti-viral immune reaction in the host, evolutionarily distant viruses have evolved a variety of strategies to evade their sensing by the host cells[114,49]. Interestingly, autophagy has been shown to impact such pathways in the context of viral infection[110]. For example, autophagy can limit VSV-induced IFN-β[115,116]. Using poly(I:C) to mimic viral PAMPs (poly(I:C) is a TLR3, RIG-I and melanoma-differentiation-associated gene 5 (MDA5) agonist[117]) laboratories have proposed two models. In the first one, formation of the ATG5–ATG12 complex has been proposed to limit RIG-I signaling through direct association with RIG-I and MAVS[115] (**Figure 5 A**). Alternatively, targeting of damaged mitochondria to degradation by autophagy (mitophagy) could induce a decrease in ROS and MAVS presence in the cells, thereby limiting RIG-I signaling[116] (**Figure 5 B**).

Moreover, murine cytomegalovirus induces autophagy in infected cells, which inhibits the inflammatory cascade initiated by NF-κB[118]. This inhibition occurs through targeting of NF-κB essential modulator (NEMO) to autophagic degradation via interaction with the viral protein M45. Importantly, as NF-κB is involved in type I IFN induction[119], this autophagy-mediated prevention of NF-κB activation may mitigate the infected cell type I IFN response.

7.2. Autophagy potentiates type I IFN induction in pDCs

In plasmacytoid dendritic cells, autophagy has on the contrary pro-inflammatory properties in the context of VSV. Indeed, Lee and colleagues showed that autophagy in pDCs potentiates the induction of type I IFN secretion through translocation of cytosolic viral replication intermediates to the TLR7-containing compartments[120] (**Figure 5 C**).

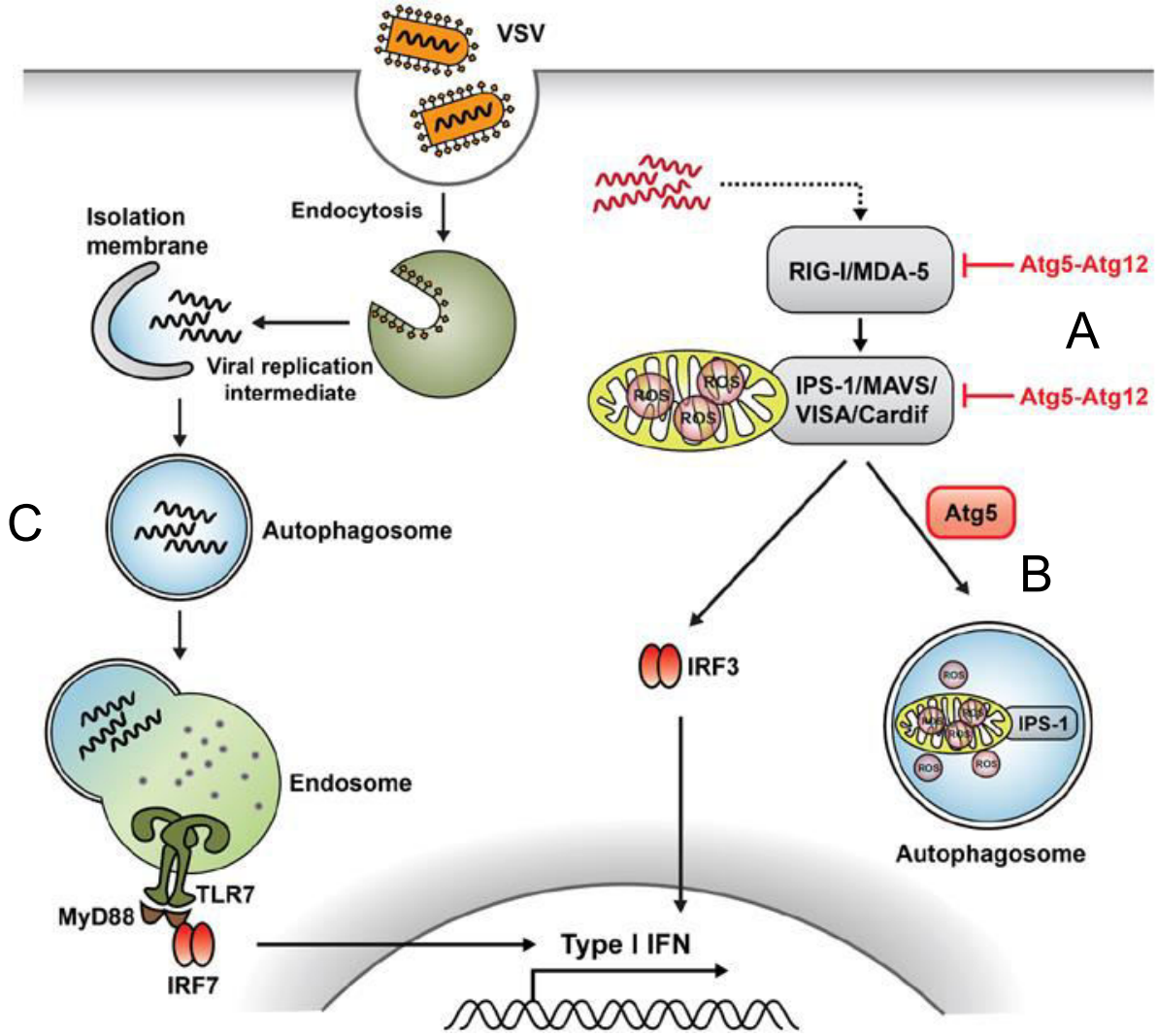

Figure 5: Autophagy as a pro- or anti-type I IFN mechanism in VSV.
(**A, B**) Studies using mouse embryonic fibroblasts proposed that the ATG5–ATG12 conjugate directly interacts with RIG-I, MDA5 and MAVS and limits their activation (**A**)115 and that mitophagy decreases MAVS and ROS levels, both limiting type I IFN induction (**B**)116. In pDCs however, autophagy allows the translocation of viral replication intermediate to TLR7-containing compartments, thereby potentiating the type I IFN response (**C**)120. Adapted from Ref. 121.

7.3. Type I IFN can induce autophagy

Interestingly, type I IFNs have been proposed to induce autophagy[122]. This induction of autophagy by type I IFN may act as an anti-viral mechanism through xenophagy for example. Conversely, type I IFN-induced autophagy may benefit other viruses such as HCV that rely on autophagy for its replication (see above).

7.4. Autophagy and the inflammasome

Autophagy also impacts inflammasome activation. Although not using viral infection, but transfection of dsDNA in macrophages, authors were able to highlight a role for autophagy—which was stimulated by this PAMP—in the degradation of inflammasome components through their ubiquitination and targeting to autophagic degradation via p62[123]. Autophagy thereby limited IL-1β production and therefore acted as an inflammatory signal–driven anti-inflammatory mechanism. Other teams have confirmed an anti-inflammasome effect of autophagy leading to a reduction in IL-1β secretion and in symptom severity in animal models of acute toxic liver injury and atherosclerotic[124,125]. However, autophagy also, perhaps through other molecular mechanisms, stimulates IL-1β secretion[126]. This presumably occurs via the targeting of this cytokine by autophagy, allowing its secretion through fusion of autophagosomes with the plasma membrane[126]. By contrast, Harris and colleagues showed that autophagy could both degrade pro–IL-1β and prevent mature IL-1β secretion upon inflammasome activation[127]. These seemingly contradictory results may come from the fact that the two teams used different macrophage cellular models as well as different autophagy/inflammasome-inducing conditions. Importantly, NF-κB stimulates mitophagy, which acts as an anti-inflammasome activation mechanism[128]. Indeed, mitochondrial ROS and mitochondrial DNA released from damage mitochondria act as a signal 2 on NLRP3 inflammasome[129]. NF-κB is therefore involved in signal 1–induced transcription of pro–IL1-β and NLRP3 but also in initiating a negative feedback pathway involving mitophagy[128].

Given that autophagy intersects with viral fitness and host responses to infection, it is not surprising that, in turn, viruses have evolved mechanisms to manipulate this pathway[14].

8. IAV crosstalks with autophagy

IAV, as many other viruses, has been shown to perturb autophagy in infected cells. Indeed, different strains of IAV are known to induce autophagosome formation[130,88,131,132]. It appears from several studies that M2 is a key inducer of autophagy in IAV infected cells[88,133,132]. HA protein and especially enzymatic cleavage products are also involved in stimulating autophagy, in particular for the highly pathogenic viruses H5 and H7[133]. Such cleavage may play a role in physiopathology since HAs are cleaved by respiratory tract transmembrane proteases[134]. The mechanism by which IAV induces autophagy is still unclear but may involve mTOR signaling[135,136].

Importantly, it appears that the large autophagosome accumulation in the context of viral infection, which has been described by several teams[130,88,131,132,133] does not rely solely on autophagosome formation stimulation but also on prevention of autophagosome maturation, mainly through M2 protein[88,132]. This M2-mediated prevention of autophagosome fusion with lysosome is thought to participate in non-matured autophagosome accumulation as it is the case for chemical inhibitors of autophagy maturation[137]. Of note, Gannage and colleagues argued that M2 anti-autophagy maturation properties are independent of its ion channel activity, whereas Chen group recently argued that ion channel activity was required[132].

It is noteworthy that some teams described that autophagy was functional (i.e. proceeded to degradation of autophagosomal contents) in their *in vitro* models[131,130], which may be due to different experimental settings (e.g. cell lines, viral strains, methods used to modulate autophagy).

Of note, as p62, M2 harbors an LC3-interacting region (LIR) which leads to LC3 localization at the plasma membrane, preventing this interaction through mutation of M2 leads to diminution of filamentous virus budding and of virion stability at room temperature[138].

A recent study, performed in macrophages, highlighted that autophagy-deficient lung macrophages are more inflammatory that their wildtype (WT) counterparts, which leads to more inflamed lung correlating with better control of lung IAV replication and less fatalities among mice[139]. Interestingly, their data suggest that, even at steady state, basal inflammation is induced by autophagy incapacity in macrophages and it is not clear if macrophages were infected in their setting and if active perturbation of autophagy in macrophages was involved in the anti-inflammatory effects of autophagy.

9. Commonly used techniques to study autophagy present strong disadvantages which can generate artifacts

The common approaches to study autophagy are [137] :

- chemical treatments to induce or inhibit autophagy
- small interfering RNA (siRNA)-mediated silencing of autophagy-related genes
- the use of cell lines that are knock-out (KO) for key autophagy genes
- the use of mice lacking autophagy capacity in specific cell subsets

However, these approaches all present disadvantages when studying cell stress and innate signaling pathways.

Indeed, most chemical treatments used to inhibit or stimulate autophagy target pathways that are not only controlling autophagy but also impact key biological processes. For example, rapamycin, a commonly used inhibitor of autophagy, acts by inhibiting the kinase activity of the mTOR. mTOR complex 1, the active complex inhibited by rapamycin is not only controlling autophagy but also other metabolic processes such as translation, transcription and mitochondrial metabolism (**Figure 6 A**). Rapamycin has been showed to perturb these key cellular metabolic pathways[140,141]. A common way of preventing autophagy is by treating cells with 3-methyladenine (3-MA) or wortmanin, which act through inhibition of class I and III or class I, II and III phosphatidylinositol 3-kinases (PI-3Ks), respectively[142,143]. PI-3Ks are involved in a variety of cell metabolic and functional pathways (**Figure 6 B**). Surprisingly, 3-MA has been shown to induce autophagy in some contexts through its inhibitory action on class I PI-3K, illustrating the fact that it does not only act on class III PI-3Ks (the described pro-autophagic pathway)[143]. Finally, 3-MA stimulates inflammation in macrophages in an autophagy-independent fashion[144]. This offers an example of the dangers of using this kind of non-specific chemicals to study complex pathways such as innate immune responses to pathogen encounter.

The use of siRNA transfection to impact the autophagic status of the cell also shows drawbacks. Indeed, siRNAs might activate innate signaling pathways in the transfected cells in a siRNA structure/sequence-dependent manner[145]. Of note, this raises the question of the reliability of the use of non-targeting siRNA as control in siRNA experiment given that they might activate innate signaling pathways differently than the siRNA targeting the protein of interest.

Finally, the use of KO cell lines such as mouse embryonic fibroblasts (MEFs) and their wildtype (WT) counterpart also presents downsides. Indeed, straightforward controlling of the drift (e.g. genetic drift) between the two genetically different immortalized cells is challenging. Yet we hypothesize that divergences between two cell lines may be important, especially in the case of the loss in stress pathway response such as autophagy.

Furthermore, *in vivo* discrepant results when using cell-specific autophagy-related (*Atg)* gene deficient mouse strains, may come from the challenge in segregating modifications of cell developmental programs and more proximal effects on inflammatory responses.

A

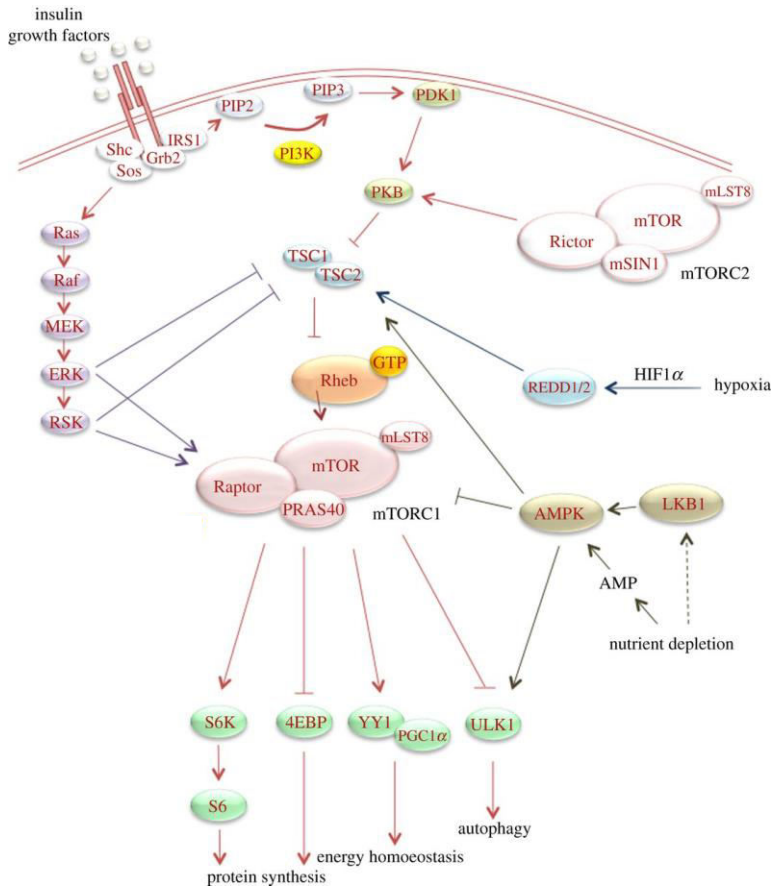
insulin
growth factors
PIP2
PIP3
PDK1
PI3K
Shc
Grb2
Sos
IRS1
PKB
mLST8
mTOR
Rictor
mSIN1
mTORC2
Ras
Raf
MEK
ERK
RSK
TSC1
TSC2
GTP
Rheb
REDD1/2
HIF1α
hypoxia
mLST8
mTOR
Raptor
PRAS40
mTORC1
AMPK
LKB1
AMP
nutrient depletion
S6K
4EBP
YY1
PGC1α
ULK1
S6
autophagy
energy homoeostasis
protein synthesis

B

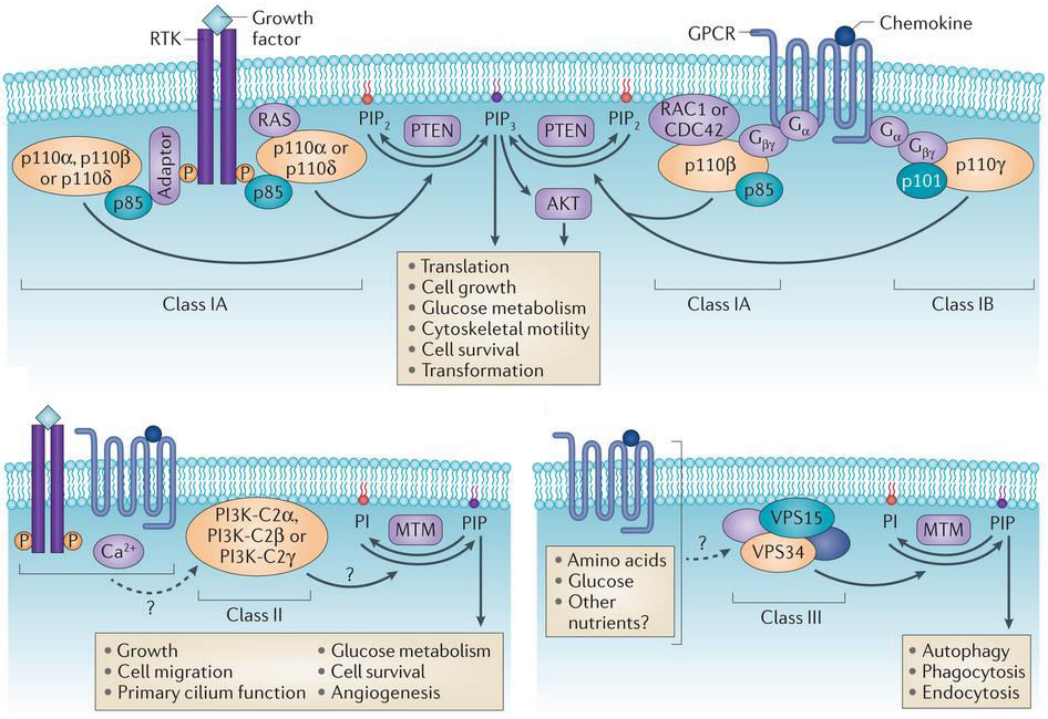
RTK
Growth
factor
GPCR
Chemokine
RAS
PIP2
PTEN
PIP3
PTEN
PIP2
RAC1 or
CDC42
p110α, p110β
or p110δ
Adaptor
P
P
p85
p110α or
p110δ
p85
Gβγ
Gα
Gα
Gβγ
p110β
p85
p101
p110γ
AKT
• Translation
• Cell growth
• Glucose metabolism
• Cytoskeletal motility
• Cell survival
• Transformation
Class IA
Class IA
Class IB
P
P
Ca2+
PI3K-C2α,
PI3K-C2β or
PI3K-C2γ
PI
MTM
PIP
?
?
Class II
• Growth
• Cell migration
• Primary cilium function
• Glucose metabolism
• Cell survival
• Angiogenesis
• Amino acids
• Glucose
• Other
nutrients?
?
VPS15
VPS34
PI
MTM
PIP
Class III
• Autophagy
• Phagocytosis
• Endocytosis

Figure 6: Upstream signaling and effector function of enzymes often targeted to study autophagy.
Signaling and effector function of mTOR (**A**) and PI3Ks (**B**) are shown highlighting their involvement in autophagy and other key cellular processes. Adapted from Ref. 146 and 147.

9. Approach and key findings

Given the fact that, as explained in the previous section, most approaches utilized to study autophagy show strong drawbacks as they are either unspecific or inclined to generate artifactual phenotypes, I developed a new approach to study the impacts of autophagy on host cells reactions to IAV infection. I took advantage of a technology that allowed us to generate new experimental models in which the cell capacity to undergo autophagy can be controlled through stabilizing critical components of the autophagy pathway that are otherwise targeted for degradation in cell proteasome. Importantly, this model does not induce autophagy, but instead restores the capacity for autophagic flux to the cell. The aim of the study was to use this newly generated cellular model (**Figure 7 A**) to investigate the impact of autophagy and its perturbation on IAV infectivity end replication (**Figure 7 B & C**) as well as the impacts on host cell reaction to infection (**Figure 7 D through F**).

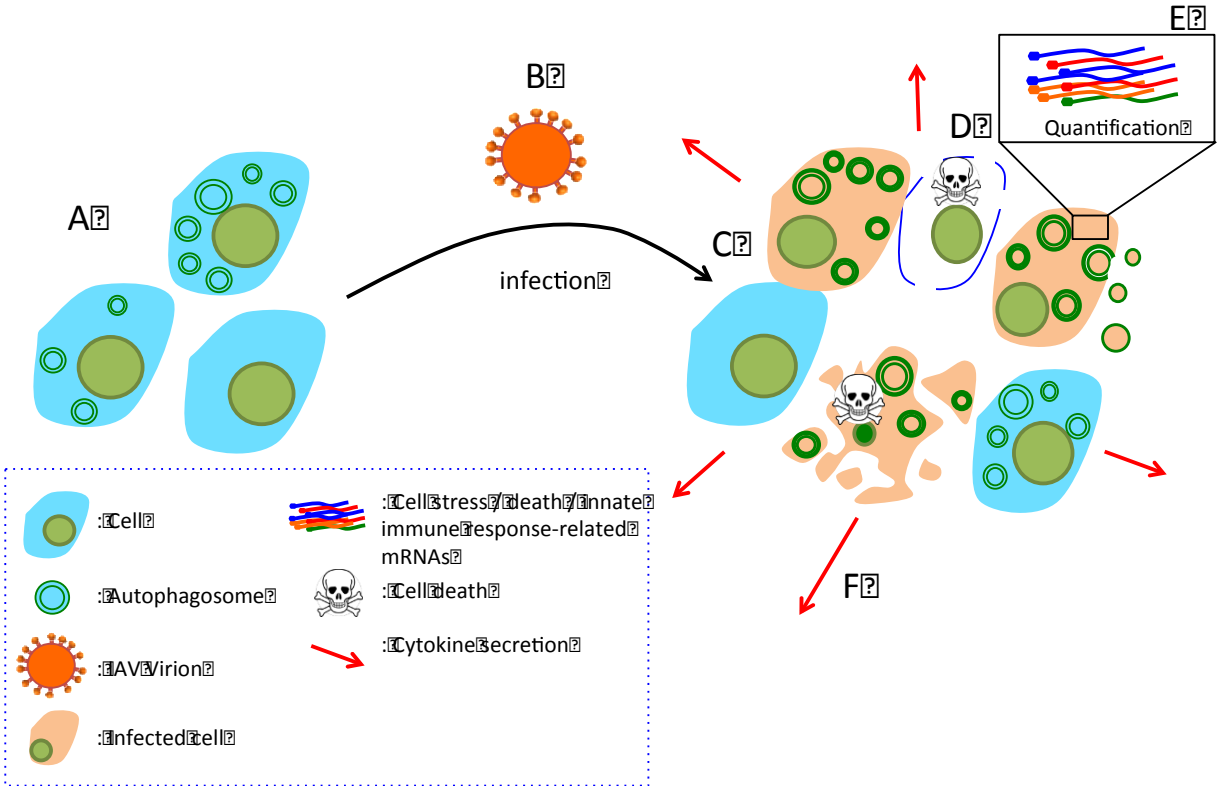

Figure 7: Aims of the study.
Given the drawbacks that current methods to study autophagy possess, I aimed to generate cellular models in which autophagy can be specifically restored (**A**). Using these models, after infection (**B**) I sought to investigate whether autophagy or autophagy perturbation by IAV results in altered viral fitness through monitoring of infected cell percentage and intracellular viral replication (**C**). I also wanted to investigate whether autophagy and its perturbation might result in alteration in the host cells response to IAV with a focus on cell death (**D**), transcription of immune, stress and death-related gene expression (**E**) and inflammatory cytokine secretion (**F**).

I confirmed that the new cellular model to study autophagy showed low autophagy-independent effect on key cellular death, stress, inflammatory, and metabolic pathways.

Using induced autophagy capacity, I observed that autophagy was dispensable for IAV infection and replication. However, I highlighted an inhibitory role for autophagy on type I IFN-induced inflammatory response at early times post-infection by IAV.

Notably, the impact of autophagy on ISG expression was not mediated by NS1 and was explained by differential production of IFN-β during the initial phase of IAV infection. These findings will help clarify the interplay of IAV infection, autophagy, and host response. Moreover, the experimental model presented herein will help establish a new path towards validating the role of autophagy during inflammatory processes.

Using a cellular model allowing accumulation of M2H37G, a mutant form of M2 devoid of proton channel activity but still capable of inducing autophagosome maturation inhibition, I showed that this protein was able to induce abortive autophagy only in the context of IAV infection. M2 and M2H37G are cleaved by caspases in the context of infection, which correlates with p62 degradation limitation, a marker of autophagic activity. This data indicates that caspase activation may be a prerequisite for autophagy maturation inhibition by M2.

Interestingly, experiment showed that among IAV-infected cells, when infecting cells at low MOI, single cell RNA quantification revealed that most IAV infected cells do not express all IAV RNAs. Cells failing to express M2 RNA and protein show limited induction of the interferon-stimulated gene *Cxcl10* as compared to bystander cells and infected cells that do express M2 protein.

RESULTS

I. Deciphering the impacts of autophagy on host cell response to IAV infection

As described in the introduction, commonly used techniques to study autophagy cause significant changes in other metabolic pathways and may also interfere with innate immune sensing and signaling, thereby limiting our capacity to understand how autophagy itself impacts infected cell response to IAV. For all these reasons, I generated a variety of cell lines with fine-tunable autophagy through treatment with a biochemically inert chemical (details will be discussed in this section). One advantage of this approach is that the cells wherein autophagy can be tuned have the same genetic background and cell culture history.

1. Generation of cellular models allowing control of autophagy capacity

1.2. Generation of *Atg5*$^{-/-}$ cells expressing ATG5^{DD}, *Atg5*$^{-/-}$ cells expressing ATG5K130R^{DD} and *Atg7*$^{-/-}$ cells expressing ATG7^{DD}

1.2.1. Inducible protein stabilization system presentation

To generate cells in which autophagy capacity can be controlled, we took advantage of a technology allowing stabilization of proteins. This system relies on the fusion of proteins to a destabilization domain (DD). The DD is a 12 kDa mutant form (V2A/F36V mutant) of the human FK506/Rapamycin binding protein 12 (FKBP12) that is targeted to degradation by the proteasome, thereby leading to the degradation of the whole fusion protein[148]. When the cell-permeable small molecule Shield1 is added, the DD is stabilized and the protein of interest accumulates in the cells (**Figure 8**). Importantly, Shield1 is relatively free of off-target effect to the cellular environment, as shown by microarray analysis[148]. Moreover, the effect of Shield1 presence on protein accumulation is reversible after its removal, which allows a reversible induction of protein presence.

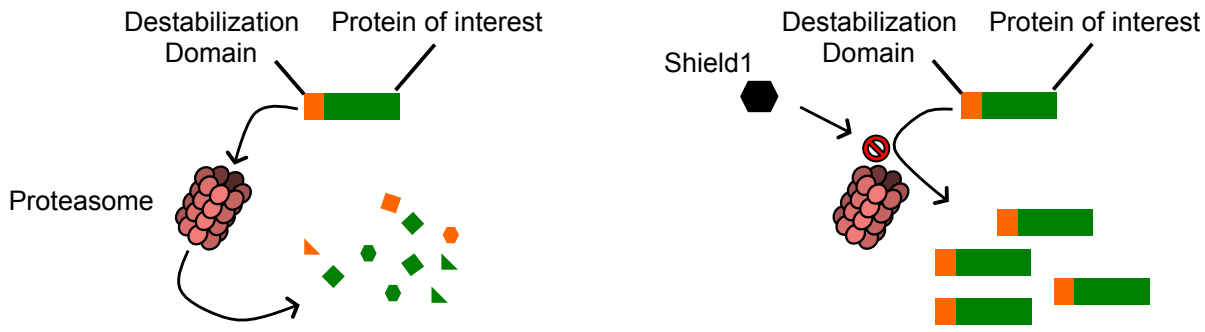

Figure 8: Inducible protein stabilization system.
(**A**) Protein fused to the destabilization domain are degraded by the proteasome. (**B**) When the small, cell permeable chemical Shield1 is added, proteasomal degradation is inhibited and the fusion protein accumulates.

1.2.2. Generation of cell lines

Taking advantage of our autophagy incompetent *Atg5*$^{-/-}$ and *Atg7*$^{-/-}$ MEFs I chose to use inducible protein stabilization system to express ATG5^{DD} and ATG7^{DD} in these cell lines, respectively.

To do so, I introduced the destabilization domain at the N-terminus of ATG5 through cloning, N-terminus fusion of DD having being shown to be more destabilizing[148]. Mutagenesis qPCR allowed introduction of 3 glycin amino acid as a flexible linker that may help limit loss of function of ATG5 due to steric hindrance by the DD[149]. The final vector for expression was a lentiviral vector, which allowed production of lentiviruses from HEK 293T cells. Lentiviral infection of *Atg5*$^{-/-}$ was followed by puromycin selection and single cell cloning. ATG5^{DD} stabilization through Shield1 addition should allow the recovery of autophagy capacity in this ATG5 deficient cell line (the strategy and expected phenotypes are exposed in **Figure 9**).

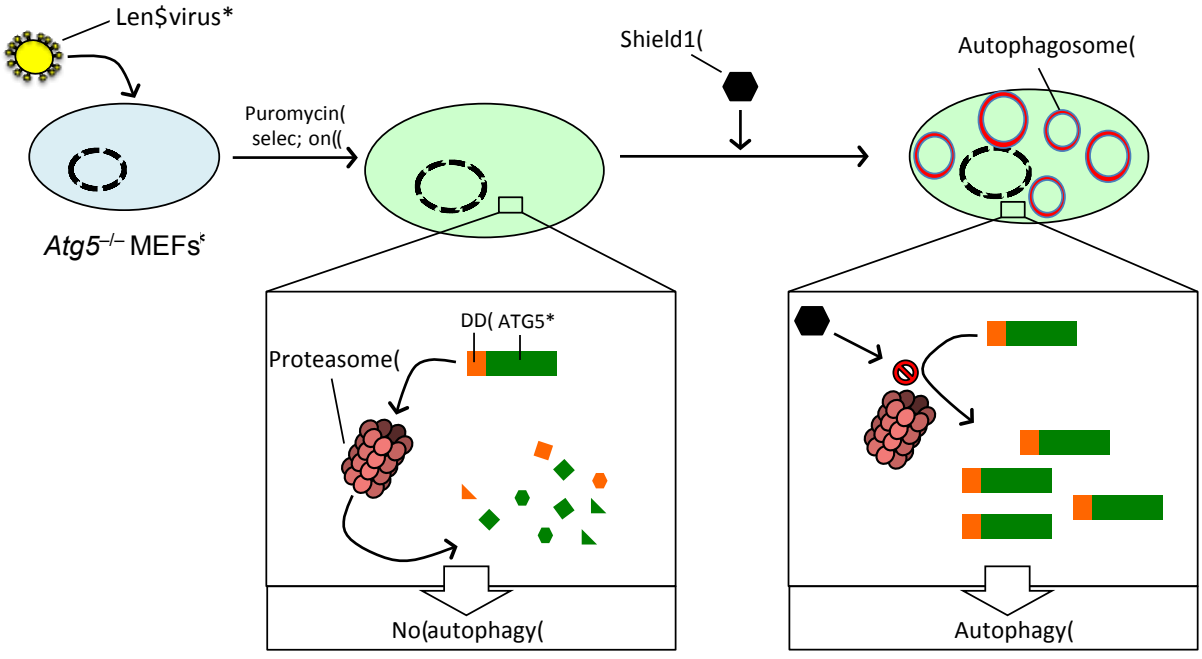

Figure 9: Strategy for *Atg5*$^{-/-}$ cells expressing ATG5^{DD} generation and expected associated phenotypes.
Lentivirus infection of Atg5$^{-/-}$ MEFS, followed by puromycin selection, should allow expression of ATG5^{DD}, although rapid degradation should occur, preventing rescue of

autophagy capacity. Addition of Shield1 in cell growth medium should prevent proteasomal ATG5^{DD} degradation, thereby rescuing autophagy.

The same strategy was followed to obtain cell lines in which ATG7^{DD} can be stabilized in *Atg7*$^{-/-}$ MEFs.

The lysine (K) 130 of ATG5 is the acceptor residue for conjugation to ATG12[150], an event required for autophagosome formation, as exposed in the introduction. Replacement of K130 to an arginine (R) in ATG5 renders it unable to exert its role in autophagosome membrane elongation[106,151,152]. I used the same strategy as for *Atg5*$^{-/-}$ cells expressing ATG5^{DD} generation to produce *Atg5*$^{-/-}$ cells expressing ATG5K130R^{DD}. This would allow me to account for possible off-autophagy effect of ATG5, which have already been described[153].

Single cell clones for each cell line were selected and Shield1 was titrated to allow best stabilization of proteins (1 µM was selected). ATG5^{DD}, ATG7^{DD} and ATG5K130R^{DD} were stabilized as expected when Shield1 was introduced. Indeed, monitoring of ATG5^{DD}, ATG5K130R^{DD} and ATG7^{DD} by immunoblot confirmed that Shield1 mediated the stabilization of the destabilized proteins (**Figure 10**). Importantly, the stabilization of ATG5^{DD} and ATG7^{DD} led to LC3-II accumulation, which showed that DD fusion did not prevent pro-autophagic activity of the destabilized proteins. ATG5K130R^{DD} was, as expected, unable to allow LC3-II accumulation and no band of the size corresponding to a form complexed to ATG12 was observed, as opposed to stabilization of ATG5^{DD} (**Figure 10 A & B**). ATG7 being involved in the conjugation of ATG5 to ATG12 (see introduction), it was of no surprise that ATG7^{DD} stabilization correlated with an increased in ATG5^{DD}–ATG12/ATG5^{DD} ratio (**Figure 10 C**).

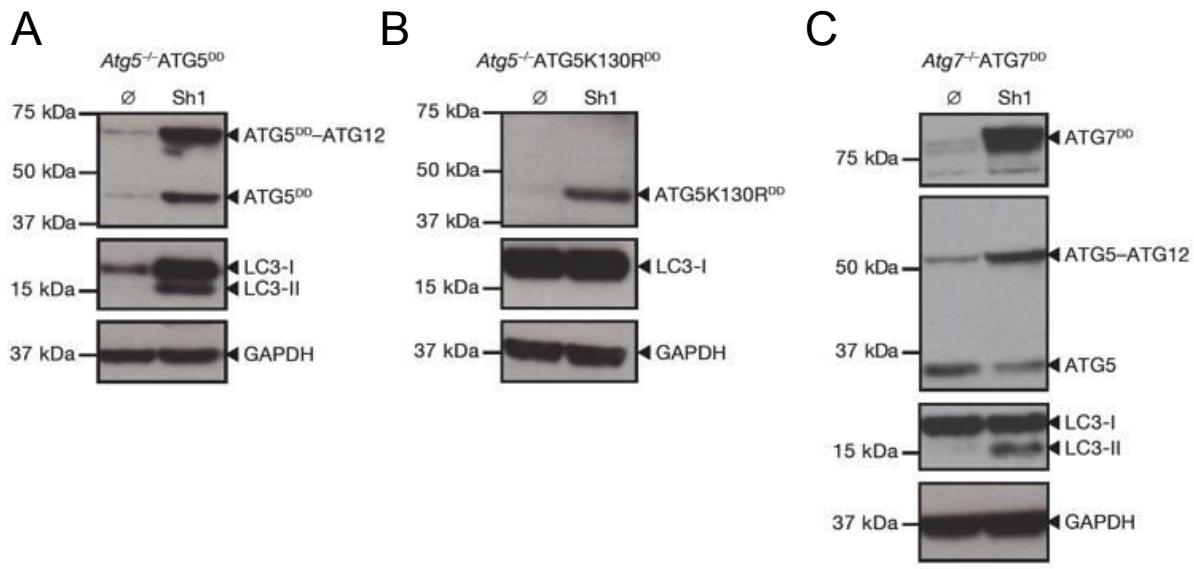

Figure 10: Phenotyping of generated cell lines.
Atg5$^{-/-}$ cells expressing ATG5^{DD} (**A**), *Atg5*$^{-/-}$ cells expressing ATG5K130R^{DD} (**B**), or *Atg7*$^{-/-}$ cells expressing ATG7^{DD} (**C**), were treated or not with Shield1 (Sh1) for 20 h before immunoblotting was performed using anti-ATG5, anti-ATG7, anti-LC3, and anti-GAPDH antibodies.

Shield1 introduction therefore allowed the restoration of basal autophagy in *Atg5*$^{-/-}$ cells expressing ATG5^{DD} and in *Atg7*$^{-/-}$ cells expressing ATG7^{DD} but not in *Atg5*$^{-/-}$ cells expressing ATG5K130R^{DD} (hereafter referred to as simply ATG5^{DD}, ATG7^{DD} and ATG5K130R^{DD} cells, respectively). I then wondered whether the generated cell lines would be able to have their autophagic activity stimulated by different autophagy inducers.

1.2.3. ATG5^{DD} stabilized cells can have their autophagy stimulated by common inducers

Autophagic activity can be measured by the increase in LC3-II/LC3-I ratio and by p62 degradation (p62 being degraded at the maturation step, see introduction)[137]. We showed that ATG5^{DD} stabilization allowed basal autophagy to be reactivated. However, I wanted to make sure that the cells were able to show higher autophagic activity when treated by commonly-used autophagy stimulator such as serum starvation, PP242, an mTOR inhibitor[137]. Introduction of these autophagy stimulators led to a Shield1-dependent increase in LC3-II/LC3-I ratio (**Figure 11**). Chloroquine (CQ), a treatment that prevents autophagosome maturation, thereby inducing non-matured autophagosome accumulation, also led to increased LC3-II/LC3-I levels as expected. However, under CQ conditions, p62 was not degraded because CQ prevents autophagosome maturation. Treatment of cells with MG132, a known

proteasome inhibitor[154], increased autophagy flux as expected, presumably through ATG5^{DD} degradation prevention.

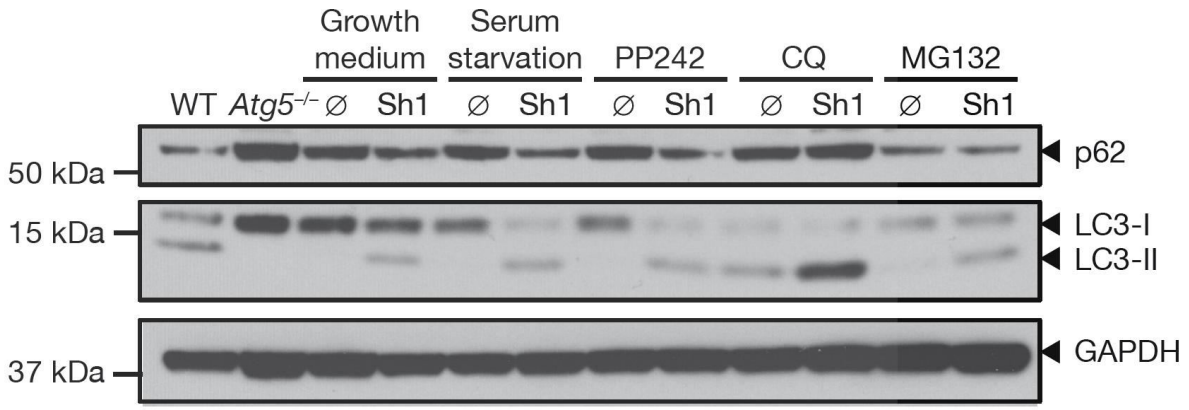

Figure 11: Basal autophagy is restored and autophagy can be stimulated in Shield1-treated ATG5^{DD} cells.
In the presence or absence of Shield1 (Sh1), cells were exposed to serum deprivation, an mTOR inhibitor (PP242), a proton pump inhibitor (chloroquine, CQ), or a proteasome inhibitor (MG132). Wildtype (WT) and *Atg5*$^{-/-}$ MEFs (*Atg5*$^{-/-}$) were used as positive and negative controls, respectively. After 4 h of culture, protein extracts were subjected to immunoblot analysis using anti-p62, anti-LC3, and anti-GAPDH.

In summary, ATG5^{DD} cells showed basal autophagy and could have their autophagic activity potentiated when treated with Shield1. I then wondered whether autophagy restoration would impact cell growth and cell transcriptional profile.

1.2.4. Autophagy restoration does not impact cell growth

Autophagy being a process involved in homeostatic maintenance and helping cells to thrive in certain conditions, I wondered whether ATG5^{DD} cell growth would be impacted by autophagy capacity restoration. Intra-incubator microscopy was used to measure cell confluence over time, with or without the addition of Shield1 to the culture media, revealing that ATG5^{DD} accumulation, in nutrient-rich conditions, did not impact the kinetics of short-term cell growth (**Figure 12**).

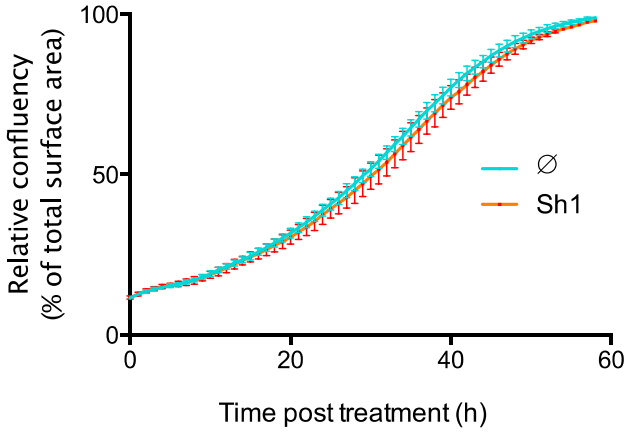

Figure 12: Autophagy capacity does not impact cell growth.
ATG5^{DD}cells were treated or not with Shied1 (Sh1) and images were obtained every hour for 60 h to assess cell growth. Points depict mean relative confluency at interval time and error bars depict standard deviation.

1.2.5. Autophagy restoration induces transcriptional changes

I then wondered whether autophagy rescue would impact the transcriptional profile of cells. I selected two clonal populations of ATG5^{DD} cells and one clonal population of ATG5K130R^{DD} cells. To test whether immune, stress or death pathways were impacted by autophagy, I used the NanoString nCounter technology, a method that allows the quantitative measurement of single mRNA molecule counts, without the need for reverse transcription or amplification procedures, across a 561-gene set that is enriched in immunology, stress and death-related gene networks (complete list for mouse Immunology kit available on nanostring.com).

Cells were treated for 24 or 48 h with Shield1 or ethanol before harvest, RNA extraction and nCounter analysis. After normalizing the data by housekeeping genes, I performed principal component analysis (PCA), an unsupervised method for visualization of multidimensional data[155]. Namely, representing a sample with values for the expression of 561 genes requires a 561-dimensional space (each axis representing one gene), which is impossible to visualize for human interpretation. PCA relies on the fact that there is a lot of redundancy in this information, i.e. these genes do not vary independently. It finds linear combinations of genes called "supervariables" or principal components (PCs) which are uncorrelated to each other (for the dataset of interest), and which explain decreasing variance. The contributions of a gene to a component gives how much and in which way the component

depends on a gene. Here, PCA for 48 h treatment revealed that most of the variability (91%) observed between samples was explained by gene expression differences between clones, with PC 1 isolating $ATG5^{DD}$ clones from the $ATG5K130R^{DD}$ clone, and PC 2 further separating all three clones (**Figure 13 A**). Three percent of the remaining sample variability was accounted for by PC 3, which separated Shield1- and ethanol-treated cells expressing $ATG5^{DD}$ but not $ATG5K130R^{DD}$ cells (**Figure 13 B**), revealing genes that were impacted by ATG5 capacity to bind to ATG12, i.e. by autophagy capacity and not by off-targets effects of ATG5. Importantly, the fact that 91% of the variance was explained by clone differences highlights the danger of comparing two different cell lines to study autophagy, which may explain contradicting results in the literature.

Since none of the first three PCs separated Shield1- from ethanol-treated $ATG5K130R^{DD}$ samples, I next tested if single genes were impacted by ATG5 capacity in an ATG12-independent fashion. Namely, unpaired t-tests were performed to compare Shield1- vs ethanol-treated samples of each clone, and p-values were subsequently corrected by false-discovery rate (q-value) to account for multiple testing. In line with the PCA results, a few genes were significantly impacted by Shield1 treatment in both $ATG5^{DD}$ clones, among which were Toll-interacting protein (TOLLIP) and *Bid* which were also main contributors to PC 3 in the PCA (**Figure 14** and **Figure 13 C**). However, no genes reached statistical significance when comparing Shield1- and ethanol-treated $ATG5K130R^{DD}$ samples (smallest q-value > 0.6, **Figure 14**), suggesting that (a) genes that were impacted by ATG5 presence were impacted by autophagy capacity and not by off-target effects of ATG5, and that (b) neither Shield1 treatment nor DD accumulation led to significant changes in the (immune-related) transcriptome of the cell, confirming the reliability of my model.

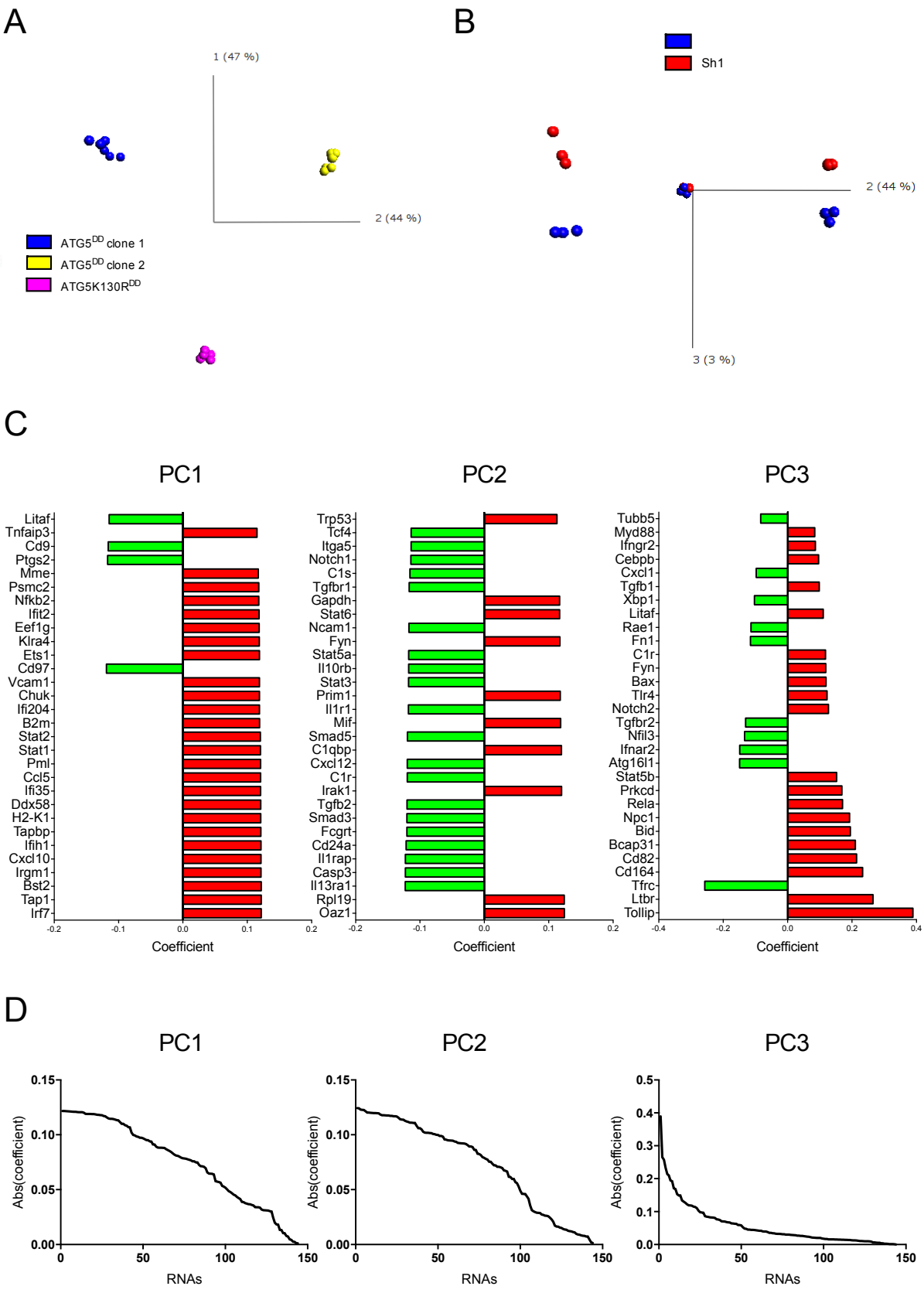

Figure 13: Clonal variability is much greater than the variance explained by autophagy capacity.

Two ATG5^{DD} and one ATG5K130R^{DD} clones were treated with ethanol or Shield1 in triplicates for 24 or 48 h, after which RNA was extracted and analyzed by the Nanostring

nCounter technology, to assess the RNA levels of 561 immune-related genes. Principal component analysis was performed for the 48 h timepoint; shown are samples lying in the principal component 1 (PC 1)–PC 2 (**A**) or PC 2–PC 3 (**B**) plane. (**C**) Genes with highest absolute contributions to each of the PCs. (**D**) Absolute contribution of all genes for each PC.

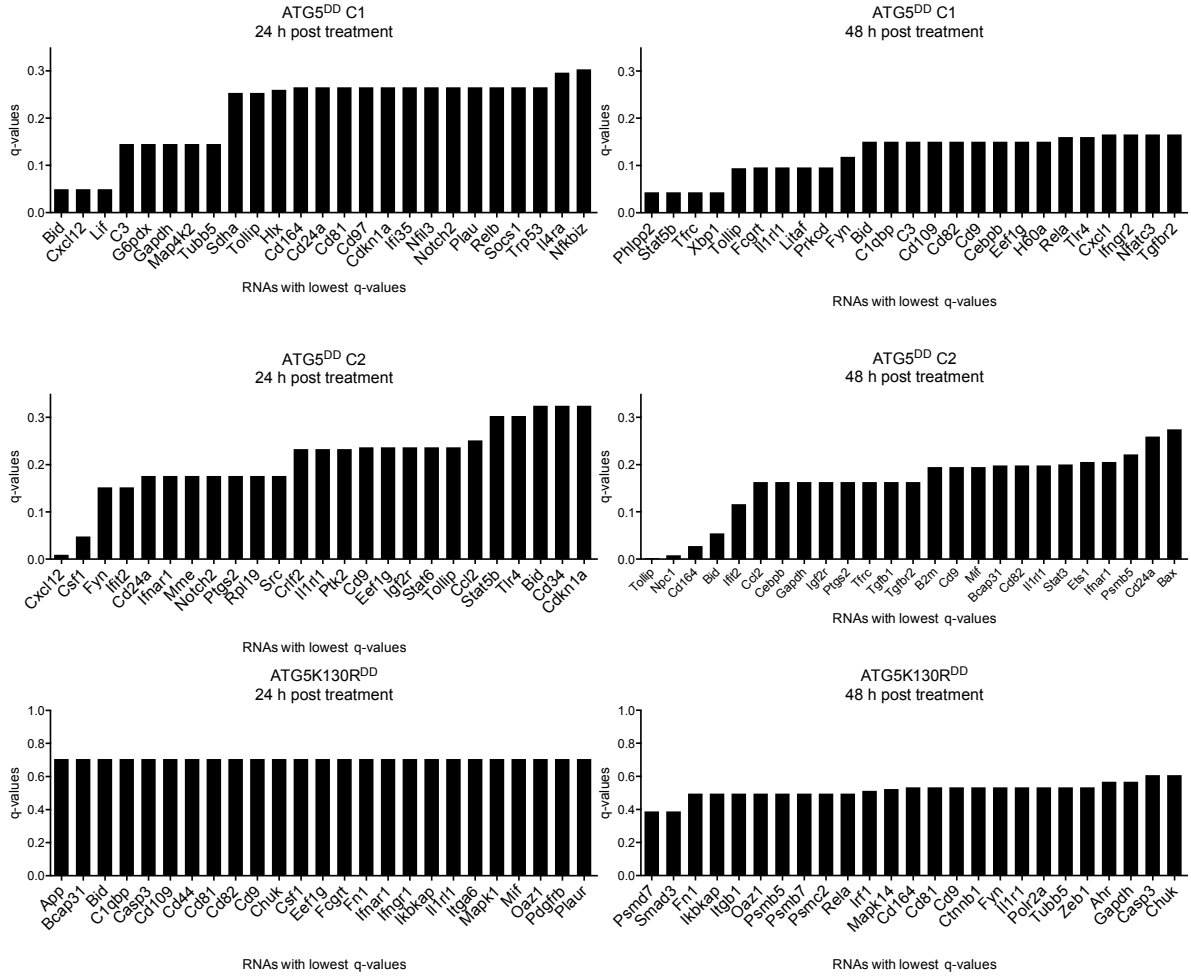

Figure 14: The immune transcriptome is impacted by steady-state autophagy capacity, with no significant off-target effect of ATG5, or impact of Shield1 or DD accumulation. T-tests were performed to compare Shield1- vs ethanol-treated samples, and p-values were corrected by false-discovery rate (q-values) to account for multiple testing. Shown are the 25 genes with lowest q-values for the indicated clone and timepoint.

2. ATG5^{DD} stabilization allows IAV-induced autophagy perturbation without impacting its replication

2.1. IAV infection leads to abortive autophagy in ATG5^{DD} stabilized cells

As described in the introduction, IAV has been showed to perturb autophagy during infection. Even if different laboratories do not agree on the fact that IAV blocks autophagy maturation, there seems to be a consensus on the fact that IAV perturbs autophagy and leads to autophagosomal vesicles (autophagosomes and/or autolysosomes) accumulation (see introduction).

To test whether I could confirm this phenotype in my cellular model, I took advantage of a protocol, developed by a student in our laboratory, which allows single cell monitoring of autophagosomal vesicles accumulation in a high throughput, high content fashion using imaging flow cytometry[156]. I infected ATG5^{DD} cells that were pre-treated or not with Shield1 with IAV at MOI 5 for 20 h.

Using imaging flow cytometry, I delineated infected and uninfected cells (**Figure 15 A**) and measured the percentage of autophagic cells within each population (**Figure 15 B**). IAV-induced LC3 puncta accumulated in a cell-intrinsic manner, i.e., in IAV-infected cells (purple) but not in uninfected cells (green) (**Figure 15 C and D**). Importantly, this confirmed with my model that IAV leads to autophagosome accumulation, and showed that Shield1-treated ATG5^{DD} cells behave as MEFs and other cell types when infected by IAV[88].

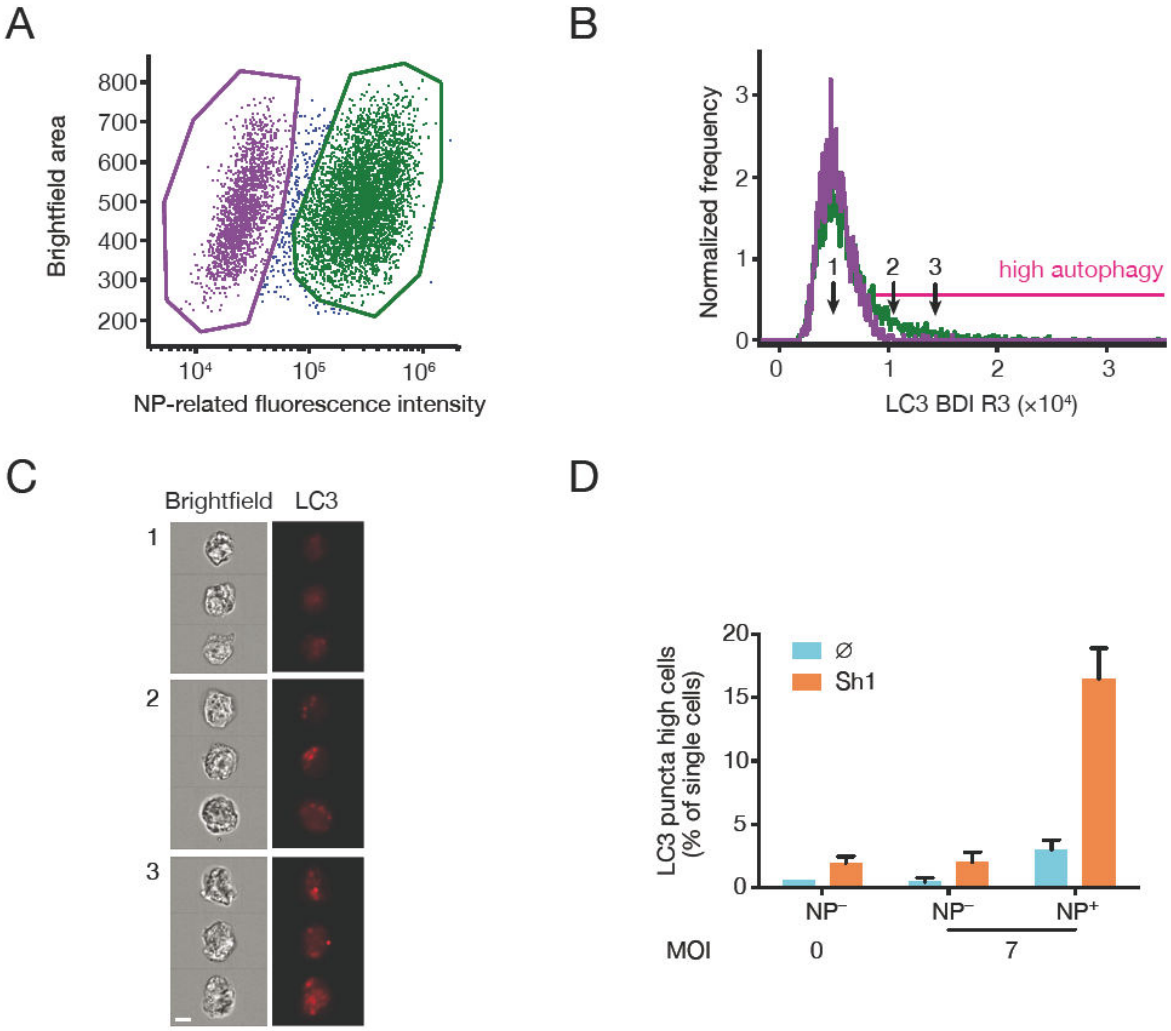

Figure 15: IAV induces autophagy in Shield1-treated ATG5^{DD} cells in a cell-intrinsic manner.
ATG5^{DD} expression was stabilized by Shield1 (Sh1) treatment and cells were infected with IAV. After 20 h, cells were fixed, permeabilized, and stained using anti-NP antibody to quantify IAV infection and anti-LC3 antibody to visualize autophagy puncta. Imaging flow cytometry permitted gating based on NP expression (representative dot plot, **A**) and quantification of autophagic vesicles using the bright detail intensity R3 (BDI R3, histogram, **B**). (**C**) Images of single cells, corresponding to the indicated numbers in (**B**) are shown. Scale bar, 10 µm. (**D**) Graphs plot showing mean percent of cells with high autophagic vesicle content and standard deviation; analysis is based on images captured from >10,000 cells per experiment (n = 2 experiments).

Next, I wondered whether, in my new cellular model, autophagy was complete, or if IAV induced a block in autophagosome maturation. Immunoblot analysis revealed that, although LC3-I/LC3-II ratio was increased in IAV-infected Sh1-treated cells, p62 degradation did not occur (**Figure 16**). Of note, basal autophagy in non-infected cells led to decreased levels of

p62, arguing for complete autophagy process, as expected. If IAV was inducing productive autophagy, p62 would be expected to be even further decreased.

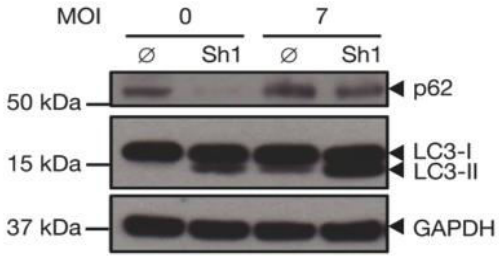

Figure 16: IAV induces abortive autophagy in Shield1-treated ATG5^{DD} cells.
After 20 h infection with IAV at the indicated MOI, with or without Shield1 (Sh1) pre-treatment, p62; LC3 and GAPDH were monitored by immunoblot.

Altogether, these data suggest that, in this cellular model, autophagy is stimulated by IAV in a cell-intrinsic and aborted manner.

I then wondered whether autophagy capacity of host cells would impact IAV replication.

2.2. Cell autophagy capacity does not impact IAV RNA levels in infected cells

Given that autophagy and its perturbation by viruses has been shown to impact viral replication (see introduction), I then wondered if induced autophagy capacity would impact IAV RNA presence in cells.

I designed qPCR primer/probe sets for detection of the IAV RNA coding for NP, NS1, PB1, M1 and M2. Of note, M2-coding RNA is a spliced variant of M1 one. The forward primer allowing M2 detection was designed to span the region where donor and acceptor site come together, hence preventing the detection of non-spliced M1-coding RNA (**Figure 17 A**). Conversely, the forward primer and half of the qPCR probe to detect M1 RNA were designed to target the region spliced out in M2 RNA, hence preventing detection of the later (**Figure 17 A**).

Results showed that, 5 h post infection, autophagy capacity did not impact the replication of viral RNA in infected cells (**Figure 17 B**).

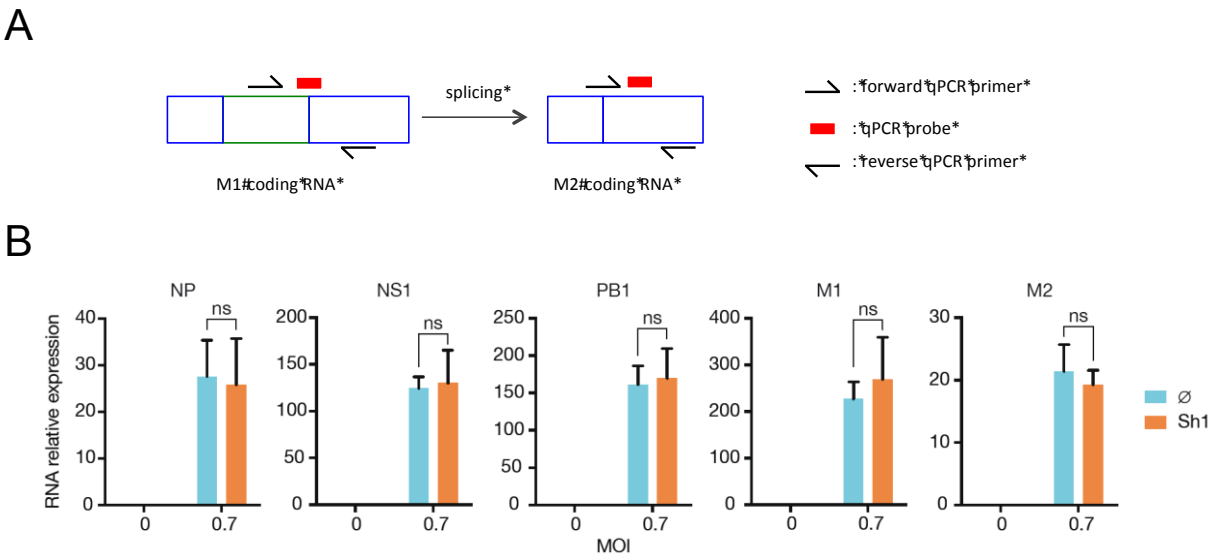

Figure 17: IAV RNA expression is not impacted by autophagy capacity.
(A) Schematic representation of the sites of binding of Taqman forward primer, reverse primer and probe to detect M1 or M2-coding RNA; the green section represents the part that is spliced out in M2-coding RNA. **(B)** Following 5 h infection, with or without Shield1 (Sh1) pre-treatment, IAV RNA expression levels were determined using RT and qPCR primer/probe sets specific for the *Np, Ns1, Pb1, M1* and *M2* genes.

2.3. Cell autophagy capacity neither impacts infectiousness of IAV nor IAV protein synthesis.

To test whether autophagy capacity impacts cell infectability, I infected cells, which were pre-treated or not with Shield1, and monitored the percentage of NP-expressing cells by flow cytometry. Data showed that the percentage of IAV-infected cells were similar between autophagy-competent and incompetent cells (**Figure 18 A**).

As a catabolic process, autophagy might degrade IAV proteins. I therefore monitored by flow cytometry the viral NP and M2 protein content in infected cells. This showed that autophagy-competent and -incompetent cells expressed comparable levels of NP and M2 proteins (**Figure 18 B & C**). Immunoblotting for M2 at a later timepoint (20 h post infection) confirmed that autophagy does not impact its level in my model (**Figure 18 D**).

In sum, induced autophagy is dispensable for IAV infection and intracellular replication. I then wondered whether autophagy or its perturbation by IAV impacts the cellular response to infection.

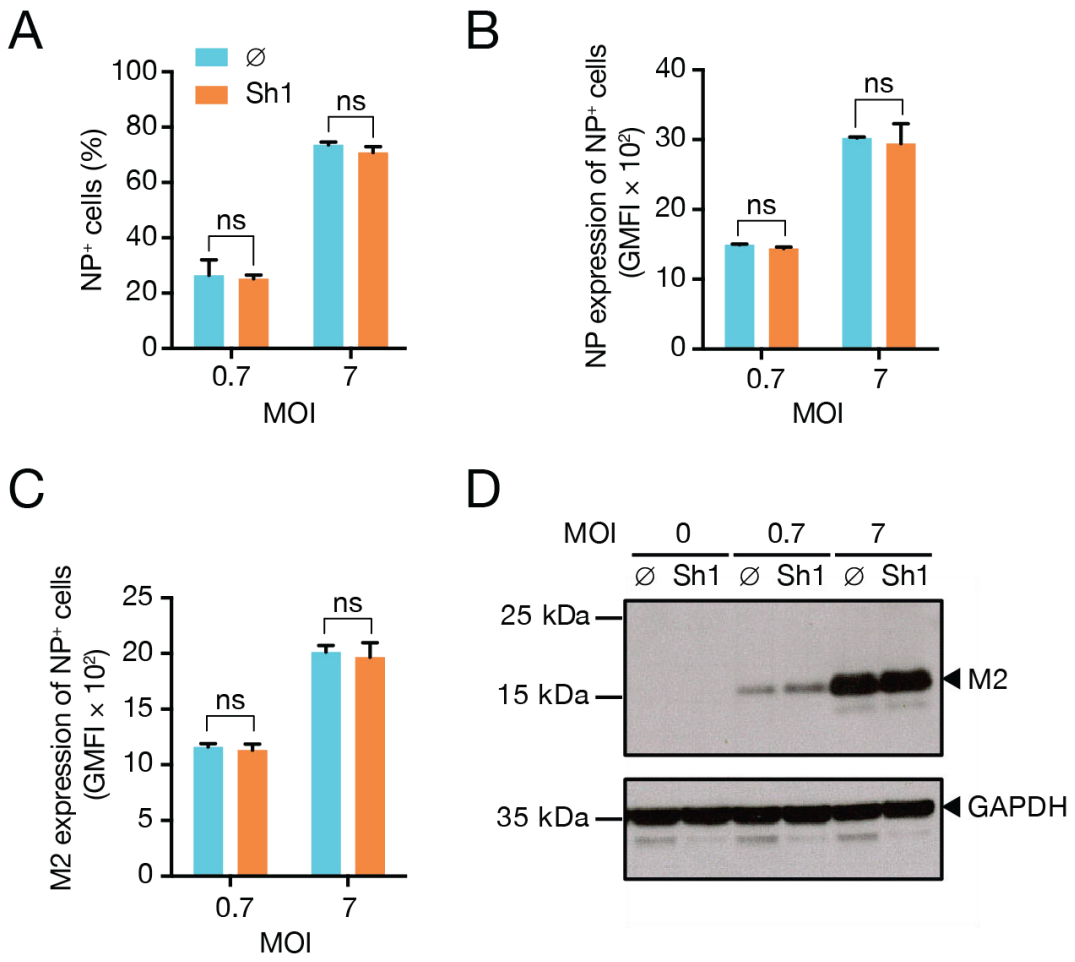

Figure 18: IAV NP and M2 protein expression are not impacted by ATG5^{DD} stabilization.
ATG5^{DD} cells, with or without Sh1 treatment, were infected with IAV for 16 h at the indicated MOI. The percentage of NP-expressing cells (**A**), the geometric mean fluorescent intensity (GMFI) of NP (**B**) and of M2 (**C**) per infected (i.e. NP-expressing) cell were determined by flow cytometry. (**D**) IAV M2 expression was determined using immunoblotting following 20 h infection at the indicated MOI. Graphs show mean and standard deviation of triplicates wells, and data are representative of three experiments. ns, not significant (two-tailed paired t-test followed by Holm's multiple testing correction).

3. Apoptosis is induced by IAV but is not impacted by autophagy

3.1. Apoptosis is induced by IAV in a cell-intrinsic manner

As described in the introduction, IAV is known to induce apoptosis. I wanted to test whether apoptosis was induced in a cell-intrinsic or cell -extrinsic manner. After infection, imaging flow cytometry allows the monitoring of caspase 3 cleavage (effector step of apoptosis), membrane permeability (necrosis or necroptosis), NP expression and LC3 vesicles at the

single cell level (**Figure 19 A**). I monitored apoptosis and cell death at 20 h post infection and showed that apoptotic cell death was induced by IAV in NP^+ cells, as I previously showed for autophagy (**Figure 14 19**). Of note, some cells showed hallmarks of both autophagy and apoptosis, as previously reported by our laboratory[156] (**Figure 19 C**).

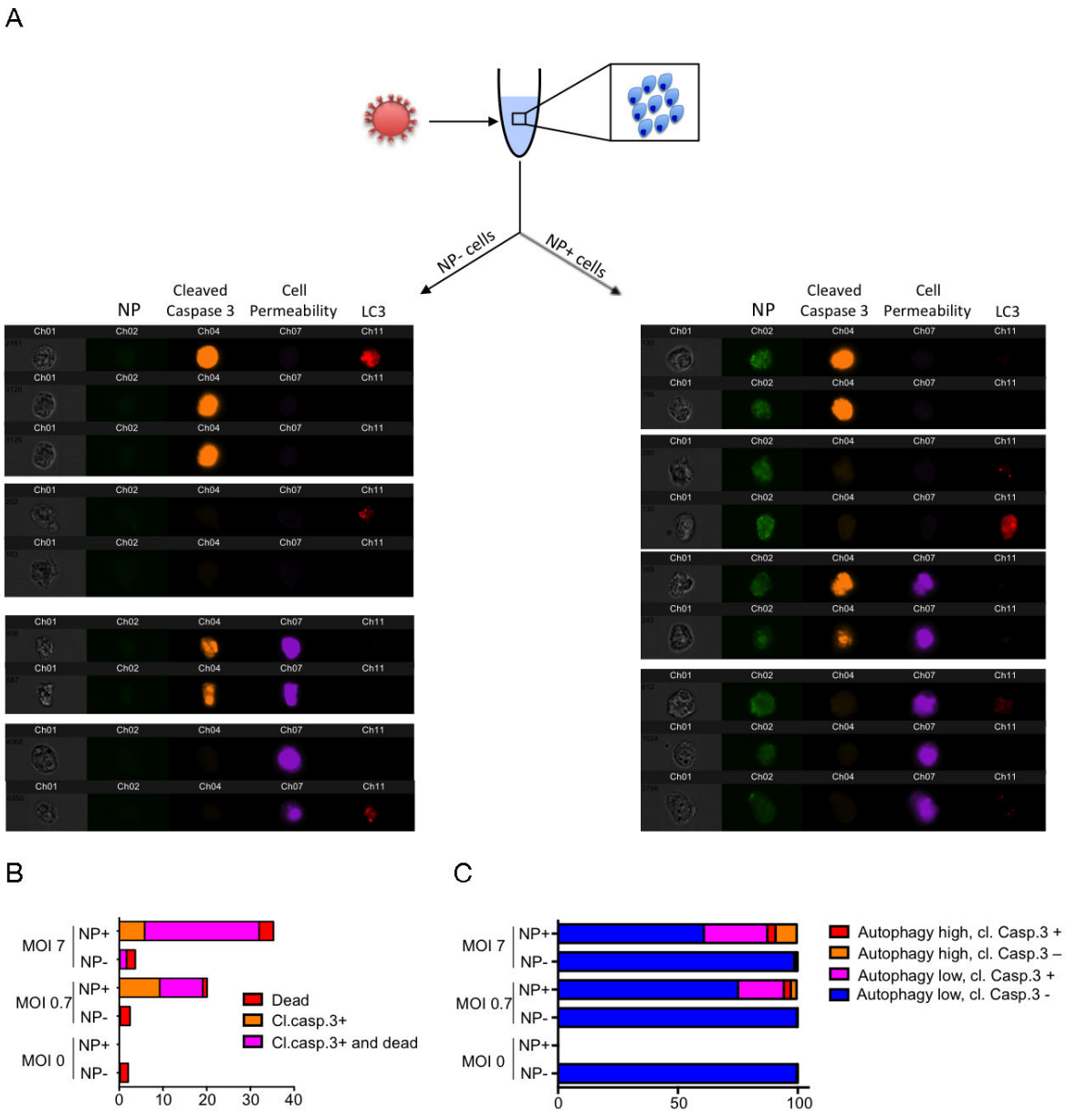

Figure 19: IAV induces autophagy and apoptosis in a cell-intrinsic manner, few cells harbor hallmarks of both apoptosis and autophagy.
Cells were infected at the indicated MOI for 20 h before harvest and staining for loss of membrane integrity (violet), NP (green), LC3 (red) and cleaved caspase 8 (orange). (A)

representative examples of single cell staining illustrating the variability in phenotype even within a single infected tube. (B) Percentage of cells being dead (violet staining), at early apoptotic stages (Cleaved caspase 3 (Cl. Casp. 3) positive, violet negative) or at secondary necrosis stage of apoptosis (Cl. Casp. 3 positive, violet positive) in NP^+ or NP^- cells. (C) Percentage of cells with high or low autophagy (high or low BDI R3) in the process of apoptosis (Cl. Casp. 3 positive) or not in NP^+ or NP^- cells.

3.2. Autophagy capacity does not impact apoptosis occurrence

Since autophagy has been shown to interfere with apoptosis, being pro- or anti-apoptotic in different models[157], I sought to monitor apoptosis after infection in autophagy-competent or -deficient cells. Using live imaging, I showed that $ATG5^{DD}$ stabilization did not impact cell confluency or apoptosis (**Figure 20**).

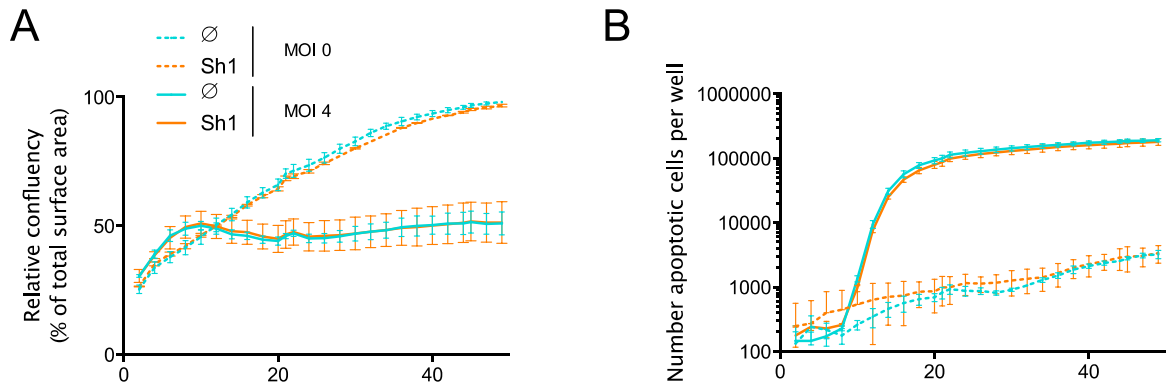

Figure 20: Autophagy capacity does not impact apoptosis levels after infection.
$ATG5^{DD}$-expressing *Atg5*$^{-/-}$ cells, pre-treated or not with Shied1 (Sh1), were infected with IAV at MOI 4 and images were obtained every hour for 50 h to assess cell growth (**A**) and apoptotic cell number (**B**). Points depict mean relative confluency at interval time and error bars depict standard deviation.

Although autophagy does not impact IAV infectiousness, RNA and protein synthesis or IAV-induced cell death, I then wondered whether host cell death, stress and inflammatory responses are impacted by autophagy.

4. Host cell inflammatory response is negatively impacted by autophagy

4.1. Induced autophagy competence limits interferon-stimulated gene (ISG) expression in the context of IAV infection

ATG5^{DD} cells, pre-treated or not with Shield1 for 16 h, were infected with IAV for 4 or 12 h. Raw RNA counts, obtained using the Nanosting nCounter technology, were normalized to the geometric mean value of 5 internal control genes (*Ppia*, *Gapdh*, *Rpl19*, *Oaz1* and *Polr2a*), selected based on the application of the geNorm method[158] (**Figure 21** and Materials and Methods).

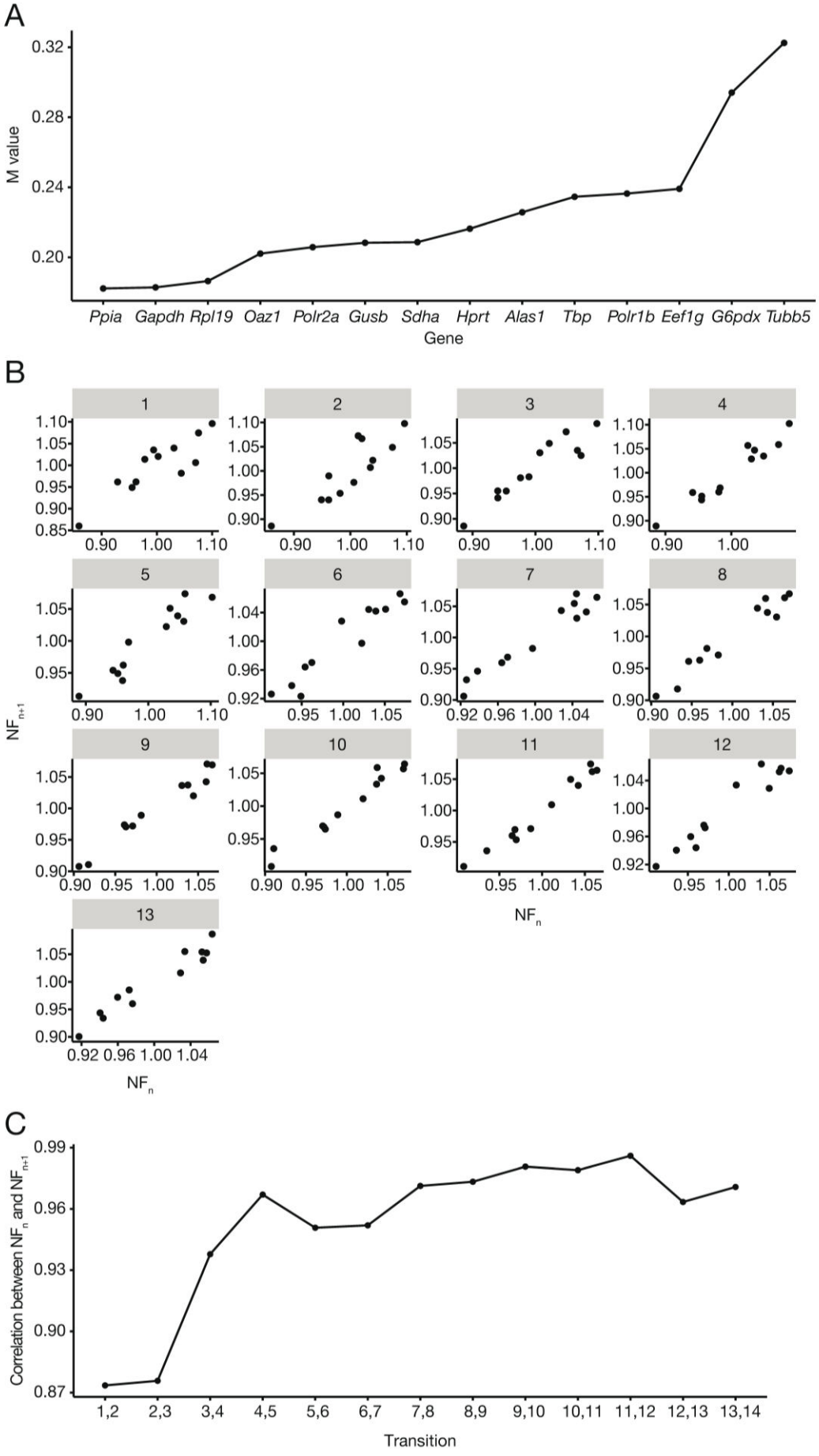
A
M value
0.32
0.28
0.24
0.20
Ppia Gapdh Rpl19 Oaz1 Polr2a Gusb Sdha Hprt Alas1 Tbp Polr1b Eef1g G6pdx Tubb5
Gene
B
1
2
3
4
5
6
7
8
9
10
11
12
13
NF n+1
NF n
C
Correlation between NF n and NF n+1
0.99
0.96
0.93
0.90
0.87
1,2 2,3 3,4 4,5 5,6 6,7 7,8 8,9 9,10 10,11 11,12 12,13 13,14
Transition

Figure 21: Strategy for selection of internal control genes following the geNorm method. (**A**) The 14 candidate control genes provided by Nanostring were ordered by increasing M value, i.e., by decreasing correlation with the other candidate control genes (see Materials and Methods). (**B to C**) Normalization factors arising from addition of one control gene were compared for each addition (**B**), and consecutive Pearson's correlation coefficients were computed and are shown in the graph (**C**).

From the results of three independent experiments, I found that the inability to induce autophagy in the context of infection led to higher expression, compared to autophagy-competent cells, of several pro-inflammatory genes, among which were known ISGs, such as *Psmb10*, *Cd274*, *Cxcl10*, and *Irf1 and Tap1* (**Figure 22 A** and **Table 1**). Of note, two members of the class I major histocompatibility complex (MHC I) pathway, *Tapbp*, *B2m*, *H2k1*, *Psmb10 and Tap1*, were decreased in autophagy-competent cells compared to autophagy-deficient cells (**Figure 22 A** and **Table 1**). To identify biological processes and signaling pathways, rather than single genes, impacted by autophagy capacity in a robust fashion, I performed a gene set enrichment analysis (GSEA).[159] Among the 129 gene sets tested (corresponding to sets from the database that included at least 5 genes measured in this experiment, and with expression levels consistently above the lower limit of quantification), this method identified four pathways that were significantly enriched in genes differentially expressed by autophagy-competent (Shield1-treated) vs autophagy-deficient (control vehicle-treated) infected cells (**Figure 22 B**): (1) IFN signaling, (2) IFN-α/β signaling, (3) cytokine signaling, and (4) IFN-γ signaling. Due to shared gene expression among IFN-γ and IFN-β signaling pathways, and given that GSEA relies on unweighted gene set lists, this method is not suited to distinguish between a type I and a type II IFN response. To address this caveat, we implemented a more quantitative approach, using recently published data comparing the gene signature of IFN-β- and IFN-γ-stimulated whole blood, analyzed by the same nCounter technology[160]. The genes most significantly impacted by autophagy and present in the gene sets of both our study and the whole blood approach (44 genes, t-test p-value < 0.05, **Table 1**) were weighted by their t-statistic, which gave rise to an "autophagy" vector lying in a 44-gene feature dimensional space. We then used data from control, IFN-β, or IFN-γ whole blood stimulation of 25 healthy donors, to create two new vectors by weighting each gene by its t-statistic (paired t-test, control vs IFN-β or control vs IFN-γ). All vectors were normalized to length 1, and the "autophagy" vector was projected onto the "IFN-β" and "IFN-γ" vectors (**Figure 22 C**). The scalar product ⟨autophagy, IFN-β⟩ was found to be greater than the ⟨autophagy, IFN-γ⟩ scalar product. Bootstrapping over the 25 donors from the whole blood

study confirmed the robustness of this result, as the difference between the two scalar products showed a consistent positive value (95% confidence interval = (0.014, 0.12)), suggesting that the autophagy signature was more characteristic of IFN-β stimulation than IFN-γ induced gene expression (**Figure 22 D**).

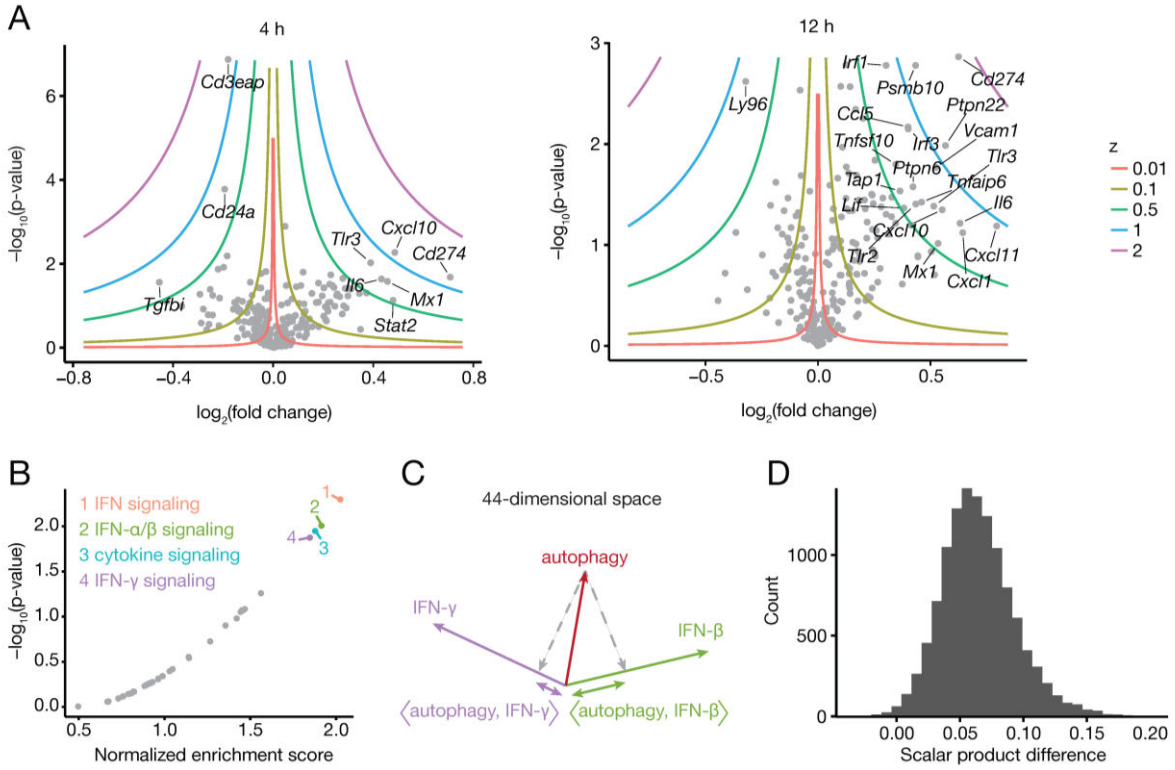

Figure 22: IAV-induced expression of type I IFN-stimulated genes is reduced when ATG5^{DD} is stabilized.
(A) ATG5^{DD} cells, pre-treated for 16 h with Shield1 (Sh1), were infected with IAV PR8 at MOI 3 for 4 or 12 h followed by RNA extraction. mRNA levels of 561 genes (see Materials and Methods) were quantified using Nanostring nCounter technology. Volcano plots show the p-value determined by two-tailed paired t-tests and fold change of gene expression in control vs Sh1-treated cells. Iso z-value curves are depicted. Data were generated from 3 independent experiments. (**B**) Gene set enrichment analysis was performed after ranking genes according to their differential expression in control vs Sh1-treated samples (see Materials and Methods for computation of t-statistic). Shown are normalized enrichment score and p-values, computed by the GSEA method.[159] Each point represents a gene set (the 40 most enriched gene sets are shown), and sets with an enrichment false-discovery rate < 0.2 (significance threshold recommended by Nanostring) are colored and labeled. **(C)** The 44 genes most significantly impacted by Sh1 treatment (paired t-test p-value < 0.05) were selected and weighted by their t-statistic, which gave rise to an "autophagy" vector lying in a 44-dimensional space (red). Data from whole-blood[160] stimulation was used to create an IFN-β vector (control vs IFN-β treatment t-statistic, green) and an IFN-γ vector (control vs IFN-β treatment t-statistic, purple), after which all vectors were normalized to length 1. **(D)**

Bootstrapping over the 25 donors of the whole-blood study was performed and the difference ⟨autophagy, IFN-β⟩ – ⟨autophagy, IFN-γ⟩ between the two scalar products was computed for each iteration. Plotted is the distribution of the differences, with a 95%-confidence interval of (0.014, 0.12).

Moreover, the only interferon gene consistently detected in our cellular model after infection was *Ifnb1* (**Figure 23**). These results led us to conclude that autophagy following IAV infection resulted in the modulation of IFN-β–stimulated genes.

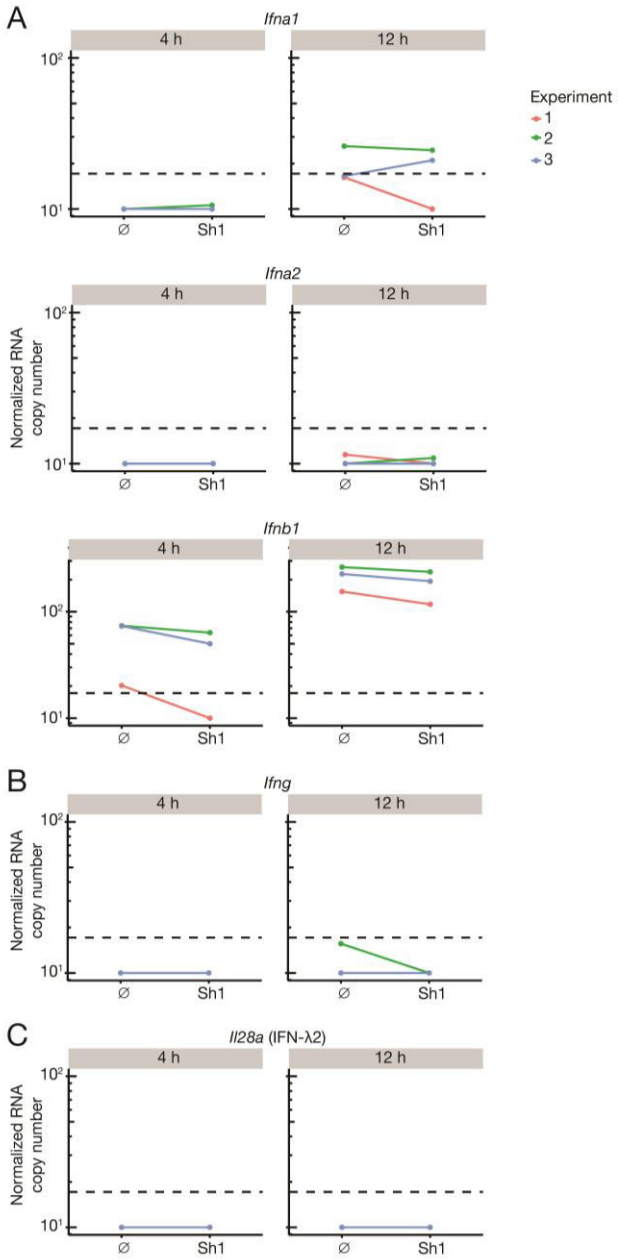

Figure 23: Only *Ifnb1* RNA is consistently expressed by ATG5^{DD} cells after IAV PR8 infection.

ATG5^{DD} cells, pre-treated for 16 h with Shield1 (Sh1), were infected with IAV PR8 at MOI 3 for 4 or 12 h after which RNA was extracted. RNA levels were quantified using Nanostring nCounter technology. Expression of type I (**A**), type II (**B**), and type III (**C**) interferons are depicted. Dashed lines represent the lower limit of quantification of the assay. A threshold of 10 was used for visualization purposes, hence points below 10 overlap at 10.

4 h

	Gene	t-statistic	p-value	q-value	FC	z-value
1	*Cd3eap*	-2730.5	1.34E-07	3.25E-05	0.88276	1.236401
2	*Cd24a*	-77.591	0.00017	0.02009	0.87429	0.732589
3	*Il6st*	27.9668	0.00128	0.10294	1.03372	0.138452
4	*Cxcl10*	13.6059	0.00536	0.30754	1.40089	1.10446
5	*Ahr*	-12.371	0.00647	0.30754	0.88044	0.402119
6	*Tlr3*	10.2275	0.00943	0.30754	1.31015	0.789482
7	*Maf*	-9.0192	0.01207	0.30754	0.87179	0.379728
8	*Il1rn*	-8.5344	0.01345	0.30754	0.85855	0.411692
9	*Psmd7*	-8.0044	0.01525	0.30754	0.98005	0.052827
10	*Nfkbiz*	7.86164	0.0158	0.30754	1.08673	0.21615
11	*Notch2*	-7.5673	0.01702	0.30754	0.96737	0.084681
12	*Pml*	7.28403	0.01833	0.30754	1.1731	0.400024
13	*Cd274*	6.82393	0.02081	0.30754	1.63318	1.190183
14	*Ifih1*	6.58922	0.02227	0.30754	1.21285	0.460012
15	*Il6*	6.47391	0.02304	0.30754	1.3499	0.708813
16	*Mx1*	6.04646	0.02628	0.30754	1.37267	0.72221
17	*Tgfbi*	-5.9061	0.02749	0.30754	0.72959	0.709921
18	*Itga6*	-5.9053	0.0275	0.30754	0.9387	0.142445
19	*Klra4*	5.77515	0.0287	0.30754	1.13367	0.279135
20	*Tlr2*	5.57668	0.03068	0.30754	1.16966	0.342093
21	*Casp2*	5.37019	0.03297	0.30754	1.07981	0.164166
22	*Cd80*	5.3628	0.03306	0.30754	1.03687	0.077348
23	*Tapbp*	5.35903	0.0331	0.30754	1.17895	0.351538
24	*B2m*	5.18974	0.03518	0.30754	1.06641	0.13485
25	*Socs1*	5.07328	0.03673	0.30754	1.18343	0.348672
26	*C1qbp*	-5.0347	0.03726	0.30754	0.96165	0.080605
27	*Ccl2*	5.0334	0.03728	0.30754	1.15082	0.28951
28	*Atg16l1*	-5.0156	0.03753	0.30754	0.96668	0.069706
29	*Irgm1*	4.96889	0.0382	0.30754	1.23329	0.428957
30	*Il15ra*	4.94069	0.03861	0.30754	1.22106	0.407223
31	*Ifit2*	4.83984	0.04014	0.30754	1.24129	0.435467
32	*Gpi1*	-4.8063	0.04067	0.30754	0.83989	0.350099
33	*Gm10499*	4.3207	0.04961	0.3274	1.29568	0.48747
34	*Cd109*	-4.3139	0.04976	0.3274	0.98599	0.026525
35	*Ddx58*	4.26495	0.05082	0.3274	1.1133	0.200364
36	*Tap1*	4.26323	0.05086	0.3274	1.27006	0.446167
37	*Ifi204*	4.20985	0.05206	0.3274	1.1944	0.328953
38	*Lef1*	-4.1638	0.05313	0.3274	0.81642	0.373004
39	*Tgfb1*	-4.0411	0.05613	0.3274	0.94348	0.104992
40	*Igf2r*	-4.0245	0.05656	0.3274	0.84591	0.301184
41	*Ikbkg*	4.01273	0.05686	0.3274	1.19221	0.315832
42	*Stat1*	3.9639	0.05815	0.3274	1.23012	0.369159
43	*Bst2*	3.96293	0.05817	0.3274	1.14567	0.242351
44	*Irf7*	3.88165	0.06042	0.33229	1.20254	0.324318
45	*Bcl2*	-3.712	0.06552	0.34629	0.86214	0.253307
46	*Itgb1*	-3.6637	0.06709	0.34629	0.98518	0.025282
47	*Mif*	-3.6432	0.06777	0.34629	0.97767	0.038087
48	*Stat3*	3.61622	0.06868	0.34629	1.05345	0.087374
49	*Tollip*	-3.4918	0.07313	0.35066	0.90736	0.159303
50	*Stat2*	3.47182	0.07389	0.35066	1.39396	0.542174
51	*Il1r1*	-3.3575	0.07842	0.35066	0.9185	0.135593
52	*Pdgfrb*	-3.3435	0.079	0.35066	0.7443	0.469668
53	*Myd88*	3.27874	0.08177	0.35066	1.13395	0.197204
54	*Irf1*	3.26307	0.08247	0.35066	1.17154	0.247532
55	*Crlf2*	-3.2458	0.08324	0.35066	0.89882	0.166162
56	*Ifi35*	3.24024	0.08349	0.35066	1.1267	0.185595
57	*Fas*	3.22168	0.08434	0.35066	1.16529	0.237022
58	*Cxcl12*	-3.2083	0.08496	0.35066	0.93781	0.099184
59	*Tfrc*	3.19679	0.08549	0.35066	1.0405	0.061182
60	*Casp3*	3.14787	0.08783	0.35423	1.07413	0.108985
61	*Jak2*	3.10007	0.0902	0.35783	1.0895	0.129207
62	*Hif1a*	3.00506	0.09519	0.37154	1.02316	0.033739
63	*H2.DMa*	2.91815	0.10011	0.3716	1.21577	0.281739
64	*Phlpp2*	-2.8892	0.10183	0.3716	0.95988	0.058602
65	*Pdgfb*	-2.8823	0.10224	0.3716	0.77622	0.361935
66	*Tnfaip6*	2.88179	0.10227	0.3716	1.18644	0.244228
67	*Fn1*	-2.8718	0.10288	0.3716	0.93414	0.097083
68	*Traf5*	2.8318	0.10536	0.37496	1.15553	0.203821
69	*C1ra*	-2.7875	0.10821	0.37951	0.90497	0.139122
70	*Tnfsf10*	2.72291	0.11256	0.38701	1.22429	0.276943
71	*Il10rb*	-2.7087	0.11354	0.38701	0.94591	0.075798
72	*Jak3*	2.6717	0.11618	0.39028	1.16211	0.20263
73	*Ptger4*	-2.623	0.11978	0.39028	0.82402	0.257357
74	*Il6ra*	-2.6168	0.12025	0.39028	0.96927	0.041424
75	*Pdcd2*	-2.6076	0.12095	0.39028	0.89553	0.146033
76	*Pparg*	-2.527	0.12736	0.40435	0.91202	0.118905
77	*Prkcd*	-2.5114	0.12866	0.40435	0.95956	0.053036
78	*Ly96*	2.44426	0.13444	0.40688	1.09302	0.111833
79	*Irf5*	2.44407	0.13445	0.40688	1.16408	0.191006
80	*Ifngr1*	-2.4309	0.13563	0.40688	0.98758	0.015649
81	*Bcl6*	-2.4248	0.13619	0.40688	0.9085	0.119879
82	*Casp8*	-2.3741	0.14087	0.41575	0.95244	0.05984
83	*Cd99*	-2.318	0.14634	0.42667	0.93022	0.087103
84	*Tnfrsf1b*	2.27972	0.15023	0.4328	1.08917	0.101443
85	*Npc1*	-2.2544	0.15288	0.43416	0.96818	0.038053
86	*Ikbkap*	-2.2412	0.15429	0.43416	0.98277	0.020356
87	*Psmb10*	2.21713	0.15691	0.43646	1.21087	0.22204
88	*Mme*	-2.158	0.1636	0.4499	0.83527	0.204167
89	*Tyk2*	-2.1363	0.16616	0.4518	0.84547	0.188768
90	*Runx1*	2.11159	0.16913	0.45477	1.0637	0.068756
91	*Rae1*	-2.0481	0.17712	0.46199	0.97849	0.023583
92	*H2.K1*	2.04567	0.17743	0.46199	1.15052	0.151912
93	*Il1rap*	2.03858	0.17835	0.46199	1.06075	0.063702
94	*Fyn*	-2.0302	0.17945	0.46199	0.96255	0.041081
95	*Bax*	-2.0037	0.18299	0.46505	0.9573	0.046431
96	*Ptk2*	1.99284	0.18448	0.46505	1.04502	0.046636
97	*Litaf*	1.96998	0.18765	0.46816	1.04183	0.042957
98	*Plaur*	-1.9321	0.19307	0.47676	0.96295	0.038907
99	*Jak1*	-1.8753	0.20158	0.48504	0.98846	0.011647
00	*Ikbke*	1.84257	0.20672	0.48504	1.10617	0.099663

12 h

	Gene	t-statistic	p-value	q-value	FC	z-value
1	*Cd274*	27.0385	0.00137	0.09074	1.54174	1.789278
2	*Ctsc*	24.6834	0.00164	0.09074	1.08992	0.346062
3	*Irf1*	24.4996	0.00166	0.09074	1.23335	0.840984
4	*Psmb10*	24.4885	0.00166	0.09074	1.35075	1.205411
5	*Ly96*	-20.391	0.0024	0.09074	0.80019	0.842688
6	*Ifngr2*	19.2717	0.00268	0.09074	1.07263	0.260134
7	*Csf1*	19.1991	0.0027	0.09074	1.10386	0.366137
8	*Ahr*	-18.443	0.00293	0.09074	0.94623	0.202037
9	*Pml*	14.8064	0.00453	0.12484	1.12305	0.392405
10	*Muc1*	13.3608	0.00556	0.13777	1.14852	0.450565
11	*Ccl5*	12.0997	0.00676	0.14661	1.31962	0.868259
12	*Irf3*	11.8096	0.00709	0.14661	1.32068	0.862403
13	*Ptpn22*	9.75634	0.01034	0.19038	1.4811	1.12504
14	*Ifi35*	9.56828	0.01075	0.19038	1.07836	0.214275
15	*Tapbp*	8.22536	0.01446	0.23154	1.19179	0.465719
16	*Tnfsf10*	7.83174	0.01592	0.23154	1.2706	0.621295
17	*Il1rap*	7.61022	0.01683	0.23154	1.09116	0.223263
18	*Vcam1*	7.54852	0.0171	0.23154	1.43893	0.927649
19	*Nfkbia*	7.06461	0.01945	0.23154	1.09894	0.23288
20	*Nfil3*	6.89357	0.0204	0.23154	1.12627	0.289972
21	*Irak1*	-6.8707	0.02053	0.23154	0.94913	0.127102
22	*Abcb10*	6.65965	0.02181	0.23154	1.06262	0.145579
23	*Zbtb7b*	-6.3467	0.02394	0.23154	0.87822	0.303674
24	*Ifngr1*	6.12621	0.02563	0.23154	1.0371	0.083621
25	*Ptpn6*	6.01936	0.02651	0.23154	1.34012	0.66591
26	*Tap1*	5.7224	0.02921	0.23154	1.28738	0.559235
27	*Eef1g*	-5.7087	0.02934	0.23154	0.975	0.055981
28	*H2.K1*	5.50763	0.03142	0.23154	1.17989	0.358643
29	*Tfrc*	5.45089	0.03205	0.23154	1.18185	0.360174
30	*Ifi204*	5.31563	0.03362	0.23154	1.2553	0.483335
31	*Fyn*	-5.2626	0.03426	0.23154	0.91158	0.195688
32	*Cd74*	5.25979	0.0343	0.23154	1.22115	0.422189
33	*B2m*	5.24762	0.03445	0.23154	1.09006	0.181987
34	*Ifih1*	5.13278	0.03592	0.23154	1.15392	0.29838
35	*Stat1*	5.12504	0.03603	0.23154	1.13328	0.260534
36	*Tnfaip6*	5.00762	0.03764	0.23154	1.37595	0.655798
37	*Irgm1*	4.91887	0.03893	0.23154	1.18558	0.34621
38	*Tlr2*	4.89733	0.03926	0.23154	1.35169	0.611321
39	*Tollip*	-4.816	0.04051	0.23154	0.86409	0.293447
40	*Tlr3*	4.76894	0.04127	0.23154	1.42878	0.712667
41	*Il13ra1*	4.72633	0.04197	0.23154	1.21507	0.387015
42	*Lif*	4.66255	0.04305	0.23154	1.30324	0.521964
43	*Cd44*	4.62044	0.04379	0.23154	1.0484	0.092653
44	*Irf7*	4.61641	0.04386	0.23154	1.15654	0.284911
45	*Atm*	4.61556	0.04387	0.23154	1.09359	0.175258
46	*Cxcl10*	4.56344	0.04482	0.23154	1.46645	0.744853
47	*Bcl6*	4.52262	0.04557	0.23154	1.11209	0.205576
48	*Ddx58*	4.51636	0.04569	0.23154	1.1003	0.184798
49	*Cebpb*	-4.5134	0.04575	0.23154	0.9007	0.202123
50	*Bax*	-4.4083	0.0478	0.23709	0.94097	0.115916
51	*Lck*	4.31939	0.04964	0.24139	1.23334	0.394592
52	*Pdcd2*	-4.2327	0.05154	0.24158	0.93437	0.126116
53	*Pou2f2*	4.19193	0.05247	0.24158	1.2543	0.418438
54	*Il6st*	4.18616	0.0526	0.24158	1.07495	0.133352
55	*Nfkb2*	4.0054	0.05705	0.25724	1.04612	0.080902
56	*Tmem173*	3.91985	0.05935	0.26072	1.16342	0.267848
57	*Fcgr2b*	3.86375	0.06093	0.26072	1.2702	0.419301
58	*Il6*	3.86215	0.06097	0.26072	1.54922	0.767232
59	*Ccl2*	3.77162	0.06366	0.26758	1.33275	0.495681
60	*Cxcl11*	3.73072	0.06493	0.26837	1.7343	0.943343
61	*Ski*	-3.6561	0.06734	0.2703	0.92041	0.140201
62	*Ncam1*	-3.6491	0.06757	0.2703	0.88338	0.20935
63	*Tgfb1*	-3.5938	0.06946	0.27186	0.95151	0.083065
64	*Ifit2*	3.5738	0.07016	0.27186	1.18303	0.279807
65	*Ifnb1*	3.5292	0.07175	0.27377	1.1967	0.296408
66	*Npc1*	-3.4362	0.07526	0.2799	0.77645	0.410104
67	*Cxcl1*	3.42692	0.07562	0.2799	1.56208	0.72156
68	*Igf2r*	-3.3691	0.07794	0.28107	0.89557	0.176346
69	*Stat2*	3.36274	0.0782	0.28107	1.24358	0.348081
70	*Itgb1*	-3.2336	0.08379	0.28901	0.96121	0.061467
71	*Fadd*	-3.2046	0.08512	0.28901	0.91115	0.143637
72	*Tnfaip3*	3.20323	0.08519	0.28901	1.20207	0.283998
73	*Ptgs2*	3.19396	0.08562	0.28901	1.162	0.231208
74	*Nfatc3*	3.16889	0.08681	0.28901	1.04441	0.066545
75	*Plaur*	3.15663	0.0874	0.28901	1.05977	0.088656
76	*Stat3*	3.08119	0.09116	0.29747	1.0723	0.104764
77	*H2.DMa*	3.02586	0.09406	0.30248	1.11307	0.158652
78	*Fn1*	-3.0004	0.09544	0.30248	0.91486	0.130978
79	*Mx1*	2.98023	0.09656	0.30248	1.44771	0.541888
80	*Ets1*	2.96215	0.09757	0.30248	1.12407	0.170533
81	*Fcgrt*	2.93505	0.09912	0.30349	1.04973	0.070288
82	*Cd99*	-2.9045	0.10091	0.30519	0.95056	0.072856
83	*Runx1*	2.8701	0.10298	0.30771	1.06598	0.091003
84	*App*	-2.8275	0.10563	0.31186	0.93325	0.097297
85	*Nfkb1*	2.77921	0.10875	0.3173	1.07285	0.097756
86	*Hlx*	2.75226	0.11055	0.31841	1.04624	0.06237
87	*Itga2b*	2.73536	0.1117	0.31841	1.18339	0.231258
88	*Tyk2*	2.68412	0.11529	0.32057	1.13083	0.166417
89	*Tslp*	2.67085	0.11624	0.32057	1.41754	0.470484
90	*Tbk1*	-2.6696	0.11634	0.32057	0.91726	0.116416
91	*Ptpn2*	2.63006	0.11925	0.32217	1.03161	0.041462
92	*Mapk11*	2.60032	0.12152	0.32217	1.19203	0.231976
93	*C1qbp*	-2.5856	0.12266	0.32217	0.99192	0.010663
94	*Stat5a*	-2.5507	0.12543	0.32217	0.84227	0.223276
95	*Psmb9*	2.51895	0.12803	0.32217	1.36015	0.396152
96	*Stat6*	-2.5184	0.12807	0.32217	0.92466	0.100856
97	*Tlr4*	-2.5083	0.12891	0.32217	0.90911	0.12231
98	*Gpi1*	2.50465	0.12922	0.32217	1.13822	0.16598
99	*Ccl7*	2.49864	0.12973	0.32217	1.19287	0.225676
100	*Prim1*	-2.4896	0.13049	0.32217	0.9383	0.081264

Table 1: Genes most impacted by autophagy capacity.
p-values were determined by two-tailed paired t-tests comparing control vs Shield1-treated cells, and z-values were subsequently computed (see **Materials and Methods** for formula). q-values correspond to false-discovery rate. The 100 genes with smallest p-values at 4 h and 12 h post infection are listed. In red are the 44 genes, present in the gene sets of both this study and the whole-blood study[160], that were weighted by their t-statistic to distinguish between a type I and a type II interferon response, with p-value < 0.05 at 12 h post infection
FC, fold change.

I next tested whether IAV-induced autophagy impacted the inflammatory response at the protein level, using ELISA and flow cytometry read-outs to measure interferon-induced effector molecules. Indeed, in the context of IAV infection, CXCL10 secretion was negatively impacted by $ATG5^{DD}$ stabilization, with differential expression detected as early as 5 h (**Figure 24 A**). Furthermore, surface expression of CD274 and class I major histocompatibility protein H-$2K^b$ were both negatively impacted by $ATG5^{DD}$ stabilization at 16 h post infection (**Figure 24 B and C**). Of note, surface expression of H-$2K^b$ was also significantly, although to a lesser extent, impacted by autophagy in uninfected cells. Additionally, we measured PSMB10 expression, a subunit of the immunoproteasome, which also showed reduced protein expression in autophagy-competent cells, as measured by immunoblotting (**Figure 24 D**). All three of these proteins are known to be induced by type I IFN,[161,162,163,164] and support our conclusion that IAV-induced autophagy negatively regulates IFN-β-induced inflammatory responses. I confirmed that *Cd274* was indeed an ISG in our model by blocking interferon-α/β receptor (IFNAR) signaling through use of a neutralizing anti-IFNAR1 antibody (**Figure 24 E**), and as it was the most differentially expressed ISG at the level of RNA, we used this molecule as well as H-$2K^b$ expression as functional readouts of the impact of autophagy in the remainder of our study. I next investigated whether NS1, a key negative regulator of the type I IFN response,[56] played a role in the suppression of ISGs following infection. I infected cells with wildtype and ΔNS1 IAV PR8 in the presence or absence of Shield1. Stabilization of ATG5 decreased CD274 expression following infection with either viral strain (**Figure 24 F**).

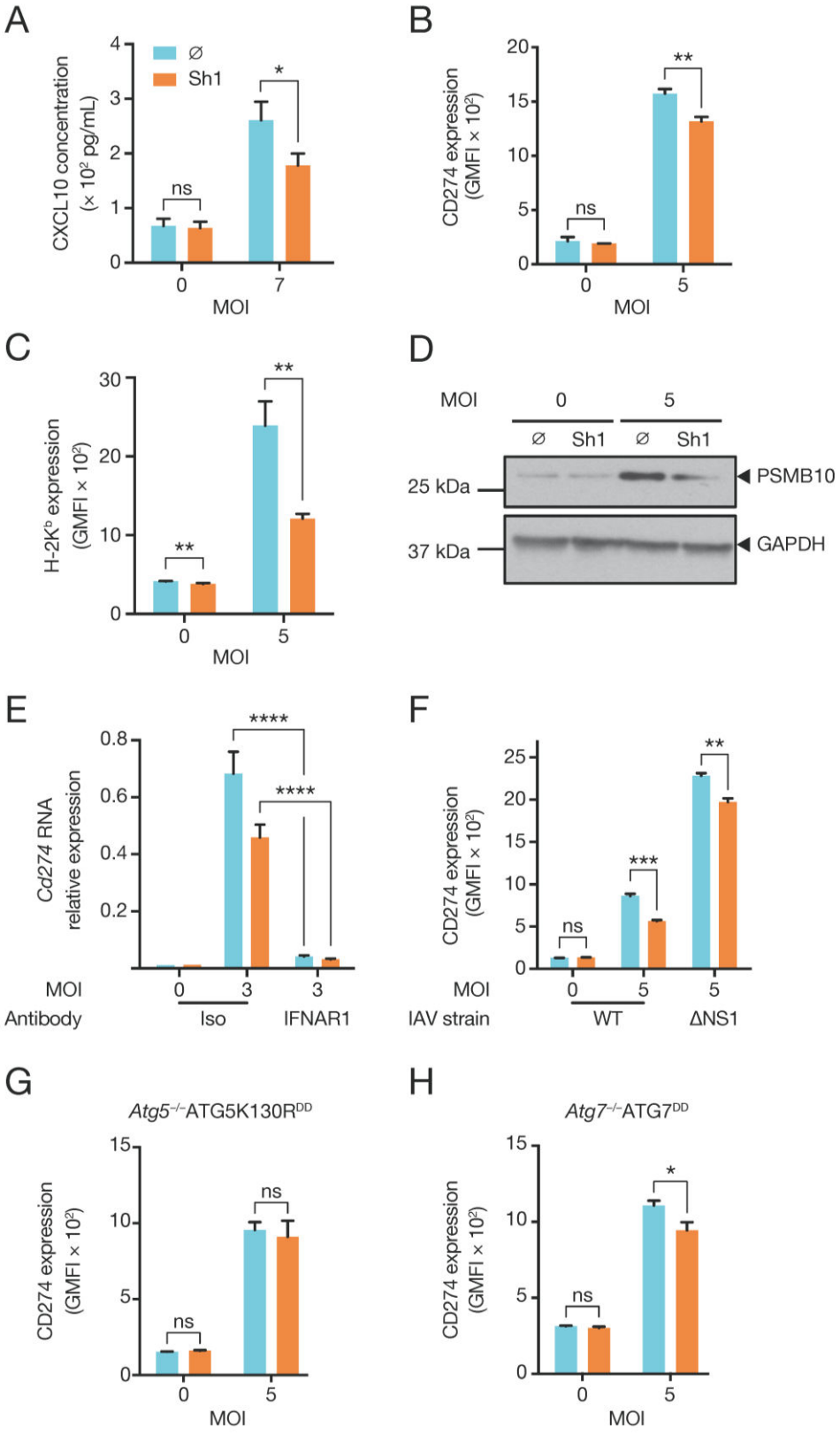

Figure 24: Expression levels of ISGs are negatively impacted by autophagy machinery during IAV infection.

(**A**) ATG5^{DD} cells, pre-treated or not with Shield1 (Sh1) for 16 h, were infected with IAV at the indicated MOIs for 5 h. CXCL10 concentration in the supernatants was measured by

ELISA. (**B and C**) ATG5^{DD} cells, pre-treated or not with Sh1 for 20 h, were infected with IAV at the indicated MOI for 16 h. Surface expression of CD274 (**B**) and H-2K^{b} (**C**) was measured by flow cytometry. (**D**) ATG5^{DD} cells, pre-treated or not with Sh1 for 20 h, were infected with IAV PR8 at the indicated MOI for 20 h before analyzing PSMB10 expression by immunoblot. (**E**) ATG5^{DD} cells, pre-treated or not with Sh1 for 16 h and with anti-IFNAR1 antibody for 1 h, were infected for 5 h at the indicated MOI and *Cd274* expression was assayed by RT–qPCR (calculated as 2^(Ct_{Hprt1}–Ct_{Cd274}). (**F**) ATG5^{DD} cells, pre-treated or not with Sh1 for 20 h, were infected with PR8 or ΔNS1 PR8 at the indicated MOI for 16 h before measuring CD274 surface expression by flow cytometry. (**G** and **H**) ATG5K130R^{DD} (**G**) or ATG7^{DD} (**H**) cells were treated as in (B) and (C) before monitoring of surface CD274 expression by flow cytometry. (**A to C, E to H**). Graphs show mean and standard deviation of triplicates, and data are representative of three experiments. ns, not significant; *, q < 0.05; **, q < 0.01; ***, q < 0.001; ****, q < 0.0001 (one-tailed unpaired t-test followed by Holm's multiple testing correction).

Of note, ATG5 has been reported to mediate several non–autophagy-related phenotypes[153]. As mentioned previously, I confirmed that ATG5K130R^{DD} accumulated upon Shield1 treatment; however, as expected, I did not detect a band corresponding to the ATG5–ATG12 complex in the Shield1-treated ATG5K130R^{DD} cell line. I infected ATG5K130R^{DD} cells in the presence or absence of Shield1 and observed that lysine 130 of ATG5 is required for suppression of CD274 expression (**Figure 24 G**). Validating my findings using the ATG5^{DD} cell lines, I demonstrated that ATG7^{DD} stabilization also resulted in the reduced CD274 expression in infected cells (**Figure 24 H**). Together, these findings highlight ATG5–ATG12 formation as a key process that limits ISG induction in response to IAV infection.

4.2. Autophagic flux, induced early post infection, results in decreased levels of IFN-β and accounts for the diminished ISG expression

Based on the differential expression of type I IFN-induced genes, I considered two hypotheses: that IFNAR signaling was negatively impacted by autophagy or alternatively, that IAV-infected, autophagy-competent cells produce less IFN-β. To address the first possibility, I directly tested whether autophagic flux impacted IFNAR signaling. Following treatment with Shield1 or control media for 16 h, ATG5^{DD} cells were exposed to increasing amounts of recombinant IFN-β. CD274 and H-2K^{b} surface protein expression was measured by flow cytometry over time. CD274 and H-2K^{b} expression was equally increased following IFN-β treatment of control and Shield1-treated cells, suggesting that ATG5^{DD} stabilization did not alter IFNAR signaling (**Figure 25 A & B**).

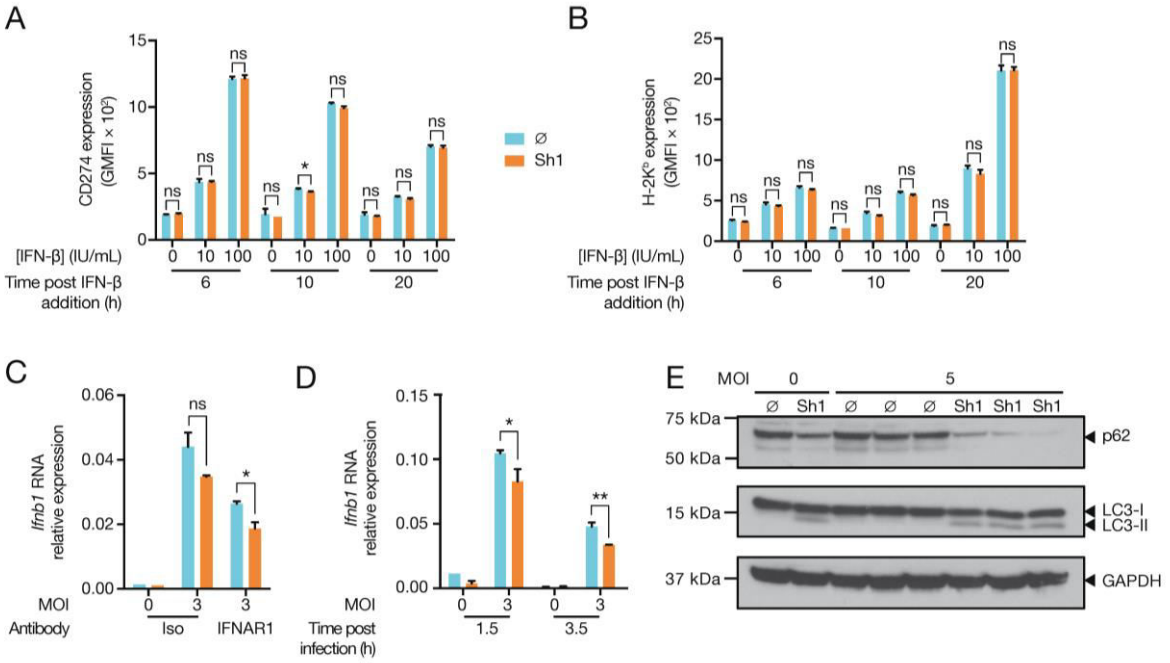

Figure 25: Autophagy inhibits ISG expression via cell-intrinsic modulation of IFN-β expression and not through desensitization to IFNAR signaling.
(**A to B**) ATG5^{DD} cells, pre-treated or not with Shield1 (Sh1), were treated with recombinant mouse IFN-β at the indicated concentration for 6, 10, or 20 h, followed by surface expression analysis of CD274 (**A**) and H-2K^{b} (**B**) by flow cytometry. (**C**) ATG5 ^{DD} cells were pre-treated with anti-IFNAR1 antibodies followed by IAV infection. *Ifnb1* expression was assayed by RT–qPCR. (**D**) In independent experiments, *Ifnb1* induction was measured at 1.5 and 3.5 h post-infection in autophagy-competent (Sh1) vs autophagy-null cells (∅). (**A to D**) Graphs show mean and standard deviation of triplicates, and data are representative of three experiments. ns, not significant; *, q < 0.05; **, q < 0.01 (one-tailed unpaired t-test followed by Holm's multiple testing correction). (**E**) ATG5^{DD} cells were pre-treated or not with Sh1 for 16 h and infected with IAV at the indicated MOI. One hour post infection, p62, LC3-I, LC3-II, and GAPDH levels were measured by immunoblot. Three biological replicates were run for infected control or Sh1-treated samples.

I therefore hypothesized that IAV-stimulated cells may express less IFN-β when competent for autophagy. I treated cells with IFNAR blocking antibody and observed by RT–qPCR that ATG5^{DD} stabilization limited *Ifnb1* expression independently of IFNAR signaling (**Figure 25 C**). Importantly, I determined that RT–qPCR was sensitive enough to detect fold changes as small as 1.4 with 80% power using triplicate samples, thus permitting confirmation of the results we observed in the nCounter analysis (**Figure 26**). ATG5^{DD} stabilization resulted in reduced IFN-β expression as early as 1.5 h post-infection (**Figure 25 D**). I, therefore, tested whether autophagy was induced by IAV at this early timepoint. Immunoblot analysis revealed that the LC3-II/LC3-I ratio was increased at 1 h post infection. This result correlated with

decreased levels of p62 when Shield1 was present, arguing that autophagy was rapidly induced and that IAV-mediated inhibition of autophagy maturation emerges later in the viral life cycle (**Figure 25 E, see also Figure 16**). This highlights that perturbation of autophagy by IAV permits the early inhibition of IFN-β induction, independently of the reported actions of NS1.

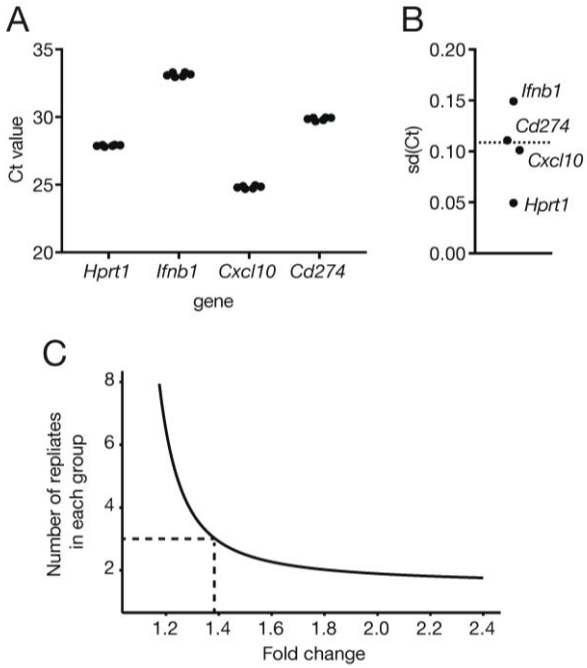

Figure 26: Detection power of RT–qPCR for *Hprt1*, *Ifnb1*, *Cxcl10* and *Cd274*.
(A and **B)** ATG5^{DD} cells treated with Shield1 were infected with IAV at MOI 3 for 4 h before RNA extraction. For each RNA product, 6 different RT–qPCR were performed for the specified gene. Threshold cycle (Ct) values (**A**) and standard deviation of Ct are shown for each gene (**B**). (**C**) After estimation of the standard deviation of ΔCt values, shown is the power curve giving the number of technical replicates required to detect different fold changes with 80% power at a confidence level of 95%; e.g., 3 replicates allow the detection of a ~1.4 fold change (dashed line).

4.3. Inducing autophagy capacity limits NF-κB activation

As the transcription of *Ifnb1* relies on RIG-I activation-mediated formation of an enhanceosome that contains NF-κB and activated (phosphorylated) IRF3/IRF7[119], I wondered if autophagy was exerting its anti–IFN-β property at this step.

To test this, I monitored the degradation of IκBα, a protein that directly interacts with NF-κB, thereby preventing it from translocating to the nucleus[165]. Upon activating signal,

IκBα is phosphorylated, ubiquitinated and degraded by the proteasome which allows NF-κB to act as a transcription factor (**Figure 27 A**). Immunoblot analysis showed that IAV infection led to degradation of IκBα, which was limited by Shield1 introduction (**Figure 27 B & C**).

Moreover, data using intra-incubator microscopy to monitor GFP florescence from a GFP NF-κB reporter showed that NF-κB transcriptional activity was limited when cells were rendered autophagy competent (**Figure 27 D**).

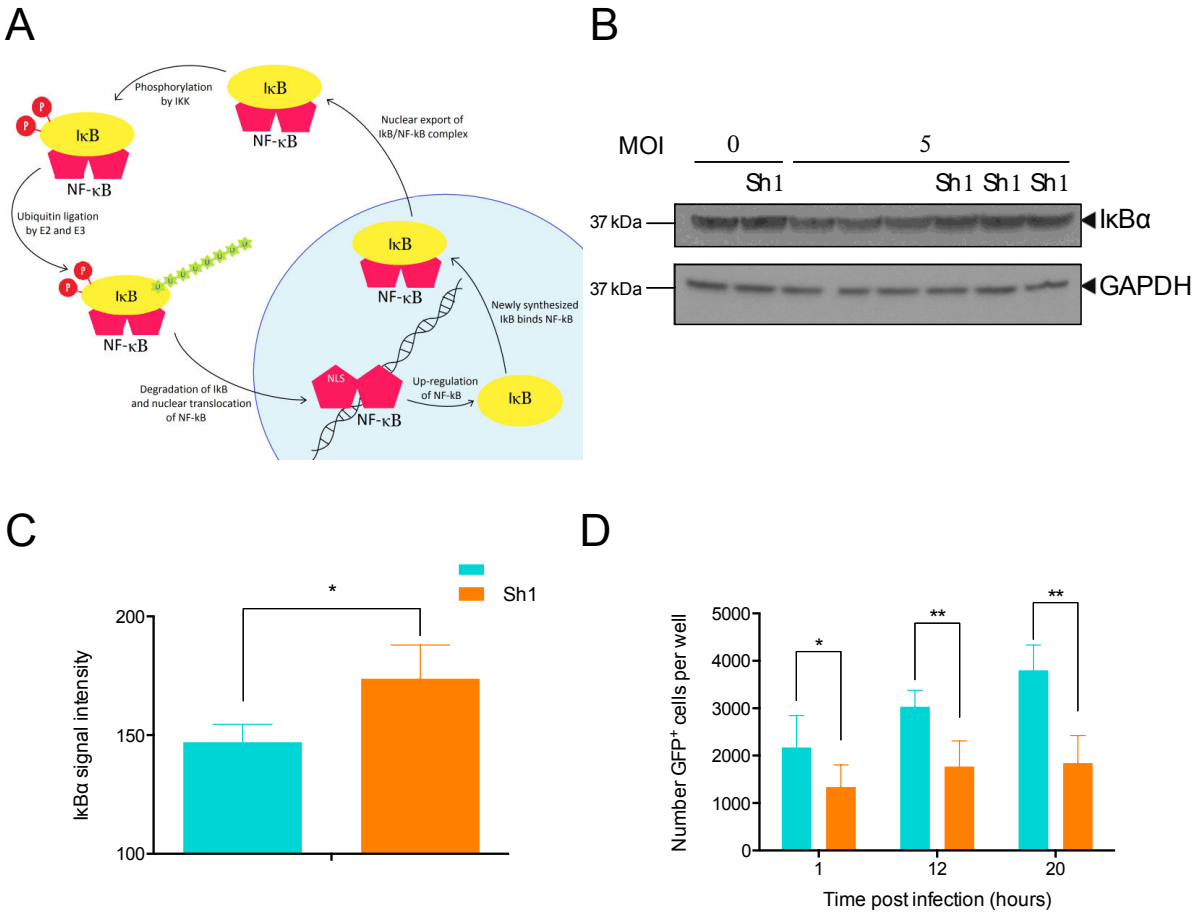

Figure 27: Activation of the NF-κB pathway is negatively impacted by autophagy.
(**A**) NF-κB activation, involves IκB phosphorylation, ubiquitination and proteasomal degradation, which frees NF-κB and allows it to translocate to the nucleus for stimulation of transcription. (from sites.tufts.edu). (**B**,**C**) ATG5^{DD} cells pre-treated or not with Shield1 (Sh1) were infected by PR8 for 1 h before monitoring IκBα degradation by immunoblot (**B**) and quantification with ImageJ (**C**). ATG5^{DD} cells transfected by with NF-κB transcription activity GFP reporter for 20 hours were pre-treated or not with Shield1 (Sh1) and infected by PR8. Incucyte intra-incubator microscope allowed the monitoring of GFP positive cell number.

In summary, I showed that after IAV infection, autophagy is rapidly induced and correlates with decreased capacity of the cell to generate IFN-β hence to induce ISGs. Autophagy negative impact on IFN-β stimulation seems to act on RIG-I signal transduction, since I could observe limited NF-κB activation in autophagy-competent cells.

As introduced previously, some teams have found that IAV induces abortive form of autophagy while others described complete forms of autophagy. With my model, autophagy is induced and complete at early timepoints (see **Figure 25E**), whereas at late timepoints, autophagy is abortive (see **Figure 16**). M2 has been shown to be the key IAV protein for autophagy perturbation. I therefore sought to generate cellular model to study its impacts on autophagy.

II. Understanding the role of M2 in IAV-mediated autophagy perturbation

M2 has been described to be the IAV protein inducing abortive autophagy (see introduction). I investigated the mechanisms allowing autophagy maturation inhibition using engineered cells systems comparable to the ones used to study the overall effects of autophagy on cell responses to infection.

1. M2H37G^{DD}-expressing cell line generation.

To study the role of M2 on autophagy perturbation, I took the same approach that the one chosen to study the impact of autophagy capacity on host cell response to infection. At the time, M2 histidine (H) 37 to glycine (G) mutant (M2H37G) had been shown to retain its anti-autophagy maturation capacity while abolishing its proton channel activity[88]. Only by the end of my Phd did Ren and colleagues challenged this idea, arguing that the proton channel activity was necessary for autophagy maturation inhibition[132]. Therefore, I generated clonal populations of *Atg5*$^{+/+}$ and *Atg5*$^{-/-}$ cells expressing M2H37G^{DD} as, by the time, I expected this protein to block autophagy maturation inhibition while having low proton gated ion channel-mediated stress effect on cells. Immunoblot showed that M2H37G^{DD} accumulated when Shield1 was introduced (**Figure 28 A**). Given that M2 has been proposed to induce cell death in infected cells[88], I monitored cell growth in my model, with or without M2H37G^{DD}

stabilization. Shield1 addition did not impact cell growth as measured by intra-incubator microscopy (**Figure 28 B and C**).

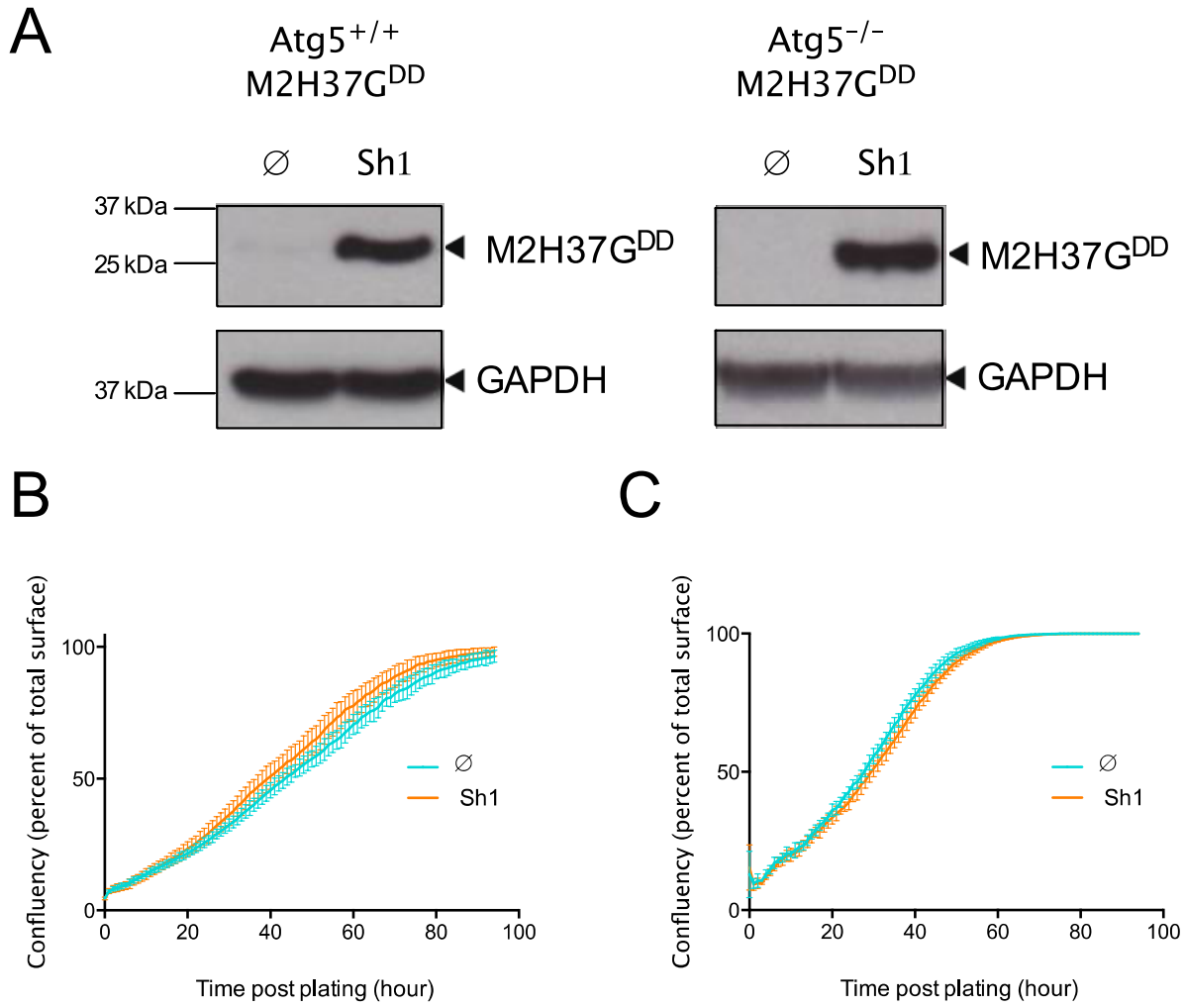

Figure 28: M2H37G^{DD} accumulates in Atg5$^{+/+}$ and Atg5$^{-/-}$ MEFs expressing M2H37G^{DD} without impacting cell growth.
(**A**) Atg5$^{+/+}$ or Atg5$^{-/-}$ MEFs expressing M2H37G^{DD} were treated or not with Shield1 (Sh1) for 20 hours before monitoring M2H37G^{DD} presence by immunoblotting. (**B**, **C**) Cell growth of Atg5$^{+/+}$ (**B**) or Atg5$^{-/-}$ MEFs (**C**) expressing M2H37G^{DD} was followed by Incucyte intra-incubator microscope after addition of Sh1 or not.

2. M2H37G^{DD} stabilization does not prevent autophagy completion

After having generated cell lines with inducible autophagy capacity, I wanted to know whether M2H37G stabilization would prevent autophagosome maturation. Stabilization of

M2H37G^{DD}, although in some conditions potentiating LC3-II/LC3-I ratio, did not rescue p62 degradation as monitored by immunoblotting (**Figure 29**).

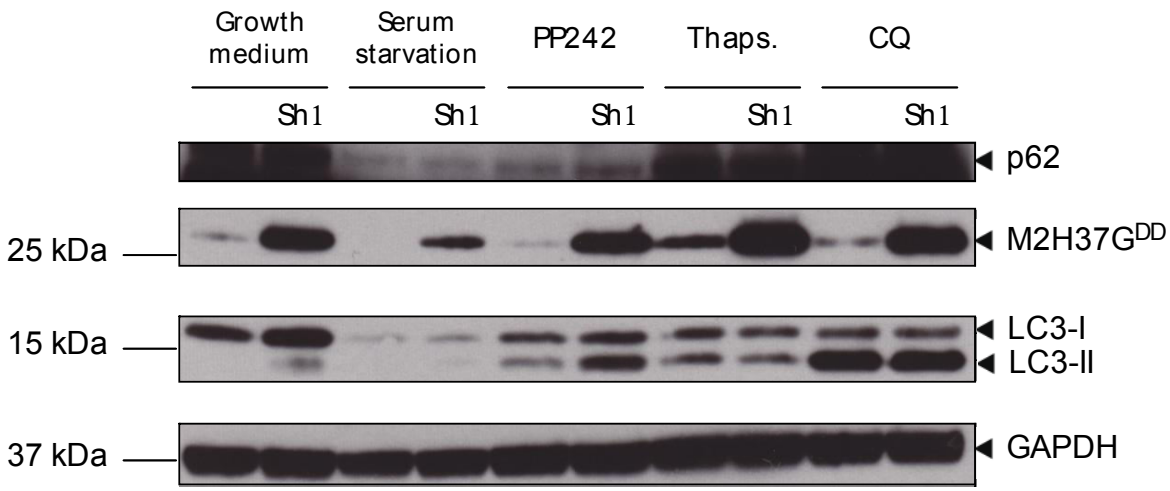

Figure 29: M2H37G^{DD} stabilization does not prevent autophagy maturation.
ATG5$^{+/+}$ MEFs stably-expressing M2H37GDD pre-treated with Shield1 (Sh1) for 16 h were treated with autophagy inducers (serum starvation, PP242) or autophagy maturation inhibitors (Thapsigargin or Thaps., chloroquine or CQ) before monitoring p62, M2H37G^{DD}, LC3 and GAPDH presence by immunoblotting.

I then wondered whether M2H37G^{DD} required infection to exert its anti-autophagy maturation property.

3. M2H37G^{DD} stabilization induces abortive autophagy in the context of IAV infection

ΔM2 A/Udorn/1972 (H3N2, Udorn strain), an IAV strain of Udorn IAV mutated in the slicing site of the M segment, rendering it unable to generate M2 but still capable of producing M1[166]. This virus was produced in Jeremy Rossman's group at Kent University in M2-producing Madin-Darby canine kidney epithelial (MDCK) cells stably-expressing M2 protein. This allows the generation of virions that contain M2 as a structural protein (which is involved in IAV entry in cells, see introduction) but lack M2-coding capacity (**Figure 30 A**).

Stabilization of M2H37G^{DD} in ATG5$^{+/+}$ cells infected with ΔM2 IAV led to aborted autophagy as monitored by LC3-II and p62 accumulation (**Figure 30 B**). Of note, CQ was even more potent in preventing p62 degradation and led to further M2H37G^{DD} accumulation that may be a sign that M2H37G^{DD} might be degraded by autophagy as p62.

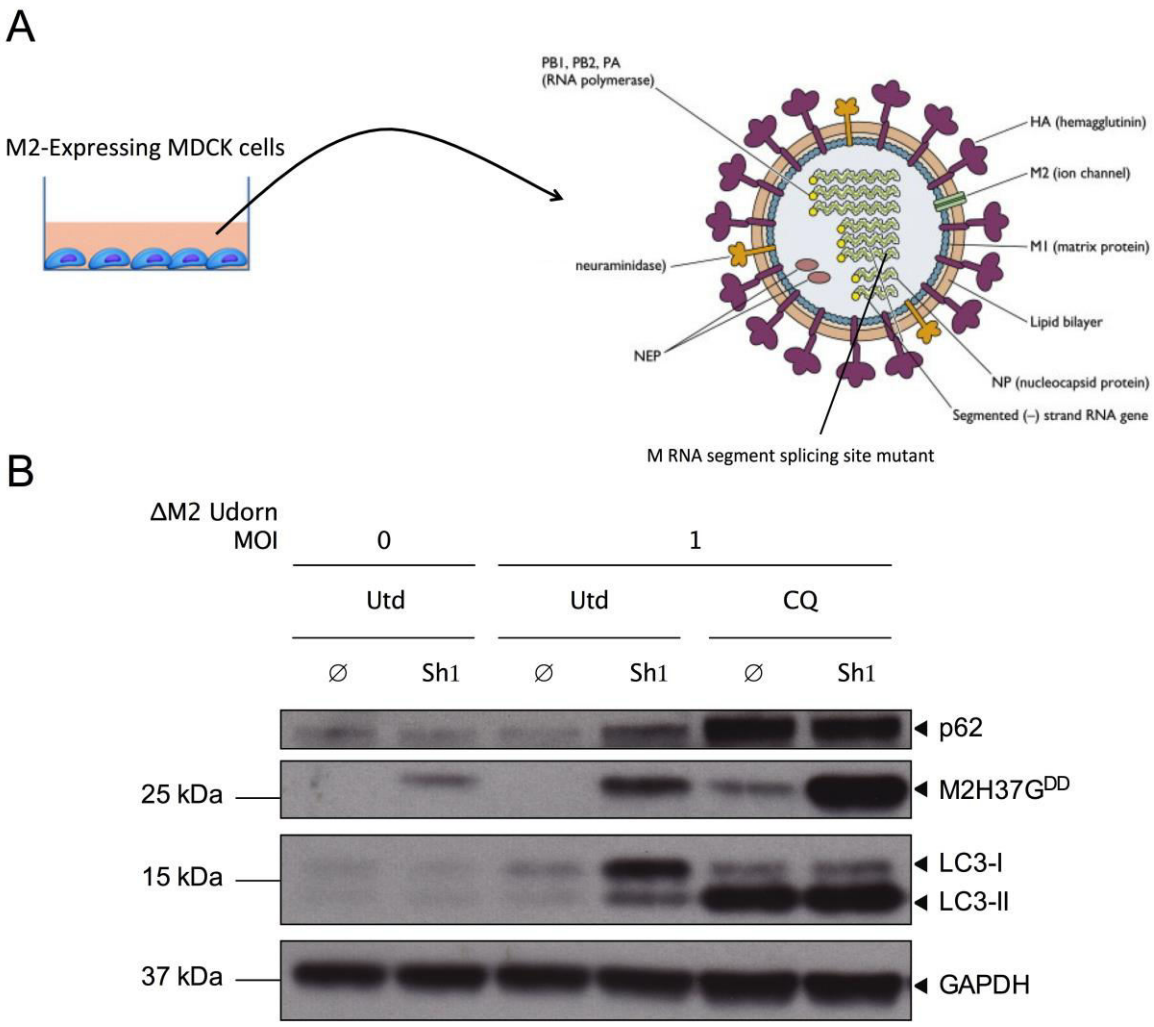

Figure 30: M2H37G^{DD} induces abortive autophagy in the context of IAV infection.
(**A**) ΔM2 IAV virion are produced from M2 stably-expressing MDCK cells, which allows M2 to be present on the virion even if ΔM2 IAV does not have the coding capacity to generate M2. M2 presence on the virion is required for IAV entry in the host cell. (**B**) *Atg5*$^{+/+}$ MEFs stably expressing M2H37G^{DD}, treated or not with Shield1 (Sh1) were infected with ΔM2 Udorn for 20 h before immunoblotting for p62, M2H37G^{DD}, LC3I and II and GAPDH.

I then wondered what could explain that M2H37G^{DD} would be able to block autophagy maturation only in the context of viral infection.

4. Caspase activation during IAV infection leads to M2 cleavage and limitation of p62 degradation

Interestingly, Jeremy Rossman had preliminary data suggesting that, in the context of infection, activated caspase 8 cleaves M2, which harbors a caspase 8 cleavage site (**Figure 31**

A). NIH 3T3 cells that stably express caspase 8 fused to a FK506 binding protein were generated in our laboratory by a student, Nader Yatim. In these cells, caspase 8 can be activated by dimerization through the addition of cell permeable molecule (BB homodimerizer)[167]. Using plasmid transfection to express M2 or M2H37G before activation of caspase 8, I could confirm that caspase 8 activation leads to M2 and M2H37G cleavage by immunoblot (**Figure 31B**).

Furthermore, infection of WT MEFs with PR8 at MOI 10 for 20 h led to the presence of a M2 smaller band that could be prevented by treatment with ZVAD, a pancaspase inhibitor (**Figure 31 C**). ZVAD-mediated prevention of M2 cleavage led to decreased levels of p62 detected by immunoblot (**Figure 31 C**).

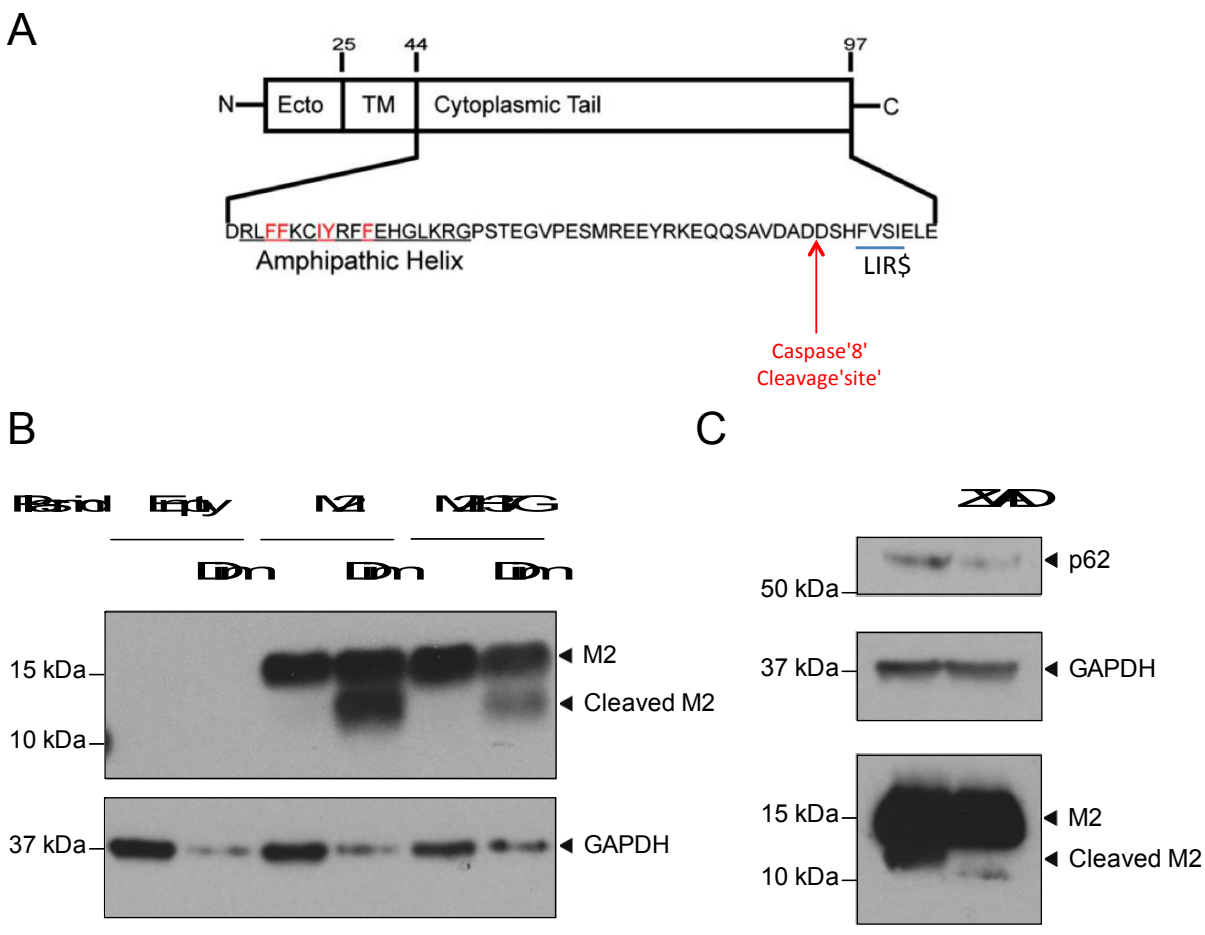

Figure 31: M2 and M2H37G^{DD} are cleaved by caspase 8 and/or caspase 8-activated effector caspases.

(**A**) M2 harbors a caspase 8 cleavage site in its cytoplasmic tail between its amphiphatic helix its LC3-interacting region involved in membrane curvature and interaction with LC3, respectively[28,138]. Adapted from Ref. 28. (**B**) NIH3T3 cells expressing dimerizable caspase 8 were transfected with control, M2 or M2H37G-expression plasmid for 70 h with dimerizer (dim.) added for the last 20 h before immunoblot monitoring of M2 and GAPDH. (**C**) WT MEFS were infected with PR8 IAV at MOI 10 for 20 h with or without post-infection addition of ZVAD. The levels of p62, GAPDH and M2 were monitored by immunoblotting.

In summary, M2 and M2H37G are able to induce aborted autophagy in cells in the context of IAV infection but cannot block autophagy maturation when autophagy was stimulated by other means. Data suggest that IAV-induced caspase activation leads to the cleavage of M2 that correlates with increased p62 degradation. M2 cleavage by caspase may be a necessary event allowing M2 to block autophagosome maturation.

DISCUSSION AND FUTURE DIRECTIONS

I. Novel cellular models allow fine tuning of autophagy

Our study describes the generation of new cellular models in which the capacity of a cell to undergo autophagy can be experimentally controlled through stabilization of ATG5^{DD} or ATG7^{DD} in *Atg5*$^{-/-}$ or *Atg7*$^{-/-}$ MEFs, respectively. Importantly, autophagy is mainly regulated by kinase activity and phosphorylation of proteins[168,169]. Several mechanisms of transcriptional regulation of *Atg* genes have been uncovered, but it seems that they act as a feedback mechanism to renew autophagy proteins when autophagy is induced, to keep the cell autophagy-competent[168,170]. Stabilization of ATG5^{DD} or ATG7^{DD} is therefore unlikely to stimulate autophagy by itself but renders the cell autophagy-capable. This constitutes a key advantage of my model as, as introduced previously, among the commonly used chemicals to study autophagy are mTOR inhibitors, which not only harbor important off-autophagy effects (potentially leading to artifactual phenotypes and erroneous data interpretation) but also stimulate autophagy[137]. In the case of IAV for example, this autophagy overstimulation may prevent researchers from understanding the impact of autophagy perturbation by the virus.

ATG5 has been shown to possess non-ATG5–ATG12—i.e. non-autophagy-related—properties[153,171]. *Atg5*$^{-/-}$ MEFs expressing ATG5K130R^{DD} allow to control for such off-autophagy effects. Strikingly, stabilization of ATG5K130R^{DD} in *Atg5*$^{-/-}$ cells induced no statistically significant changes in gene expression among the 561 immunity, stress and death-related genes. This suggests that neither Shield1, nor the DD itself, nor ATG5K130R impacts these genes. Unlike stabilization of ATG5K130R^{DD}, the stabilization of ATG5^{DD} led to changes in the levels of several genes including the pro-apoptotic protein BID, the negative regulator of TLR2, TLR4, and IL1R signaling TOLLIP[172] that has also interestingly been showed to act as an autophagy receptor by interaction with LC3 and ubiquitinated protein aggregates for their selective degradation by autophagy[173,174].

Importantly, the immune-related transcriptome analysis of ATG5^{DD} and ATG5K130R^{DD} cells revealed that the inter-clonal cell line variability (axes 1 and 2 in the PCA in **Figure 13 A**) is far greater than the autophagy competence-induced variability. This suggests that, as suggested in the introduction, comparing *Atg* gene-deficient cell lines with their WT counterparts may lead to inaccurate conclusion of autophagy involvement in some mechanisms, when in fact the observed phenotype results from genetic drift between cell lines.

Of note, rescuing autophagy capacity did not impact cell growth, which may be explained by the fact that I worked with nutrient-rich media. Alternatively, the parental cell lines from which autophagy-inducible cells were made being autophagy-deficient, they may have adapted to grow well without autophagy.

II. Autophagy does not impact viral replication and cell death

Using this inducible-autophagy cellular model, I showed that the propensity of cells to get infected by IAV was independent of their autophagy capacity. This suggests that autophagy is not involved in viral docking, entry and early replication.

Autophagy did not impact viral RNA expression and NP and M2 protein levels in infected cells at later timepoints, which argues that autophagy is also dispensable for viral intracellular replication efficacy.

Data showed that IAV induces autophagy and apoptosis in a cell-intrinsic manner, with some cells harboring hallmarks of both autophagy and apoptosis. However, autophagy capacity of cells did not impact IAV-induced cell death in my model. These data contradict Gannage and colleagues' findings, since they witnessed substantially more cell death in *Atg5*$^{-/-}$ MEFs as compared to WT MEFs[88]. This may be explained by the differences in viral stock or differential cell line basal phenotype (see previous section for considerations on cell line-to-cell line variability).

III. Autophagy perturbation by IAV: impact on inflammation

1. Autophagy limits IFN-β simulation post infection in an NS1-independent fashion.

Portions of the manuscript "Autophagy represses the early interferon-β response to influenza A virus resulting in differential expression of interferon stimulated genes" submitted to Autophagy have been reproduced here.

During IAV infection, the induction of specific ISGs was reduced when autophagy was active. Among the most impacted ISGs was *Cd274* (coding for PD-L1), a gene that has been

shown to negatively regulate $CD8^+$ T cell effector function, with a notable role in the response to pandemic IAV strains[175]. The use of a mutant ATG5K130R cell line and ATG7 stabilization in *Atg7*$^{-/-}$ cells demonstrated that ATG5–ATG12 complex–mediated autophagy plays a critical negative role in regulating CD274 expression levels. Autophagy also negatively impacted MHC I expression at the cell surface. I hypothesize that the negative impact of $ATG5^{DD}$ stabilization on several MHC I presentation pathway genes (*Psmb10, Tapbp, H2-K1, B2m* and *Tap1*), may be an underlying reason for the decreased surface expression of MHC I complexes. These findings are in agreement with Loi and colleagues, who recently reported that autophagy-deficient dendritic cells express more MHC I on their surface at steady state and more efficiently prime anti-IAV–specific $CD8^+$ T cell responses.[176] Importantly, they did not observe any impact of autophagy on MHC I heavy chain transcription or traffic to the plasma membrane but report that *Atg5*/*7* deficiency compromises endocytosis and degradation of class I MHC complexes. This mechanistic study was performed on non-infected DCs. In line with these findings, I also witnessed that autophagy incompetence led to higher presence of MHC I complexes at the cell surface, which, although caution should be taken when comparing cell lines as different as MEFs and DCs, may be resulting from the same mechanism (described in their model, see **Figure 32**). However, my results suggest that, in the context of IAV infection, the negative impact of autophagy on MHC I upregulation may, at least in part, be the result of limitation in IFN-β–induced stimulation of several genes belonging to the class I MHC pathway.

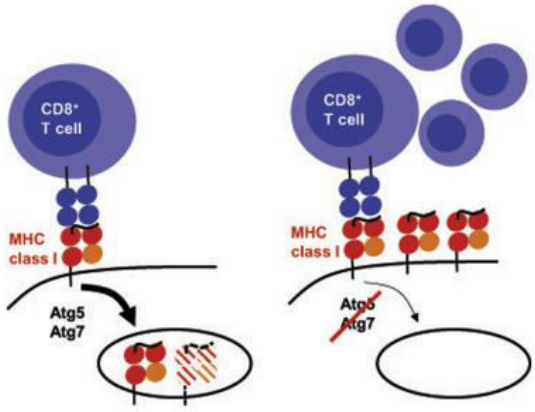

Figure 32: Model proposed by Gannage's group for the increased expression of class I MHC at the surface of DCs.
Class I MHC of DCs are endocytosed and degraded. This process is negatively impacted by autophagy deficiency. From the graphical abstract of Ref. 176.

The decreased expression of key proteins involved in immune regulation and/or defense against IAV infection was a result of autophagy impacting *Ifnb1* expression. The modulation of IFN-β effect of autophagy was measurable as early as 1.5 h post-infection. Interestingly, the best described mechanism by which IAV inhibits PRR signaling and subsequent IFN-β and ISG induction is by the action of NS1.[177] However, NS1 is only present in minute amounts within incoming virions and it is suggested that IAV replication and *de novo* NS1 synthesis within IAV-infected cells is necessary for NS1 to exert its anti–IFN-β function[37,178]. However, Liedmann and colleagues argued that shielding of IAV 5'triphosphate RNA by the polymerase complex is a mechanism that limits IFN-β induction early after infection (i.e., before replication commences)[37]. Here I propose another mechanism by which IAV limits early IFN-β responses through manipulation of autophagy (**Figure 33**).

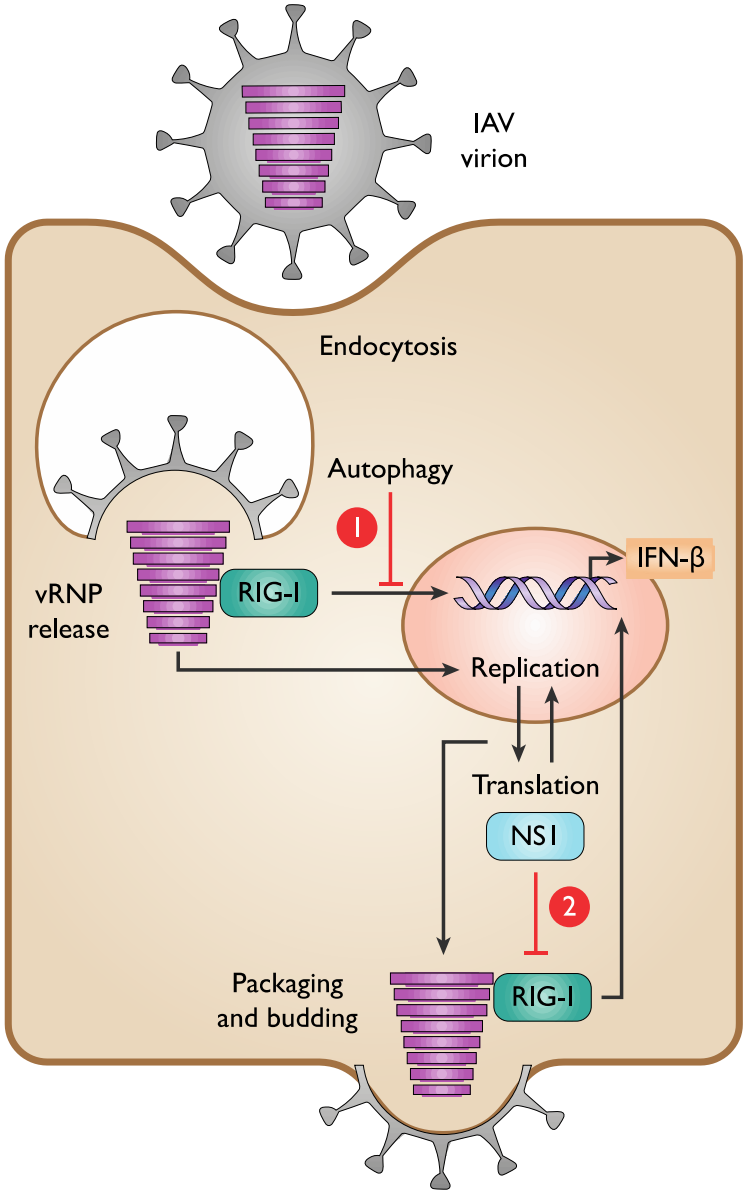

Figure 33: Model of early and late prevention of RIG-I detection in the course of viral infection.
After IAV virion is endocytosed, viral RNPs (vRNPs), which are released in the cytoplasm, are sensed by RIG-I. This event leads to stimulation of *Ifnb1* transcription but is repressed by autophagy (1), which is induced by the virus. vRNPs then translocate to the nucleus where vRNAs are produced and hidden from RIG-I, which resides in the cytosol (see introduction). Translation of IAV NS1 protein occurs and allows the inhibition of RIG-I activation when vRNPs exit the nucleus and traffic to the plasma membrane for virion packaging and budding (2); this constitutes a later IFN-β–inhibition mechanism.

2. M2 cleavage as a switch between complete and aborted autophagy?

I observed that IAV required the autophagy machinery to potently repress IAV-induced IFN-β induction, which led to the dampening of the host ISG response. Importantly, the impact of IAV on autophagy is still debated with studies arguing that autophagy flux is induced by IAV while other work has shown that IAV blocks the maturation of autophagosomes through the activity of M2[131,132,88,130]. Moreover, the laboratories that showed that M2 blocks autophagosome maturation do not agree about the requirement for the ion channel activity of M2 in its ability to block maturation[88,132].

My results suggest that autophagy flux is induced early post-infection (1 h), but at later times post-infection (20 h), autophagy maturation is compromised. I suggest that at early stages post-infection, IAV induces complete autophagy due to lower amounts of M2 present in the cell; and during the course of viral gene expression, elevated intracellular levels of M2 begins to inhibit autophagosome–lysosome fusion, as previously reported by the Munz laboratory[88]. The impact of this switch from complete to abortive autophagy on the inflammatory state of infected cells remains to be elucidated.

M2H37G^{DD} stabilization in WT MEFs showed that this protein is capable of blocking autophagy maturation only in the context of viral infection in a process that involves caspase activation. Activation of caspase 8 and/or downstream effector caspases was also involved in cleavage of M2 (and M2H37G). Data are missing and experiments in collaboration with Jeremy Rossman's team using IAV with uncleavable M2 will be performed, with the hypothesis that caspase activation induces abortive autophagy by cleaving M2. In other words, M2 cleavage product(s) may act as the autophagosome maturation inhibitor. Interestingly, caspase activation and subsequent apoptosis stimulation are thought to be required at later stage of infection to produce viral progeny (see introduction). Caspase activation might also allow the inhibition of late stage IFN-β stimulation in the infected cells in an autophagy-dependent manner.

3. Complete or abortive autophagy: implications for IFN-β production

The observation that autophagy inhibits IFN-β induction may also apply to other viral models. Indeed, autophagy has been shown to limit VSV-induced IFN-β[115,116]. Using poly(I:C) to mimic viral PAMPs (poly(I:C) is a TLR3, RIG-I and MDA5 agonist[117]) different laboratories have proposed two models. In the first one, formation of the ATG5–ATG12 complex has been proposed to limit RIG-I signaling through direct association with RIG-I and MAVS[115].

Alternatively, mitophagy could induce a decrease in ROS and MAVS presence in the cells, thereby limiting RIG-I signaling[116].

It is unclear whether these models could explain my observations using the autophagy-tunable cell systems. In light of the study of Jounai and colleagues[115], one hypothesis could be that autophagy induction by IAV induces ATG5–ATG12 complex, which limits RIG-I signal signaling. Abortive autophagy then induces accumulation of autophagosomes, which are decorated by ATG5–ATG12 complexes, thereby further limiting RIG-I signaling (**Figure 34 A & B)**. Besides, when autophagy is aborted, mitochondria that are trapped in non-matured autophagosome may not be able to signal because of their isolation within the double membrane of autophagosomes (**Figure 34 C & D**).

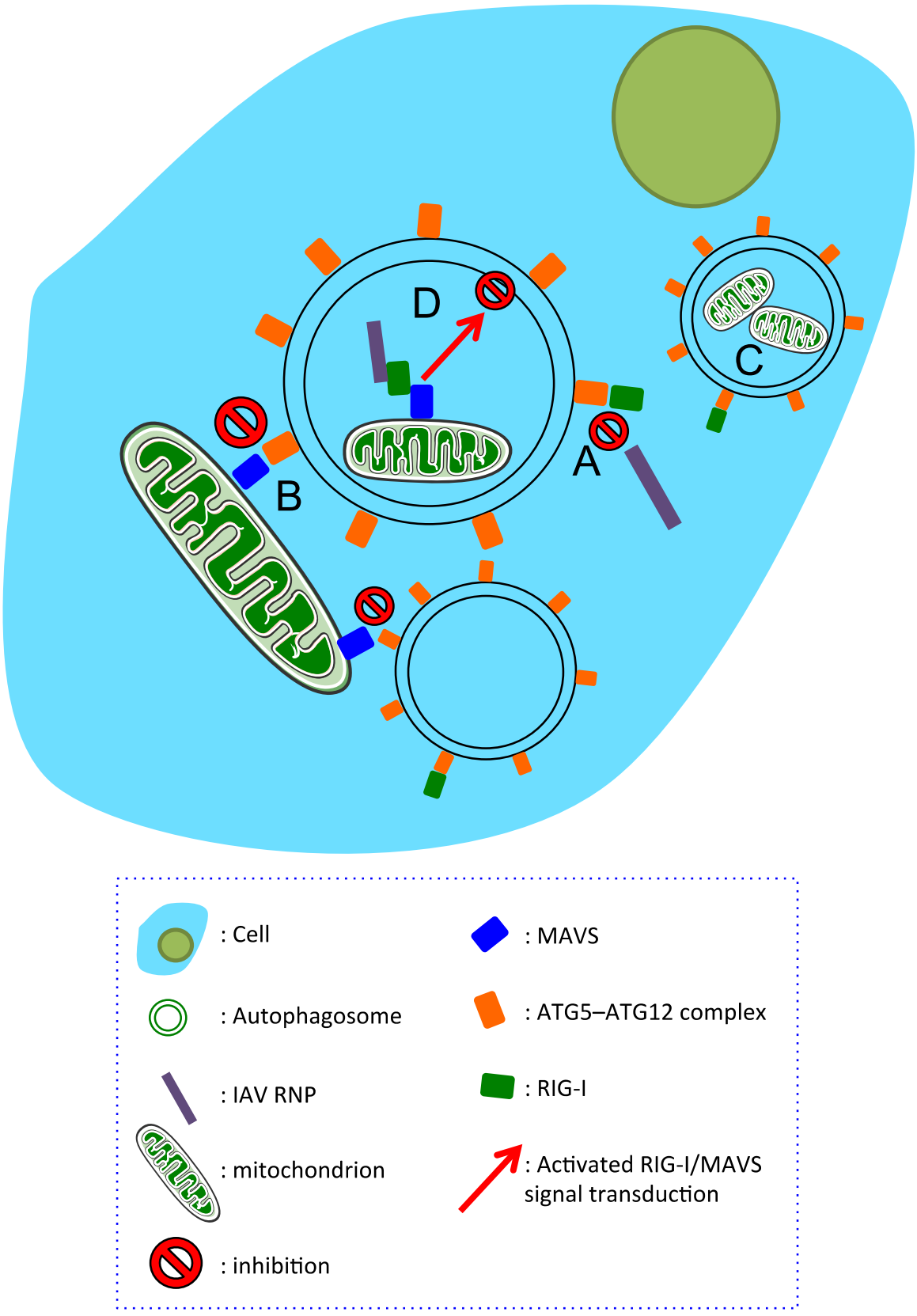

Figure 34: Hypothetical model showing how abortive autophagy might limit RIG-I–mediated type I IFN induction in the context of IAV.
Accumulation of non-matured autophagosomes decorated by ATG5–ATG12 might prevent RIG-I (**A**) and MAVS (**B**) stimulation by viral ribonucleoproteins (vRNPs) through direct interaction. Mitochondria isolation within these structures may reduce MAVS accessible to

cytoplasmic vRNPs (**C**). Mitochondria, which MAVS has been activated by RIG-I might not be able to induce productive signal transduction due to their isolation within the double membrane autophagosome (**D**).

Interestingly, Coxsackievirus, human parainfluenza virus type 3 and rotavirus RNA viruses that activate RIG-I and/or MDA5[179,180,181,182] have been proposed to induce abortive autophagy[183,184,185]. Although the impact of such perturbation on PRR induction and signaling have not been studied, I hypothesize that this induction of abortive autophagy may limit IFN-β induction by these viruses.

4. Potential implications in vaccine development and therapy improvement

My new *in vitro* model permitted restoration of autophagy capacity in otherwise autophagy-incompetent cells, allowing us to uncover the negative impact of IAV infection on ISG expression while avoiding potential confounding effects of genetic drift between cell lines. As the inflammatory response to IAV impacts viral propagation and symptom severity, future studies will be important to determine the role of autophagy *in vivo* in infected lung epithelial cells.

A better understanding of viral perturbation of autophagy and its impacts on inflammation may, in the future, help fight IAV through new antiviral molecules targeting autophagy or autophagy perturbation capacity of M2 to tune the inflammatory response in order to limit viral fitness and/or decrease host symptom severity. Alternatively, designing live attenuated viruses modified in their ability to hijack autophagy, leading to improved protective immunity may be possible. For example, viruses devoid of M2-coding capacity and/or of M2 autophagy-impacting region (mutated in the LIR, the amphiphatic helix, and/or in the caspase cleavage site) may be impacted in their ability to prevent inflammation and induce more potent immune responses. Interestingly, this study showed that autophagy incapacity particularly stimulated IFN-β. Type I IFNs are known to potentiate the anti-IAV cytotoxic T lymphocytes cell response *in vivo*[186,18,187] and to bias the adaptive immune response toward a $CD8^+$ T cell response in different models[188]. Tuning IAV live attenuated vaccine autophagy perturbation capacity may allow the robust induction of IAV-specific $CD8^+$ T cells that is anticipated to allow long lasting cross-strain/cross-subtype immunity through targeting of more conserved IAV intracellular epitopes that are not accessible to antibodies[189].

IV. Cell-to-cell variability and contribution to inflammation

As highlighted in the introduction, infection with low MOI results in most infected cells expressing only subsets of IAV proteins *in vitro*, resulting in the incapacity of most infected cells to produce infectious viral progeny[32]. Taking advantage of this observation as a means to study the impact of viral protein—in particular M2—expression on inflammation, I tested the hypothesis that infected cells failing to express M2 have dampened inflammatory gene expression due to the absence of M2-mediated autophagy perturbation, using single-cell approaches; preliminary results are described hereafter. First, I tested whether I could make the same observation as Brooke and colleagues[32] at the IAV RNA level, or whether the failure of expressing some IAV proteins is the result of translational/post-translational defects.

1. Infected cells are heterogeneous in the IAV RNA they express

I infected WT MEFs for 16 h at low MOI and used single cell RT–qPCR to monitor the expression of three IAV RNAs, namely NP, NS1 and M2. Among the 46 cells analyzed, only 7 expressed all three measured IAV RNAs (**Figure 35**). Of note, the percentages of cells expressing at least NP and NS1 among infected cells were similar to previous studies at the protein level[32] (71.5 and 69.5% respectively).

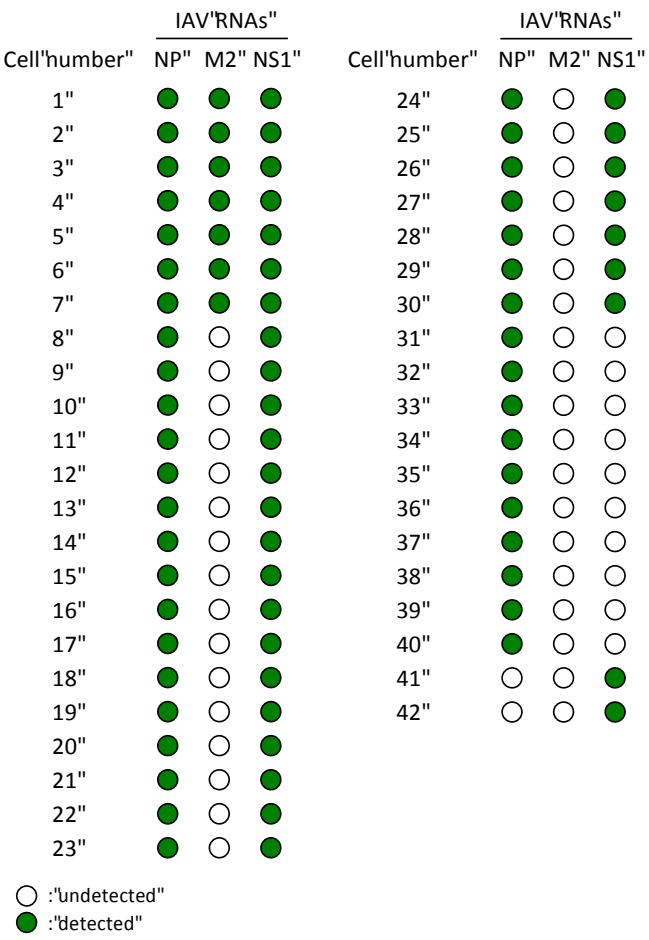

Figure 35: Most IAV-infected cells fail to express at least one IAV RNA.
WT MEFs were infected with IAV at MOI 0.07 for 16 h. After harvest, cells were sorted, lysed, RNA was extracted and reverse transcribed before cDNA pre-amplification (using the Fluidigm C1 technology). qPCR was performed to detect IAV NP, NS1 and M2 RNA. Each row represents a cell. Samples with detected cDNA were the ones with a sigmoid fluorescence curve.

2. Infected cells that express M2 show less *Cxcl10* expression than other infected and bystander cells

Flow cytometry data confirmed in WT MEFs, at 20 h post infection, that some infected cells failed to express M2 (**Figure 36 A**). After fluorescence-activated cell sorting of NP^-M2^-, NP^+M2^- and NP^+M2^+, I confirmed that these three populations expressed the expected IAV RNA subsets (**Figure 36 B**). Moreover, expression of *Cxcl10*—a type I, type II[160] and type III[190] IFN and NF-κB–induced[191] pro-inflammatory cytokine—was induced by infection in NP^-M2^- and NP^+M2^- cells, and to a lesser extent in NP^+M2^+, suggesting that M2 may exert an anti-ISG function (**Figure 36 C**).

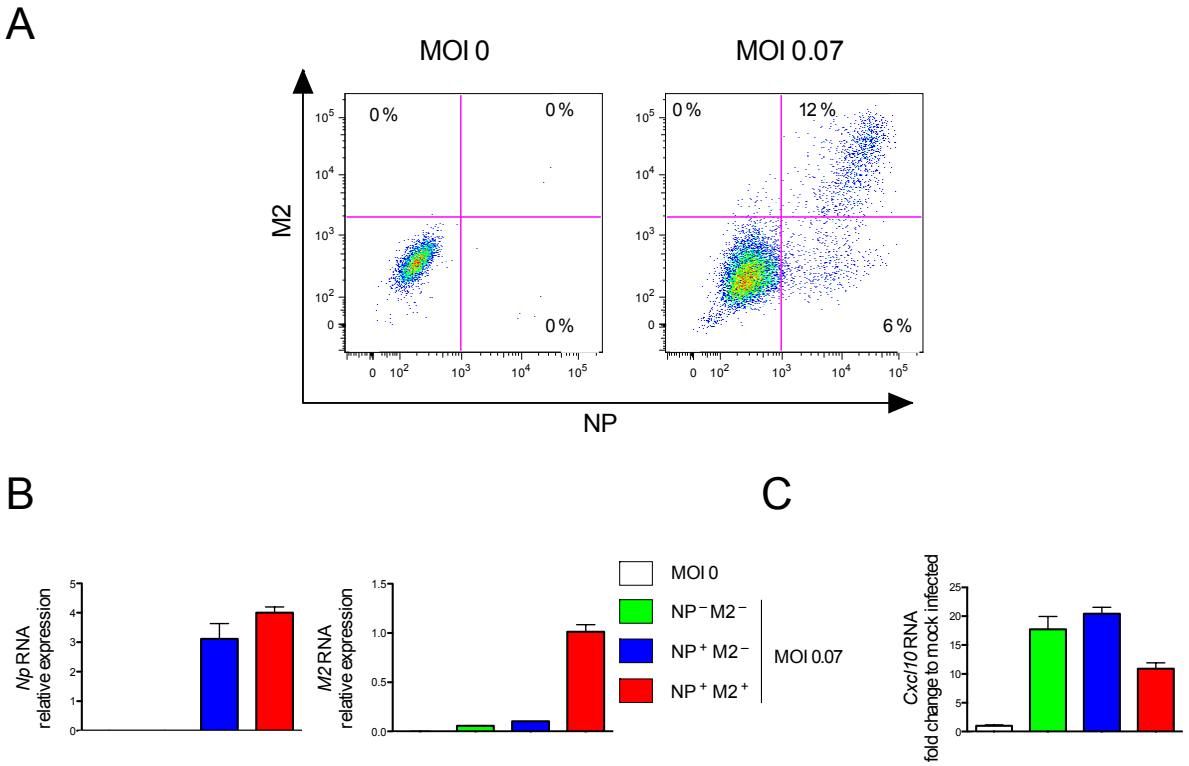

Figure 36: Infected cells that fail to express M2 show higher levels of *Cxcl10* RNA after infection.
WT MEFs were infected with PR8 IAV at MOI 0.07 for 20 h. (**A**) Flow cytometry data showing NP and M2 expression in mock-infected (MOI 0) or infected sample. (**B**, **C**) In a different experiment, $NP^{-}M2^{-}$, $NP^{+}M2^{-}$ and $NP^{+}M2^{+}$ were sorted and RNA extraction and RT–qPCR was performed to monitor *Np* and *M2* expression (**B**) as well as *Cxcl10* expression in the different populations.

3. Possible implications in the establishment of inflammation

Interestingly, and in line with Brooke and colleagues, I observed that some cells failed to express NS1 RNA/protein[32]. Given that NS1 is a key viral protein acting to limit IFN-β and other inflammatory cytokines (see introduction), I hypothesize that cells failing to express it are the major contributors to the establishment of inflammatory microenvironment, acquisition of anti-viral vigilance phenotype by bystander cells and recruitment of innate then adaptive immune cells (**Figure 37**).

Similarly, given that autophagy perturbation by IAV limits IFN-β induction, cells that fail to express M2 may secrete more IFN-β and pro-inflammatory cytokines as compared to those that do express it, as I observed for *Cxcl10* (**Figure 37**).

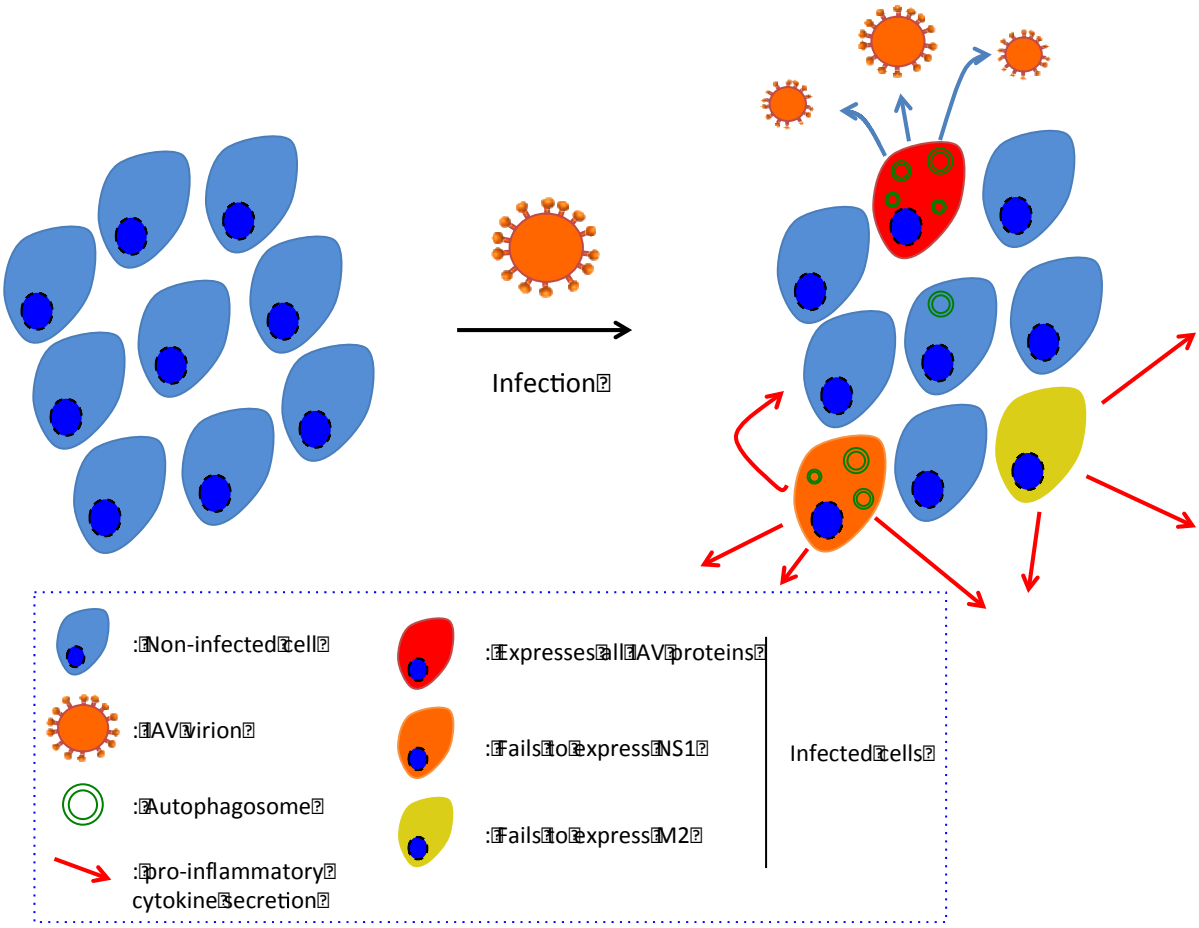

Figure 37: Cells that fail to express anti-PRR signaling IAV proteins may be the major source of pro-inflammatory cytokines.
When infected with IAV at low MOI, some cells fail to express at least one IAV protein. Cells that fail to express NS1 may secrete high levels of pro-inflammatory cytokines. Cells that do not express M2 are unable to perturb autophagy and are therefore also better pro-inflammatory cytokine producers. Finally, cells that express all IAV proteins have strong viral protein and autophagy perturbation preventing pro-inflammatory cytokine secretion; they are the producers of infectious progeny, estimated to represent 1 out of 10 infected cells. Ref. 32.

V. Autophagy and cancer

1. Autophagy, a double-edged sword in cancer

Autophagy is often deregulated in cancer and is generally believed to be an anti-tumorigenesis mechanism while being pro-tumor development and pro-malignant phenotype

acquisition[192,193]. Decrease/loss of autophagy has been proposed to cause misfolded, potentially harmful, protein accumulation, mitochondria clearance defects leading to genotoxic ROS accumulation and cell death accompanied by inflammation, which all have pro-tumor properties[193]. Conversely, autophagy pro-tumor development role is presumably linked to the increase in stress tolerance. Autophagy being involved in nutrient and energy homeostasis, it may allow tumors to thrive in the biologically hostile environment limited in glucose and oxygen[193]. Moreover, the high protein synthesis rate in cancer and increased mutation rate leading to more damaging misfolded proteins (which activate the unfolded protein response and apoptosis) and a stronger need for amino-acid available pool may also render cancer cells addicted to protein catabolism pathways such as autophagy as they are to the proteasome[194,195].

2. $CD8^+$ T cells, type I IFN, autophagy and cancer

It is becoming clear that successful anti-tumor chemotherapies necessitate the activation, recruitment and activity of tumor cell killing $CD8^+$ T cells[196]. The priming of tumor antigen-specific $CD8^+$ T cells relies on cross-presentation, a process allowing DCs to present antigens acquired from engulfed dying cells onto MHC I thereby stimulating $CD8^+$ T cells harboring a cognate TCR receptor[16]. Importantly, the way cells die has been correlated to the efficiency of cross-priming of $CD8^+$ T cells by DCs[197,18,167].

Autophagy in the dying cells (chemotherapy-induced death) was proposed, in a heterotopic model of colon carcinoma, to potentiate ATP release from chemotherapy-exposed dying cells, thereby potentiating the recruitment of T lymphocyte and DCs in the tumor bed[198].

Type I IFN axis promotes $CD8^+$ T cell response through potentiation of cross-presentation[199,18]. Interestingly, anthracycline-based chemotherapies were shown to induce an immune response mimicking those induced by viral pathogens, in part explaining the efficiency of chemotherapies in an IFN-β and CXCL10-mediated fashion[200]. The use of cellular vaccination therapies, using virus-infected cancer cells as vaccines, may therefore allow the induction of potent anti-tumor $CD8^+$ T cell response in cancer patients.

3. Autophagy, virotherapy and cellular anti-cancer therapy

Oncolytic viruses are promising and anticipated to become part of our anti-cancer arsenal. It seems that their immunogenicity may be key for their anti-cancer potential[201,202]. I

believe that strategies using dying cancer cells within which autophagy is finely tuned may allow the elicitation of a potent anti-cancer cytotoxic T lymphocyte (CTL)-mediated immune response. In this context, using IAV as a model shows a three-pronged interest: it elicits an inflammatory response in the dying cell, it induces abortive autophagy (see results section) and is a potent inducer of dying cell antigen-specific CTL response through cross-presentation *in vivo*[18]. Limiting autophagy in the context of virus-mediated immunotherapy may potentiate the mounting of anti-tumor immune response through potentiation of IFN-β secretion. For example, infecting patient cancer cells *ex vivo* by live attenuated IAV while preventing autophagy perturbation in the infected cells by chemical treatment or by using M2-mutant or ΔM2 viruses before reinjecting the cells intradermally to the patient may allow potent type I IFN-boosted induction of $CD8^+$ T cells response directed toward tumor antigens.

MATERIAL AND METHODS

Cell lines, cell growth media, treatments, and viruses

Atg5$^{+/+}$ cells and *Atg5*$^{-/-}$ MEFs were obtained from Christian Munz, University of Zurich, Switzerland. *Atg7*$^{-/-}$ MEFs were obtained Stephen Tait, University of Glasgow. All cell lines in this study were cultivated in completed growth medium, comprised of DMEM with high glucose, pyruvate, GlutaMAX, and supplemented with non-essential amino-acids, HEPES buffer, penicillin/streptomycin (all reagents, ThermoFisher Scientific) and 10% fetal calf serum (GE Healthcare, A15-502). Shield1 (Clontech, 632188) was added at a final concentration of 1µM in growth media. EtOH, the solvent for Shield1, was used as a control at a 1:1,000 dilution in growth media. Treatments were used at the following concentrations: chloroquine (Sigma, C6628), 50 µM; PP242 (Selleck chemical, S2218), 1 µM; MG132 (Sigma, C2211) 10 µM; ZVAD (R&D systems, FMK001) 50 µM; recombinant interferon-beta, at indicated concentrations (BioLegend, 581302). Blocking IFNAR antibody (BD Pharmingen, 561183) or isotype control (BD Pharmingen, 553447) were used at 10 µg/mL, added to culture media 1 h before infection for the duration of the experiment. Influenza A/PR/8/76 (PR8) and ΔNS1 PR8 were purchased as purified allantoic fluid or purified antigen respectively from Charles River Laboratories (Spafas, CT, USA).

Lentivirus production and clonal stably-modified cell line generation

pLVX pTuner lentiviral vector (Clontech) with a puromycin resistance gene and destabilization domain at the 5'P end of the multiple cloning site was from Clontech. Mutagenesis PCR allowed the introduction of an AgeI site and 3 glycin codons (to increase flexibility between the DD and ATG5 protein) at the 5'-terminus of the ATG5 coding site in the pmCherry–ATG5 plasmid (Plasmid #13095; Addgene). Mutagenesis qPCR was performed using Phusion polymerase (ThermoFisher Scientific) following the manufacturer's protocol and using primers: ACCGGTGGAGGAGGAACAGATGACAAAGATGTGCTT and CATGGTACCGTCGACTG. The ATG5^{DD} coding insert was then subjected to using AgeI and BamHI restriction enzyme cleavage and ligated into pLVX pTuner lentiviral vector (all enzymes from New England Biolabs). The final plasmid (pATG5^{DD}) was confirmed to have the expected sequence.

For the generation of the ATG5K130R^{DD} coding plasmid, mutagenesis PCR was performed using Phusion polymerase to change codon 130 from AAA to CGA in the pATG5DD plasmid with the primers: CGAGAAGCTGATGCTTTAAAGCA and ATACACGACAT AAAGTGAGCC. pBabeATG7^{DD}, a retroviral vector coding for ATG7^{DD},

was a generous gift from Douglas Green, St. Jude Children's Research Hospital. Lentiviruses (from pATG5^{DD} and pATG5K130R^{DD}) and retroviruses (pATG7^{DD}) were produced and *Atg5*$^{-/-}$ or *Atg7*$^{-/-}$ MEFs were infected. pCAGGS-WSNM2H37G plasmid (a kind gift of Christian Münz laboratory, described in [88]) was used to generate pLVX-M2H37G^{DD}and cells stably expressing M2H37G^{DD}. Puromycin was used at 4 µg/mL for 1 week for selection (ThermoFisher Scientific, A11138-03) before single cell cloning and phenotyping were performed.

IAV infection

For infection, adherent cells were washed with growth medium without fetal calf serum. Growth medium, without serum, containing IAV was added to cells and plates were incubated at 37 °C for 1 h with gentle shaking every 15 min. Cells were then washed with complete growth medium before adding fresh complete growth medium with or without additional treatments.

Immunoblotting

Cells were harvested by trypsinization, centrifuged, and resuspended in 100 µl per million cells in lysis buffer: 1% Nonidet P40 substitute (Sigma, 74385) with protease inhibitor (Sigma, 11836145001). Protein concentration in the resulting supernatants was determined by BCA assay (ThermoFisher Scientific, 23225) following lysis on ice and clarification by centrifugation according to the manufacturer's guidelines. 30 µg of protein per sample were prepared in Lithium Dodecyl Sulfate sample buffer (ThermoFisher Scientific, NP0007) with dithiothreitol (DTT, 20 mM final concentration) and loaded in 4–12% gradient polyacrylamide gel (Biorad, 3450124). Following transfer, polyvinylidene fluoride membranes (BioRad, 1704157) were blocked for 1 h in 5% w/v non-fat dry milk in TBS with 0.05% Tween 20 (Sigma P5927) (blocking solution). Membranes were then incubated for 15 h in 1:1,000 dilution of the following antibodies in blocking solution with gentle shaking at 4 °C: anti-ATG5 (Abcam, ab108327), anti-GAPDH (CST, 2118), anti-LC3B (CST, 2775S), anti-p62 (CST, 5114) anti-M2 (Abcam, ab5416), anti-IκBα (CST, 9242) and anti-PSMB10 (Abcam, ab77735) antibodies. Membranes were then incubated in 1:1,000 horseradish peroxidase-conjugated anti-mouse antibody (CST, 7076S) or anti-rabbit antibody (CST, 7074S) in blocking solution for 1 h at room temperature with gentle shaking. Membranes were revealed with Supersignal Enhanced Chemoluminescence Substrate (ThermoFisher

Scientific, 34080) according to the manufacturer's guidelines and exposed to film. For quantitation, ImageJ software was used.

Intra-incubator microscopy

Cells were plated at 10,000 cells per well in 24 well plates. Images were taken every hour using Incucyte ZOOM System (EssenBioScience). When apoptosis was monitored, Yopro-1 iodide was added to the cell culture media (ThermoFisher Scientific, Y3603). For NF-κB activity, cells were transfected with GFP NF-κB reporter plasmid with Lipofectamin2000 (ThermoFisher Scientific, 11668019) according to the manufacturer's protocol. Analysis was performed using Incucyte ZOOM software (EssenBioScience).

Flow cytometry and imaging flow cytometry

Cells were harvested and washed as for immunoblotting. After washing, cells were incubated for 20 min in 1:500 dilution of LIVE/DEAD Fixable Violet Dead Cell Stain (ThermoFisher, L34955) in PBS, then 30 minutes in 1:100 antibody dilution for surface staining, all at 4 °C. Antibodies included: APC-conjugated anti-mouse CD274 (BD Pharmingen, 564715) or PE-conjugated anti-mouse H-2K^{b} (BD Pharmingen, 553570).

For intracellular staining (ICS), cells were fixed using BD Cytofix/Cytoperm Fixation and Permeabilization Solutions (BD Biosciences, 554722). Cells were then washed twice in BD Perm/wash buffer (PWB, BD Biosciences, 554723). Immunostaining was performed at 4 °C for 45 min with 1:100 dilution of FITC-conjugated anti-influenza A Virus nucleoprotein antibody (Abcam, ab20921) or 1:500 dilution of anti-influenza A virus M2 protein antibody (Abcam, ab5416) in PWB for 45 min at 4 °C. For M2 staining, cells were then incubated in 1:500 dilution of Alexa Fluor 647 goat anti-mouse IgG (H+L) (Jackson ImmunoResearch, 115-606-062) for 45 minutes at 4 °C. Cells were then washed in PWB buffer twice and in PBS once before resuspension in PBS and acquisition using a BD LSR Fortessa flow cytometer. Data analysis was performed using FlowJo 9 (Flowjo, LLC).

For imaging flow cytometry, the antibodies used for ICS were: mouse anti-LC3 antibody (MBL International) at 1:500 dilution, rabbit anti-cleaved caspase 3 antibody (CST, 9661) at 1:500 dilution, mouse FITC-conjugated anti-influenza A virus nucleoprotein antibody (Abcam, ab20921) at 1:100 dilution. Staining of LC3 and cleaved caspase 3 were performed before washing and staining with Alexa Fluor 647 goat anti-mouse IgG (H+L) (Jackson ImmunoResearch, 115-606-062) or Goat anti-Rabbit IgG (H+L) Secondary

Antibody, Alexa Fluor546 conjugate (ThermoFisher, A-11035). After washes, the anti-NP antibody was introduced. Cells were then washed in PWB buffer twice and in PBS once before resuspension in PBS and acquisition using Amnis Imagestream X imaging flow cytometer. Data analysis was performed using Ideas software (Amnis).

RNA extraction, Reverse transcription, and qPCR

For RNA extraction, cells were harvested and washed as for protein extraction. High pure RNA isolation kit (Roche, 11828665001) was used to extract RNA according to the provider's protocol. Reverse transcription (RT) was performed using Maxima reverse transcriptase (ThermoFisher Scientific, catalogue number: EP0741) and random primers (ThermoFisher Scientific, SO142). Taqman primer/probe mixes were used for cDNA quantification of *Hprt1* (Mm03024075_m1), *Ifnb1* (Mm00439546_s1), *Cd274* (Mm00452054_m1), and *Cxcl10* (Mm00445235_m1). For viral gene detection, we designed the following primer/probe sets:

	primer 1	primer 2	FAM MGB probe
NS1	CACTGTGTCAAGCTTTCAGGTAGATT	GCGAAGCCGATCAAGGAAT	TTTCTTTGGCATGTCCG
M1	TCCAGTGCTGGTCTGAAAAATG	GGATCACTTGAACCGTTGCAT	AAAATTTGCAGGCCTATCA
M2	ACCGAGGTCGAAACGCCTAT	AAAAAAGACGATCAAGAATCCACAAT	TGCAGATGCAACGGT
NP	CGGAAAGTGGATGAGAGAACTCA	AGTCAGACCAGCCGTTGCAT	CCTTTATGACAAAGAAGAAA
PB1	TGTCAATCCGACCTTACTTTTCTTAA	TGTTGACAGTATCCATGGTGTATCC	CCAGCACAAAATG

Custom gene expression assays were synthesized by ThermoFisher Scientific. 2 uL of cDNA diluted 4 times in water was used at concentration per qPCR reaction. qPCR was performed using Taqman Fast Advanced Master Mix (ThermoFisher Scientific) according to the provider's protocol. StepOnePlus Real-Time PCR System (ThermoFisher Scientific) was used for thermocycling and data acquisition using the Fast Advanced Master Mix recommended conditions. The StepOnePlus software (ThermoFisher Scientific) was used for analysis.

Power calculation for RT–qPCR

Standard deviation of Ct values did not show mean dependence. We therefore modeled Ct values of technical replicates for gene *i* as independent normally distributed random variables with mean μ_i and standard deviation σ (this latter parameter being independent of the gene). Estimation of σ was performed using pooled variance. RNA levels are compared using normalized data (ΔCt values), and by error propagation, ΔCt values follow a normal distribution with standard deviation $\sigma' = \sqrt{2}\,\sigma$. The power curve was computed using the function power.t.test in R (CRAN), with parameters sd = σ', power = 0.8, sig.level = 0.05 and delta = log2(fold change).

Nanostring nCounter assays, normalization, and analysis

Infected or treated cells were harvested and RNA was extracted as detailed above. nCounter Mouse Immunology immunology kit was used, following Nanostring guidelines. Raw RNA counts were exported from the nSolver Analysis Software (Nanostring).Raw RNA counts were normalized by housekeeping genes to account for the inter-sample variation of RNA quantity. The 14 housekeeping genes were used to normalize the nCounter data for steady state effect of Shield1 treatment of $ATG5^{DD}$ and$ATG5K130R^{DD}$-expressing cells (non-infected samples). For infected samples with or without autophagy, the selected housekeeping gene pool was built from the 14 candidate control genes provided by Nanostring, following the geNorm method.[158] Briefly, for each two genes $j \neq k$, pairwise variation coefficient V_{jk} is defined as

$$V_{jk} = \mathrm{sd}_i\left(\log_2\left(\frac{a_{ij}}{a_{ik}}\right)\right),$$

where a_{ij} is the number of counts for the gene j in the sample i. The gene stability measure M_j for control gene j is the arithmetic mean of all pairwise variations V_{jk} for $k \neq j$. M_j evaluates the degree of correlation of gene j to other control genes (the smaller M_j is, the more correlated gene j is to other control genes). Genes were ranked by increasing M (**Figure 21 A**), and to determine a threshold, the normalization factors NF_n was computed for all n (defined as the geometric mean of the housekeeping gene counts) of each sample when considering the n genes with lowest M as a housekeeping gene set (**Figure 21 B**). Correlations between consecutive normalization factors increased then decreased when adding the 6th gene with lowest M (**Figure 21 C**). This threshold was confirmed by studying the pairwise

variation between consecutive NF_ns (data not shown). The final housekeeping gene set consisted of the following 5 genes: *Ppia*, *Gapdh*, *Rpl19*, *Oaz1* and *Polr2a*. Normalization was performed as follows: the scaling factor for a sample was defined as the ratio of the average across all geometric means and the geometric mean of the sample. For each sample, all gene counts were multiplied by the corresponding scaling factor.

As protein and mRNA data are generally close to log-normally distributed,[203] normalized RNA counts were subsequently log-transformed. For each timepoint, only genes that were consistently expressed above the lower limit of quantification were tested. Paired t-tests, which are shown to be extremely robust against non-normality,[204] were performed to compare Shield1-treated vs -untreated mRNA (log-transformed) normalized copy numbers. z-score was defined as

$$z = -\log_{10}(\text{p-value}) \times |\log_2(\text{fold change})|.$$

Gene set enrichment analysis

Each gene was scored using the absolute value of the sum of the t-statistics from paired t-tests at 4 and 12 h. Genes were ranked by decreasing score, and gene set enrichment analysis was performed using GSEA v. 2.2.1 (Broad Institute), with the following settings: method, pre ranked gene list; gene setsdatabase, reactome (c2.cp.reactome.v5.1.symbols.gmt); number of permutations, 10,000; enrichment statistic, classic; min set size, 5; max set size, 100; and all other parameters as default.

Quantitative approach to distinguish between IFN-β and IFN-γ signatures

Genes present in both nCounter panels (mouse immunology in this study and human immunology v.2 for the human whole blood study[160]) and consistently expressed above the lower limit of quantification were considered. Those for which the EtOH vs Shield1 t-test p-value was < 0.05 at 12 h were selected and weighted by their t-statistic, resulting in a 44-dimensional vector which was subsequently normalized by its L2 norm. Similar vectors were obtained by weighting the same 44 genes by the t-statistic from t-test comparing control vs IFN-β or control vs IFN-γ in the human whole blood study, after which they were also normalized. The difference ⟨autophagy, IFN-β⟩ – ⟨autophagy, IFN-γ⟩ between the scalar products was computed for 100,000 iterations through bootstrapping over the 25 donors of the whole-blood study.

ELISA

CXCL10 ELISAs (R&D Biosystems, DY466) were performed using cell supernatant clarified by spinning at 850 g for 5 min.

Plasmid transfection for the expression of M2 or M2H37G

pCAGGS-M2 and pCAGGS-M2H37G plasmids were kind gifts of Christian Münz laboratory, described in [88]. They were transfected by Lipofectamine2000 (ThermoFisher Scientific, 11668019) according to the manufacturer's protocol for 70 hours. B/B homodimerizer (Clontech, 635069) was added at 0.1 µM for the last 20 h.

Statistical analysis

Given that Shield1 treatment resulted in the reduced expression of ISGs (**Figure 22**), statistical analysis in the s

ubsequent figures was performed using one-tailed tests to test for downregulation of ISG expression upon Shield1 treatment. T-tests were performed using GraphPad Prism 6 or R when multiple testing correction had to be performed.

References

1 Anderson, R. E., Sogin, M. L. & Baross, J. A. Evolutionary strategies of viruses, bacteria and archaea in hydrothermal vent ecosystems revealed through metagenomics. *PLoS One* **9**, e109696, doi:10.1371/journal.pone.0109696 (2014).

2 Koonin, E. V., Dolja, V. V. & Krupovic, M. Origins and evolution of viruses of eukaryotes: The ultimate modularity. *Virology* **479-480**, 2-25, doi:10.1016/j.virol.2015.02.039 (2015).

3 Parkin, J. & Cohen, B. An overview of the immune system. *Lancet* **357**, 1777-1789, doi:10.1016/S0140-6736(00)04904-7 (2001).

4 Brubaker, S. W., Bonham, K. S., Zanoni, I. & Kagan, J. C. Innate immune pattern recognition: a cell biological perspective. *Annu Rev Immunol* **33**, 257-290, doi:10.1146/annurev-immunol-032414-112240 (2015).

5 Yang, Y., Jiang, G., Zhang, P. & Fan, J. Programmed cell death and its role in inflammation. *Military Medical Research* **2**, 12, doi:10.1186/s40779-015-0039-0 (2015).

6 Janeway, C. A., Jr. & Medzhitov, R. Innate immune recognition. *Annu Rev Immunol* **20**, 197-216, doi:10.1146/annurev.immunol.20.083001.084359 (2002).

7 McNab, F., Mayer-Barber, K., Sher, A., Wack, A. & O'Garra, A. Type I interferons in infectious disease. *Nat Rev Immunol* **15**, 87-103, doi:10.1038/nri3787 (2015).

8 Buckwalter, M. R. & Albert, M. L. Orchestration of the immune response by dendritic cells. *Curr Biol* **19**, R355-361, doi:10.1016/j.cub.2009.03.012 (2009).

9 Krummel, M. F., Bartumeus, F. & Gerard, A. T cell migration, search strategies and mechanisms. *Nat Rev Immunol* **16**, 193-201, doi:10.1038/nri.2015.16 (2016).

10 Dorner, T. & Radbruch, A. Antibodies and B cell memory in viral immunity. *Immunity* **27**, 384-392, doi:10.1016/j.immuni.2007.09.002 (2007).

11 Schmolke, M. & Garcia-Sastre, A. Evasion of innate and adaptive immune responses by influenza A virus. *Cell Microbiol* **12**, 873-880, doi:10.1111/j.1462-5822.2010.01475.x (2010).

12 Sanchez, E. L. & Lagunoff, M. Viral activation of cellular metabolism. *Virology* **479-480**, 609-618, doi:10.1016/j.virol.2015.02.038 (2015).

13 Gonzalez Plaza, J. J., Hulak, N., Kausova, G., Zhumadilov, Z. & Akilzhanova, A. Role of metabolism during viral infections, and crosstalk with the innate immune system. *Intractable & rare diseases research* **5**, 90-96, doi:10.5582/irdr.2016.01008 (2016).

14 Perot, B. P., Ingersoll, M. A. & Albert, M. L. The impact of macroautophagy on CD8(+) T-cell-mediated antiviral immunity. *Immunol Rev* **255**, 40-56, doi:10.1111/imr.12096 (2013).

15 Hunter, P. Molecular fossils probe life's origins. Research into molecular fossils and modern viruses is shedding light on the evolution of archaea, prokaryotes and eukaryotes. *EMBO Rep* **14**, 964-967, doi:10.1038/embor.2013.162 (2013).

16 Albert, M. L., Sauter, B. & Bhardwaj, N. Dendritic cells acquire antigen from apoptotic cells and induce class I-restricted CTLs. *Nature* **392**, 86-89, doi:10.1038/32183 (1998).

17 Albert, M. L. *et al.* Immature dendritic cells phagocytose apoptotic cells via alphavbeta5 and CD36, and cross-present antigens to cytotoxic T lymphocytes. *J Exp Med* **188**, 1359-1368 (1998).

18 Uhl, M. *et al.* Autophagy within the antigen donor cell facilitates efficient antigen cross-priming of virus-specific CD8+ T cells. *Cell Death Differ* **16**, 991-1005, doi:cdd20098 [pii]

10.1038/cdd.2009.8 [doi] (2009).

19 Taubenberger, J. K. & Morens, D. M. 1918 Influenza: the mother of all pandemics. *Emerging infectious diseases* **12**, 15-22, doi:10.3201/eid1201.050979 (2006).

20 Yewdell, J. & Garcia-Sastre, A. Influenza virus still surprises. *Current opinion in microbiology* **5**, 414-418 (2002).

21 Taubenberger, J. K. & Morens, D. M. The pathology of influenza virus infections. *Annual review of pathology* **3**, 499-522, doi:10.1146/annurev.pathmechdis.3.121806.154316 (2008).

22 de Jong, M. D. *et al.* Fatal outcome of human influenza A (H5N1) is associated with high viral load and hypercytokinemia. *Nat Med* **12**, 1203-1207, doi:10.1038/nm1477 (2006).

23 Eisfeld, A. J., Neumann, G. & Kawaoka, Y. At the centre: influenza A virus ribonucleoproteins. *Nature reviews. Microbiology* **13**, 28-41, doi:10.1038/nrmicro3367 (2015).

24 Rossman, J. S., Leser, G. P. & Lamb, R. A. Filamentous influenza virus enters cells via macropinocytosis. *J Virol* **86**, 10950-10960, doi:10.1128/JVI.05992-11 (2012).

25 Rejmanek, D., Hosseini, P. R., Mazet, J. A., Daszak, P. & Goldstein, T. Evolutionary Dynamics and Global Diversity of Influenza A Virus. *J Virol* **89**, 10993-11001, doi:10.1128/JVI.01573-15 (2015).

26 Kido, H. *et al.* Role of host cellular proteases in the pathogenesis of influenza and influenza-induced multiple organ failure. *Biochim Biophys Acta* **1824**, 186-194, doi:10.1016/j.bbapap.2011.07.001 (2012).

27 Yang, J., Li, M., Shen, X. & Liu, S. Influenza A virus entry inhibitors targeting the hemagglutinin. *Viruses* **5**, 352-373, doi:10.3390/v5010352 (2013).

28 Rossman, J. S., Jing, X., Leser, G. P. & Lamb, R. A. Influenza virus M2 protein mediates ESCRT-independent membrane scission. *Cell* **142**, 902-913, doi:S0092-8674(10)00960-8 [pii]

10.1016/j.cell.2010.08.029 [doi] (2010).

29 Shtyrya, Y. A., Mochalova, L. V. & Bovin, N. V. Influenza virus neuraminidase: structure and function. *Acta naturae* **1**, 26-32 (2009).

30 Medina, R. A. & Garcia-Sastre, A. Influenza A viruses: new research developments. *Nature reviews. Microbiology* **9**, 590-603, doi:10.1038/nrmicro2613 (2011).

31 Taubenberger, J. K. & Kash, J. C. Influenza virus evolution, host adaptation, and pandemic formation. *Cell Host Microbe* **7**, 440-451, doi:10.1016/j.chom.2010.05.009 (2010).

32 Brooke, C. B. *et al.* Most influenza a virions fail to express at least one essential viral protein. *J Virol* **87**, 3155-3162, doi:10.1128/JVI.02284-12 (2013).

33 Schulz, O. *et al.* Toll-like receptor 3 promotes cross-priming to virus-infected cells. *Nature* **433**, 887-892, doi:10.1038/nature03326 (2005).

34 Perales-Linares, R. & Navas-Martin, S. Toll-like receptor 3 in viral pathogenesis: friend or foe? *Immunology* **140**, 153-167, doi:10.1111/imm.12143 (2013).

35 Diebold, S. S., Kaisho, T., Hemmi, H., Akira, S. & Reis e Sousa, C. Innate antiviral responses by means of TLR7-mediated recognition of single-stranded RNA. *Science* **303**, 1529-1531, doi:10.1126/science.1093616 (2004).

36 Kawasaki, T. & Kawai, T. Toll-like receptor signaling pathways. *Front Immunol* **5**, 461, doi:10.3389/fimmu.2014.00461 (2014).

37 Liedmann, S. *et al.* Viral suppressors of the RIG-I-mediated interferon response are pre-packaged in influenza virions. *Nature communications* **5**, 5645, doi:10.1038/ncomms6645 (2014).

38 Iwasaki, A. & Pillai, P. S. Innate immunity to influenza virus infection. *Nat Rev Immunol* **14**, 315-328, doi:10.1038/nri3665 (2014).

39 Schlee, M. *et al.* Recognition of 5' triphosphate by RIG-I helicase requires short blunt double-stranded RNA as contained in panhandle of negative-strand virus. *Immunity* **31**, 25-34, doi:10.1016/j.immuni.2009.05.008 (2009).

40 Schmidt, A. *et al.* 5'-triphosphate RNA requires base-paired structures to activate antiviral signaling via RIG-I. *Proc Natl Acad Sci U S A* **106**, 12067-12072, doi:10.1073/pnas.0900971106 (2009).

41 Hornung, V. *et al.* 5'-Triphosphate RNA is the ligand for RIG-I. *Science* **314**, 994-997, doi:10.1126/science.1132505 (2006).

42 Loo, Y. M. & Gale, M., Jr. Immune signaling by RIG-I-like receptors. *Immunity* **34**, 680-692, doi:10.1016/j.immuni.2011.05.003 (2011).

43 Lamkanfi, M. & Dixit, V. M. Mechanisms and functions of inflammasomes. *Cell* **157**, 1013-1022, doi:10.1016/j.cell.2014.04.007 (2014).

44 Bergsbaken, T., Fink, S. L. & Cookson, B. T. Pyroptosis: host cell death and inflammation. *Nature reviews. Microbiology* **7**, 99-109, doi:10.1038/nrmicro2070 (2009).

45 Shimada, K. *et al.* Oxidized mitochondrial DNA activates the NLRP3 inflammasome during apoptosis. *Immunity* **36**, 401-414, doi:10.1016/j.immuni.2012.01.009 (2012).

46 Shao, B. Z., Xu, Z. Q., Han, B. Z., Su, D. F. & Liu, C. NLRP3 inflammasome and its inhibitors: a review. *Frontiers in pharmacology* **6**, 262, doi:10.3389/fphar.2015.00262 (2015).

47 Ichinohe, T., Pang, I. K. & Iwasaki, A. Influenza virus activates inflammasomes via its intracellular M2 ion channel. *Nat Immunol* **11**, 404-410, doi:10.1038/ni.1861 (2010).

48 McAuley, J. L. *et al.* Activation of the NLRP3 inflammasome by IAV virulence protein PB1-F2 contributes to severe pathophysiology and disease. *PLoS Pathog* **9**, e1003392, doi:10.1371/journal.ppat.1003392 (2013).

49 Chan, Y. K. & Gack, M. U. Viral evasion of intracellular DNA and RNA sensing. *Nature reviews. Microbiology* **14**, 360-373, doi:10.1038/nrmicro.2016.45 (2016).

50 Moerdyk-Schauwecker, M., Hwang, S. I. & Grdzelishvili, V. Z. Cellular proteins associated with the interior and exterior of vesicular stomatitis virus virions. *PLoS One* **9**, e104688, doi:10.1371/journal.pone.0104688 (2014).

51 Weber, M. *et al.* Incoming RNA virus nucleocapsids containing a 5'-triphosphorylated genome activate RIG-I and antiviral signaling. *Cell Host Microbe* **13**, 336-346, doi:10.1016/j.chom.2013.01.012 (2013).

52 Weber, M. *et al.* Influenza virus adaptation PB2-627K modulates nucleocapsid inhibition by the pathogen sensor RIG-I. *Cell Host Microbe* **17**, 309-319, doi:10.1016/j.chom.2015.01.005 (2015).

53 Hatada, E. & Fukuda, R. Binding of influenza A virus NS1 protein to dsRNA in vitro. *J Gen Virol* **73 (Pt 12)**, 3325-3329, doi:10.1099/0022-1317-73-12-3325 (1992).

54 Qian, X. Y., Chien, C. Y., Lu, Y., Montelione, G. T. & Krug, R. M. An amino-terminal polypeptide fragment of the influenza virus NS1 protein possesses specific RNA-binding activity and largely helical backbone structure. *RNA* **1**, 948-956 (1995).

55 Donelan, N. R., Basler, C. F. & Garcia-Sastre, A. A recombinant influenza A virus expressing an RNA-binding-defective NS1 protein induces high levels of beta interferon and is attenuated in mice. *J Virol* **77**, 13257-13266 (2003).

56 Gack, M. U. *et al.* Influenza A virus NS1 targets the ubiquitin ligase TRIM25 to evade recognition by the host viral RNA sensor RIG-I. *Cell Host Microbe* **5**, 439-449, doi:10.1016/j.chom.2009.04.006 (2009).

57 Rajsbaum, R. *et al.* Species-specific inhibition of RIG-I ubiquitination and IFN induction by the influenza A virus NS1 protein. *PLoS Pathog* **8**, e1003059, doi:10.1371/journal.ppat.1003059 (2012).

58 Tawaratsumida, K. *et al.* Quantitative proteomic analysis of the influenza A virus nonstructural proteins NS1 and NS2 during natural cell infection identifies PACT as an NS1 target protein and antiviral host factor. *J Virol* **88**, 9038-9048, doi:10.1128/JVI.00830-14 (2014).

59 Chakrabarti, A. K. & Pasricha, G. An insight into the PB1F2 protein and its multifunctional role in enhancing the pathogenicity of the influenza A viruses. *Virology* **440**, 97-104, doi:10.1016/j.virol.2013.02.025 (2013).

60 Yoshizumi, T. *et al.* Influenza A virus protein PB1-F2 translocates into mitochondria via Tom40 channels and impairs innate immunity. *Nature communications* **5**, 4713, doi:10.1038/ncomms5713 (2014).

61 Varga, Z. T., Grant, A., Manicassamy, B. & Palese, P. Influenza virus protein PB1-F2 inhibits the induction of type I interferon by binding to MAVS and decreasing mitochondrial membrane potential. *J Virol* **86**, 8359-8366, doi:10.1128/JVI.01122-12 (2012).

62 Nemeroff, M. E., Barabino, S. M., Li, Y., Keller, W. & Krug, R. M. Influenza virus NS1 protein interacts with the cellular 30 kDa subunit of CPSF and inhibits 3'end formation of cellular pre-mRNAs. *Mol Cell* **1**, 991-1000 (1998).

63 Ramanathan, A., Robb, G. B. & Chan, S. H. mRNA capping: biological functions and applications. *Nucleic acids research*, doi:10.1093/nar/gkw551 (2016).

64 Dias, A. *et al.* The cap-snatching endonuclease of influenza virus polymerase resides in the PA subunit. *Nature* **458**, 914-918, doi:10.1038/nature07745 (2009).

65 Marazzi, I. *et al.* Suppression of the antiviral response by an influenza histone mimic. *Nature* **483**, 428-433, doi:10.1038/nature10892 (2012).

66 Pauli, E. K. *et al.* Influenza A virus inhibits type I IFN signaling via NF-kappaB-dependent induction of SOCS-3 expression. *PLoS Pathog* **4**, e1000196, doi:10.1371/journal.ppat.1000196 (2008).

67 Garcia, M. A. *et al.* Impact of protein kinase PKR in cell biology: from antiviral to antiproliferative action. *Microbiology and molecular biology reviews : MMBR* **70**, 1032-1060, doi:10.1128/MMBR.00027-06 (2006).

68 Min, J. Y., Li, S., Sen, G. C. & Krug, R. M. A site on the influenza A virus NS1 protein mediates both inhibition of PKR activation and temporal regulation of viral RNA synthesis. *Virology* **363**, 236-243, doi:10.1016/j.virol.2007.01.038 (2007).

69 Bergmann, M. *et al.* Influenza virus NS1 protein counteracts PKR-mediated inhibition of replication. *J Virol* **74**, 6203-6206 (2000).

70 Choi, U. Y., Kang, J. S., Hwang, Y. S. & Kim, Y. J. Oligoadenylate synthase-like (OASL) proteins: dual functions and associations with diseases. *Experimental & molecular medicine* **47**, e144, doi:10.1038/emm.2014.110 (2015).

71 Min, J. Y. & Krug, R. M. The primary function of RNA binding by the influenza A virus NS1 protein in infected cells: Inhibiting the 2'-5' oligo (A) synthetase/RNase L pathway. *Proc Natl Acad Sci U S A* **103**, 7100-7105, doi:10.1073/pnas.0602184103 (2006).

72 Hale, B. G., Randall, R. E., Ortin, J. & Jackson, D. The multifunctional NS1 protein of influenza A viruses. *J Gen Virol* **89**, 2359-2376, doi:10.1099/vir.0.2008/004606-0 (2008).

73 Banerjee, S., Chakrabarti, A., Jha, B. K., Weiss, S. R. & Silverman, R. H. Cell-type-specific effects of RNase L on viral induction of beta interferon. *MBio* **5**, e00856-00814, doi:10.1128/mBio.00856-14 (2014).

74 Ameisen, J. C., Pleskoff, O., Lelievre, J. D. & De Bels, F. Subversion of cell survival and cell death: viruses as enemies, tools, teachers and allies. *Cell Death Differ* **10 Suppl 1**, S3-6, doi:10.1038/sj.cdd.4401117 (2003).

75 Kaminskyy, V. & Zhivotovsky, B. To kill or be killed: how viruses interact with the cell death machinery. *Journal of internal medicine* **267**, 473-482, doi:10.1111/j.1365-2796.2010.02222.x (2010).

76 Mayank, A. K., Sharma, S., Nailwal, H. & Lal, S. K. Nucleoprotein of influenza A virus negatively impacts antiapoptotic protein API5 to enhance E2F1-dependent apoptosis and virus replication. *Cell death & disease* **6**, e2018, doi:10.1038/cddis.2015.360 (2015).

77 Herold, S., Ludwig, S., Pleschka, S. & Wolff, T. Apoptosis signaling in influenza virus propagation, innate host defense, and lung injury. *J Leukoc Biol* **92**, 75-82, doi:10.1189/jlb.1011530 (2012).

78 McLean, J. E., Datan, E., Matassov, D. & Zakeri, Z. F. Lack of Bax prevents influenza A virus-induced apoptosis and causes diminished viral replication. *J Virol* **83**, 8233-8246, doi:10.1128/JVI.02672-08 (2009).

79 Wurzer, W. J. *et al.* Caspase 3 activation is essential for efficient influenza virus propagation. *EMBO J* **22**, 2717-2728, doi:10.1093/emboj/cdg279 (2003).

80 Shin, Y. K., Liu, Q., Tikoo, S. K., Babiuk, L. A. & Zhou, Y. Influenza A virus NS1 protein activates the phosphatidylinositol 3-kinase (PI3K)/Akt pathway by direct interaction with the p85 subunit of PI3K. *J Gen Virol* **88**, 13-18, doi:10.1099/vir.0.82419-0 (2007).

81 Zhirnov, O. P., Konakova, T. E., Wolff, T. & Klenk, H. D. NS1 protein of influenza A virus down-regulates apoptosis. *J Virol* **76**, 1617-1625 (2002).

82 Liu, H. *et al.* The ESEV PDZ-binding motif of the avian influenza A virus NS1 protein protects infected cells from apoptosis by directly targeting Scribble. *J Virol* **84**, 11164-11174, doi:10.1128/JVI.01278-10 (2010).

83 Halder, U. C., Bagchi, P., Chattopadhyay, S., Dutta, D. & Chawla-Sarkar, M. Cell death regulation during influenza A virus infection by matrix (M1) protein: a model of viral control over the cellular survival pathway. *Cell death & disease* **2**, e197, doi:10.1038/cddis.2011.75 (2011).

84 Nailwal, H., Sharma, S., Mayank, A. K. & Lal, S. K. The nucleoprotein of influenza A virus induces p53 signaling and apoptosis via attenuation of host ubiquitin ligase RNF43. *Cell death & disease* **6**, e1768, doi:10.1038/cddis.2015.131 (2015).

85 Tripathi, S. *et al.* Influenza A virus nucleoprotein induces apoptosis in human airway epithelial cells: implications of a novel interaction between nucleoprotein and host protein Clusterin. *Cell death & disease* **4**, e562, doi:10.1038/cddis.2013.89 (2013).

86 Zamarin, D., Garcia-Sastre, A., Xiao, X., Wang, R. & Palese, P. Influenza virus PB1-F2 protein induces cell death through mitochondrial ANT3 and VDAC1. *PLoS Pathog* **1**, e4, doi:10.1371/journal.ppat.0010004 (2005).

87 Zhang, C. *et al.* The NS1 protein of influenza A virus interacts with heat shock protein Hsp90 in human alveolar basal epithelial cells: implication for virus-induced apoptosis. *Virol J* **8**, 181, doi:10.1186/1743-422X-8-181 (2011).

88 Gannage, M. *et al.* Matrix protein 2 of influenza A virus blocks autophagosome fusion with lysosomes. *Cell Host Microbe* **6**, 367-380, doi:S1931-3128(09)00314-X [pii]

10.1016/j.chom.2009.09.005 [doi] (2009).

89 Ohsumi, Y. Historical landmarks of autophagy research. *Cell research* **24**, 9-23, doi:10.1038/cr.2013.169 (2014).

90 Ryter, S. W., Cloonan, S. M. & Choi, A. M. Autophagy: a critical regulator of cellular metabolism and homeostasis. *Molecules and cells* **36**, 7-16, doi:10.1007/s10059-013-0140-8 (2013).

91 Jung, C. H., Ro, S. H., Cao, J., Otto, N. M. & Kim, D. H. mTOR regulation of autophagy. *FEBS letters* **584**, 1287-1295, doi:10.1016/j.febslet.2010.01.017 (2010).

92 Rashid, H. O., Yadav, R. K., Kim, H. R. & Chae, H. J. ER stress: Autophagy induction, inhibition and selection. *Autophagy* **11**, 1956-1977, doi:10.1080/15548627.2015.1091141 (2015).

93 Holthofer, H., DeCandido, S. & Schlondorff, D. Identification of specific glomerular cell types in culture by use of lectin and antibody binding. *Cell differentiation and development : the official journal of the International Society of Developmental Biologists* **30**, 181-194 (1990).

94 Deretic, V., Saitoh, T. & Akira, S. Autophagy in infection, inflammation and immunity. *Nat Rev Immunol* **13**, 722-737, doi:10.1038/nri3532 (2013).

95 Pyo, J. O., Nah, J. & Jung, Y. K. Molecules and their functions in autophagy. *Experimental & molecular medicine* **44**, 73-80, doi:10.3858/emm.2012.44.2.029 (2012).

96 Levine, B. & Klionsky, D. J. Development by self-digestion: molecular mechanisms and biological functions of autophagy. *Dev Cell* **6**, 463-477, doi:S1534580704000991 [pii] (2004).

97 Klionsky, D. J. *et al.* A unified nomenclature for yeast autophagy-related genes. *Dev Cell* **5**, 539-545, doi:S153458070300296X [pii] (2003).

98 Joubert, P. E. & Albert, M. L. Antigen Cross-Priming of Cell-Associated Proteins is Enhanced by Macroautophagy within the Antigen Donor Cell. *Front Immunol* **3**, 61, doi:10.3389/fimmu.2012.00061 [doi] (2012).

99 Carlsson, S. R. & Simonsen, A. Membrane dynamics in autophagosome biogenesis. *Journal of cell science* **128**, 193-205, doi:10.1242/jcs.141036 (2015).

100 Hyttinen, J. M., Niittykoski, M., Salminen, A. & Kaarniranta, K. Maturation of autophagosomes and endosomes: a key role for Rab7. *Biochim Biophys Acta* **1833**, 503-510, doi:10.1016/j.bbamcr.2012.11.018 (2013).

101 Stolz, A., Ernst, A. & Dikic, I. Cargo recognition and trafficking in selective autophagy. *Nat Cell Biol* **16**, 495-501, doi:10.1038/ncb2979 (2014).

102 Rusten, T. E. & Stenmark, H. p62, an autophagy hero or culprit? *Nat Cell Biol* **12**, 207-209, doi:10.1038/ncb0310-207 (2010).

103 Knodler, L. A. & Celli, J. Eating the strangers within: host control of intracellular bacteria via xenophagy. *Cell Microbiol* **13**, 1319-1327, doi:10.1111/j.1462-5822.2011.01632.x (2011).

104 Orvedahl, A. *et al.* Autophagy protects against Sindbis virus infection of the central nervous system. *Cell Host Microbe* **7**, 115-127, doi:10.1016/j.chom.2010.01.007 (2010).

105 Talloczy, Z., Virgin, H. W. t. & Levine, B. PKR-dependent autophagic degradation of herpes simplex virus type 1. *Autophagy* **2**, 24-29 (2006).

106 Dreux, M., Gastaminza, P., Wieland, S. F. & Chisari, F. V. The autophagy machinery is required to initiate hepatitis C virus replication. *Proc Natl Acad Sci U S A* **106**, 14046-14051, doi:10.1073/pnas.0907344106 (2009).

107 Sir, D. *et al.* Replication of hepatitis C virus RNA on autophagosomal membranes. *J Biol Chem* **287**, 18036-18043, doi:10.1074/jbc.M111.320085 (2012).

108 Guevin, C. *et al.* Autophagy protein ATG5 interacts transiently with the hepatitis C virus RNA polymerase (NS5B) early during infection. *Virology* **405**, 1-7, doi:10.1016/j.virol.2010.05.032 (2010).

109 Tanida, I. *et al.* Knockdown of autophagy-related gene decreases the production of infectious hepatitis C virus particles. *Autophagy* **5**, 937-945 (2009).

110 Chiramel, A. I., Brady, N. R. & Bartenschlager, R. Divergent Roles of Autophagy in Virus Infection. *Cells* **2**, 83-104, doi:10.3390/cells2010083 [doi] (2013).

111 Li, J. *et al.* Subversion of cellular autophagy machinery by hepatitis B virus for viral envelopment. *J Virol* **85**, 6319-6333, doi:10.1128/JVI.02627-10 (2011).

112 Bird, S. W., Maynard, N. D., Covert, M. W. & Kirkegaard, K. Nonlytic viral spread enhanced by autophagy components. *Proc Natl Acad Sci U S A* **111**, 13081-13086, doi:10.1073/pnas.1401437111 (2014).

113 Heaton, N. S. & Randall, G. Dengue virus-induced autophagy regulates lipid metabolism. *Cell Host Microbe* **8**, 422-432, doi:10.1016/j.chom.2010.10.006 (2010).

114 Bowie, A. G. & Unterholzner, L. Viral evasion and subversion of pattern-recognition receptor signalling. *Nat Rev Immunol* **8**, 911-922, doi:10.1038/nri2436 (2008).

115 Jounai, N. *et al.* The Atg5 Atg12 conjugate associates with innate antiviral immune responses. *Proc Natl Acad Sci U S A* **104**, 14050-14055, doi:0704014104 [pii]

10.1073/pnas.0704014104 [doi] (2007).

116 Tal, M. C. *et al.* Absence of autophagy results in reactive oxygen species-dependent amplification of RLR signaling. *Proc Natl Acad Sci U S A* **106**, 2770-2775, doi:0807694106 [pii]

10.1073/pnas.0807694106 [doi] (2009).

117 Palchetti, S. *et al.* Transfected poly(I:C) activates different dsRNA receptors, leading to apoptosis or immunoadjuvant response in androgen-independent prostate cancer cells. *J Biol Chem* **290**, 5470-5483, doi:10.1074/jbc.M114.601625 (2015).

118 Fliss, P. M. *et al.* Viral mediated redirection of NEMO/IKKgamma to autophagosomes curtails the inflammatory cascade. *PLoS Pathog* **8**, e1002517, doi:10.1371/journal.ppat.1002517 (2012).

119 Panne, D., Maniatis, T. & Harrison, S. C. An atomic model of the interferon-beta enhanceosome. *Cell* **129**, 1111-1123, doi:10.1016/j.cell.2007.05.019 (2007).

120 Lee, H. K., Lund, J. M., Ramanathan, B., Mizushima, N. & Iwasaki, A. Autophagy-dependent viral recognition by plasmacytoid dendritic cells. *Science* **315**, 1398-1401, doi:10.1126/science.1136880 (2007).

121 Oh, J. E. & Lee, H. K. Autophagy as an innate immune modulator. *Immune network* **13**, 1-9, doi:10.4110/in.2013.13.1.1 (2013).

122 Schmeisser, H., Bekisz, J. & Zoon, K. C. New function of type I IFN: induction of autophagy. *Journal of interferon & cytokine research : the official journal of the International Society for Interferon and Cytokine Research* **34**, 71-78, doi:10.1089/jir.2013.0128 (2014).

123 Shi, C. S. *et al.* Activation of autophagy by inflammatory signals limits IL-1beta production by targeting ubiquitinated inflammasomes for destruction. *Nat Immunol* **13**, 255-263, doi:10.1038/ni.2215 (2012).

124 Razani, B. *et al.* Autophagy links inflammasomes to atherosclerotic progression. *Cell metabolism* **15**, 534-544, doi:10.1016/j.cmet.2012.02.011 (2012).

125 Ilyas, G. *et al.* Macrophage autophagy limits acute toxic liver injury in mice through down regulation of interleukin-1beta. *Journal of hepatology* **64**, 118-127, doi:10.1016/j.jhep.2015.08.019 (2016).

126 Dupont, N. *et al.* Autophagy-based unconventional secretory pathway for extracellular delivery of IL-1beta. *EMBO J* **30**, 4701-4711, doi:emboj2011398 [pii]

10.1038/emboj.2011.398 [doi] (2011).

127 Harris, J. *et al.* Autophagy controls IL-1beta secretion by targeting pro-IL-1beta for degradation. *J Biol Chem* **286**, 9587-9597, doi:10.1074/jbc.M110.202911 (2011).

128 Zhong, Z. *et al.* NF-kappaB Restricts Inflammasome Activation via Elimination of Damaged Mitochondria. *Cell* **164**, 896-910, doi:10.1016/j.cell.2015.12.057 (2016).

129 Gurung, P., Lukens, J. R. & Kanneganti, T. D. Mitochondria: diversity in the regulation of the NLRP3 inflammasome. *Trends in molecular medicine* **21**, 193-201, doi:10.1016/j.molmed.2014.11.008 (2015).

130 Comber, J. D., Robinson, T. M., Siciliano, N. A., Snook, A. E. & Eisenlohr, L. C. Functional macroautophagy induction by influenza A virus without a

contribution to major histocompatibility complex class II-restricted presentation. *J Virol* **85**, 6453-6463, doi:10.1128/JVI.02122-10 (2011).

131 Zhou, Z. *et al.* Autophagy is involved in influenza A virus replication. *Autophagy* **5**, 321-328 (2009).

132 Ren, Y. *et al.* Proton Channel Activity of Influenza A Virus Matrix Protein 2 Contributes to Autophagy Arrest. *J Virol* **90**, 591-598, doi:10.1128/JVI.00576-15 (2016).

133 Zhirnov, O. P. & Klenk, H. D. Influenza A virus proteins NS1 and HA along with M2 are involved in stimulation of autophagy in infected cells. *J Virol*, doi:10.1128/JVI.02148-13 (2013).

134 Zhirnov, O. P., Klenk, H. D. & Wright, P. F. Aprotinin and similar protease inhibitors as drugs against influenza. *Antiviral research* **92**, 27-36, doi:10.1016/j.antiviral.2011.07.014 (2011).

135 Sun, Y. *et al.* Inhibition of autophagy ameliorates acute lung injury caused by avian influenza A H5N1 infection. *Sci Signal* **5**, ra16, doi:10.1126/scisignal.2001931 (2012).

136 Ma, J., Sun, Q., Mi, R. & Zhang, H. Avian influenza A virus H5N1 causes autophagy-mediated cell death through suppression of mTOR signaling. *Journal of genetics and genomics = Yi chuan xue bao* **38**, 533-537, doi:10.1016/j.jgg.2011.10.002 (2011).

137 Klionsky, D. J. *et al.* Guidelines for the use and interpretation of assays for monitoring autophagy (3rd edition). *Autophagy* **12**, 1-222, doi:10.1080/15548627.2015.1100356 (2016).

138 Beale, R. *et al.* A LC3-interacting motif in the influenza A virus M2 protein is required to subvert autophagy and maintain virion stability. *Cell Host Microbe* **15**, 239-247, doi:10.1016/j.chom.2014.01.006 (2014).

139 Lu, Q. *et al.* Homeostatic Control of Innate Lung Inflammation by Vici Syndrome Gene Epg5 and Additional Autophagy Genes Promotes Influenza Pathogenesis. *Cell Host Microbe* **19**, 102-113, doi:10.1016/j.chom.2015.12.011 (2016).

140 Cunningham, J. T. *et al.* mTOR controls mitochondrial oxidative function through a YY1-PGC-1alpha transcriptional complex. *Nature* **450**, 736-740, doi:10.1038/nature06322 (2007).

141 Thoreen, C. C. & Sabatini, D. M. Rapamycin inhibits mTORC1, but not completely. *Autophagy* **5**, 725-726 (2009).

142 Vanhaesebroeck, B. *et al.* Synthesis and function of 3-phosphorylated inositol lipids. *Annual review of biochemistry* **70**, 535-602, doi:10.1146/annurev.biochem.70.1.535 (2001).

143 Wu, Y. T. *et al.* Dual role of 3-methyladenine in modulation of autophagy via different temporal patterns of inhibition on class I and III phosphoinositide 3-kinase. *J Biol Chem* **285**, 10850-10861, doi:10.1074/jbc.M109.080796 (2010).

144 Lin, Y. C., Kuo, H. C., Wang, J. S. & Lin, W. W. Regulation of inflammatory response by 3-methyladenine involves the coordinative actions on Akt and glycogen synthase kinase 3beta rather than autophagy. *J Immunol* **189**, 4154-4164, doi:10.4049/jimmunol.1102739 (2012).

145 Robbins, M., Judge, A. & MacLachlan, I. siRNA and innate immunity. *Oligonucleotides* **19**, 89-102, doi:10.1089/oli.2009.0180 (2009).

146 Groenewoud, M. J. & Zwartkruis, F. J. Rheb and mammalian target of rapamycin in mitochondrial homoeostasis. *Open biology* **3**, 130185, doi:10.1098/rsob.130185 (2013).

147 Thorpe, L. M., Yuzugullu, H. & Zhao, J. J. PI3K in cancer: divergent roles of isoforms, modes of activation and therapeutic targeting. *Nature reviews. Cancer* **15**, 7-24, doi:10.1038/nrc3860 (2015).

148 Maynard-Smith, L. A., Chen, L. C., Banaszynski, L. A., Ooi, A. G. & Wandless, T. J. A directed approach for engineering conditional protein stability using biologically silent small molecules. *J Biol Chem* **282**, 24866-24872, doi:10.1074/jbc.M703902200 (2007).

149 Chen, X., Zaro, J. L. & Shen, W. C. Fusion protein linkers: property, design and functionality. *Advanced drug delivery reviews* **65**, 1357-1369, doi:10.1016/j.addr.2012.09.039 (2013).

150 Otomo, C., Metlagel, Z., Takaesu, G. & Otomo, T. Structure of the human ATG12~ATG5 conjugate required for LC3 lipidation in autophagy. *Nat Struct Mol Biol* **20**, 59-66, doi:10.1038/nsmb.2431 (2013).

151 Mizushima, N. *et al.* Dissection of autophagosome formation using Apg5-deficient mouse embryonic stem cells. *J Cell Biol* **152**, 657-668 (2001).

152 Hamacher-Brady, A., Brady, N. R. & Gottlieb, R. A. Enhancing macroautophagy protects against ischemia/reperfusion injury in cardiac myocytes. *J Biol Chem* **281**, 29776-29787, doi:10.1074/jbc.M603783200 (2006).

153 Subramani, S. & Malhotra, V. Non-autophagic roles of autophagy-related proteins. *EMBO Rep* **14**, 143-151, doi:10.1038/embor.2012.220 (2013).

154 Lee, D. H. & Goldberg, A. L. Proteasome inhibitors: valuable new tools for cell biologists. *Trends in cell biology* **8**, 397-403 (1998).

155 Jolliffe, I. T. *Principal Component Analysis*. (

, 2002).

156 de la Calle, C., Joubert, P. E., Law, H. K., Hasan, M. & Albert, M. L. Simultaneous assessment of autophagy and apoptosis using multispectral imaging cytometry. *Autophagy* **7**, 1045-1051, doi:16252 [pii] (2011).

157 Marino, G., Niso-Santano, M., Baehrecke, E. H. & Kroemer, G. Self-consumption: the interplay of autophagy and apoptosis. *Nature reviews. Molecular cell biology* **15**, 81-94, doi:10.1038/nrm3735 (2014).

158 Vandesompele, J. *et al.* Accurate normalization of real-time quantitative RT-PCR data by geometric averaging of multiple internal control genes. *Genome biology* **3**, RESEARCH0034 (2002).

159 Subramanian, A. *et al.* Gene set enrichment analysis: a knowledge-based approach for interpreting genome-wide expression profiles. *Proc Natl Acad Sci U S A* **102**, 15545-15550, doi:10.1073/pnas.0506580102 (2005).

160 Urrutia, A. *et al.* Standardized whole-blood transcriptional profiling enables the deconvolution

of complex induced immune responses. *Cell reports* (In Press).

161 Kelly-Scumpia, K. M. *et al.* Type I interferon signaling in hematopoietic cells is required for survival in mouse polymicrobial sepsis by regulating CXCL10. *J Exp Med* **207**, 319-326, doi:10.1084/jem.20091959 (2010).

162 Xu, H. C. *et al.* Type I interferon protects antiviral CD8+ T cells from NK cell cytotoxicity. *Immunity* **40**, 949-960, doi:10.1016/j.immuni.2014.05.004 (2014).

163 Liu, Y. *et al.* PD-L1 expression by neurons nearby tumors indicates better prognosis in glioblastoma patients. *The Journal of neuroscience : the official journal of the Society for Neuroscience* **33**, 14231-14245, doi:10.1523/JNEUROSCI.5812-12.2013 (2013).

164 Shin, E. C. *et al.* Virus-induced type I IFN stimulates generation of immunoproteasomes at the site of infection. *J Clin Invest* **116**, 3006-3014, doi:10.1172/JCI29832 (2006).

165 Jacobs, M. D. & Harrison, S. C. Structure of an IkappaBalpha/NF-kappaB complex. *Cell* **95**, 749-758 (1998).

166 Jackson, D. & Lamb, R. A. The influenza A virus spliced messenger RNA M mRNA3 is not required for viral replication in tissue culture. *J Gen Virol* **89**, 3097-3101, doi:10.1099/vir.0.2008/004739-0 (2008).

167 Yatim, N. *et al.* RIPK1 and NF-kappaB signaling in dying cells determines cross-priming of CD8(+) T cells. *Science* **350**, 328-334, doi:10.1126/science.aad0395 (2015).

168 He, C. & Klionsky, D. J. Regulation mechanisms and signaling pathways of autophagy. *Annu Rev Genet* **43**, 67-93, doi:10.1146/annurev-genet-102808-114910 (2009).

169 Russell, R. C., Yuan, H. X. & Guan, K. L. Autophagy regulation by nutrient signaling. *Cell research* **24**, 42-57, doi:10.1038/cr.2013.166 (2014).

170 Karim, M. R., Kawanago, H. & Kadowaki, M. A quick signal of starvation induced autophagy: transcription versus post-translational modification of LC3. *Analytical biochemistry* **465**, 28-34, doi:10.1016/j.ab.2014.07.007 (2014).

171 Yousefi, S. *et al.* Calpain-mediated cleavage of Atg5 switches autophagy to apoptosis. *Nat Cell Biol* **8**, 1124-1132, doi:10.1038/ncb1482 (2006).

172 Capelluto, D. G. Tollip: a multitasking protein in innate immunity and protein trafficking. *Microbes Infect* **14**, 140-147, doi:10.1016/j.micinf.2011.08.018 (2012).

173 Shimizu, M., Oguro-Ando, A., Ohoto-Fujita, E. & Atomi, Y. Toll-interacting protein pathway: degradation of an ubiquitin-binding protein. *Methods in enzymology* **534**, 323-330, doi:10.1016/B978-0-12-397926-1.00018-4 (2014).

174 Lu, K., Psakhye, I. & Jentsch, S. Autophagic clearance of polyQ proteins mediated by ubiquitin-Atg8 adaptors of the conserved CUET protein family. *Cell* **158**, 549-563, doi:10.1016/j.cell.2014.05.048 (2014).

175 Valero-Pacheco, N. *et al.* PD-L1 expression induced by the 2009 pandemic influenza A(H1N1) virus impairs the human T cell response. *Clinical & developmental immunology* **2013**, 989673, doi:10.1155/2013/989673 (2013).

176 Loi, M. *et al.* Macroautophagy Proteins Control MHC Class I Levels on Dendritic Cells and Shape Anti-viral CD8(+) T Cell Responses. *Cell reports* **15**, 1076-1087, doi:10.1016/j.celrep.2016.04.002 (2016).

177 Marc, D. Influenza virus non-structural protein NS1: interferon antagonism and beyond. *J Gen Virol* **95**, 2594-2611, doi:10.1099/vir.0.069542-0 (2014).

178 Hutchinson, E. C. *et al.* Conserved and host-specific features of influenza virion architecture. *Nature communications* **5**, 4816, doi:10.1038/ncomms5816 (2014).

179 Feng, Q. *et al.* Coxsackievirus cloverleaf RNA containing a 5' triphosphate triggers an antiviral response via RIG-I activation. *PLoS One* **9**, e95927, doi:10.1371/journal.pone.0095927 (2014).

180 Sabbah, A. & Bose, S. Retinoic acid inducible gene I activates innate antiviral response against human parainfluenza virus type 3. *Virol J* **6**, 200, doi:10.1186/1743-422X-6-200 (2009).

181 Broquet, A. H., Hirata, Y., McAllister, C. S. & Kagnoff, M. F. RIG-I/MDA5/MAVS are required to signal a protective IFN response in rotavirus-infected intestinal epithelium. *J Immunol* **186**, 1618-1626, doi:10.4049/jimmunol.1002862 (2011).

182 Sen, A., Pruijssers, A. J., Dermody, T. S., Garcia-Sastre, A. & Greenberg, H. B. The early interferon response to rotavirus is regulated by PKR and depends on MAVS/IPS-1, RIG-I, MDA-5, and IRF3. *J Virol* **85**, 3717-3732, doi:10.1128/JVI.02634-10 (2011).

183 Kemball, C. C. *et al.* Coxsackievirus infection induces autophagy-like vesicles and megaphagosomes in pancreatic acinar cells in vivo. *J Virol* **84**, 12110-12124, doi:10.1128/JVI.01417-10 (2010).

184 Ding, B. *et al.* Phosphoprotein of human parainfluenza virus type 3 blocks autophagosome-lysosome fusion to increase virus production. *Cell Host Microbe* **15**, 564-577, doi:10.1016/j.chom.2014.04.004 (2014).

185 Crawford, S. E., Hyser, J. M., Utama, B. & Estes, M. K. Autophagy hijacked through viroporin-activated calcium/calmodulin-dependent kinase kinase-beta signaling is required for rotavirus replication. *Proc Natl Acad Sci U S A* **109**, E3405-3413, doi:10.1073/pnas.1216539109 (2012).

186 Brown, D. M., Lampe, A. T. & Workman, A. M. The Differentiation and Protective Function of Cytolytic CD4 T Cells in Influenza Infection. *Front Immunol* **7**, 93, doi:10.3389/fimmu.2016.00093 (2016).

187 Hufford, M. M., Kim, T. S., Sun, J. & Braciale, T. J. The effector T cell response to influenza infection. *Current topics in microbiology and immunology* **386**, 423-455, doi:10.1007/82_2014_397 (2015).

188 Tough, D. F. Modulation of T-cell function by type I interferon. *Immunol Cell Biol* **90**, 492-497, doi:10.1038/icb.2012.7 (2012).

189 La Gruta, N. L. & Turner, S. J. T cell mediated immunity to influenza: mechanisms of viral control. *Trends in immunology* **35**, 396-402, doi:10.1016/j.it.2014.06.004 (2014).

190 Pekarek, V., Srinivas, S., Eskdale, J. & Gallagher, G. Interferon lambda-1 (IFN-lambda1/IL-29) induces ELR(-) CXC chemokine mRNA in human peripheral blood mononuclear cells, in an IFN-gamma-independent manner. *Genes and immunity* **8**, 177-180, doi:10.1038/sj.gene.6364372 (2007).

191 Yeruva, S., Ramadori, G. & Raddatz, D. NF-kappaB-dependent synergistic regulation of CXCL10 gene expression by IL-1beta and IFN-gamma in human intestinal epithelial cell lines. *International journal of colorectal disease* **23**, 305-317, doi:10.1007/s00384-007-0396-6 (2008).

192 Thorburn, A. Autophagy and its effects: making sense of double-edged swords. *PLoS Biol* **12**, e1001967, doi:10.1371/journal.pbio.1001967 (2014).

193 White, E. The role for autophagy in cancer. *J Clin Invest* **125**, 42-46, doi:10.1172/JCI73941 (2015).

194 Almond, J. B. & Cohen, G. M. The proteasome: a novel target for cancer chemotherapy. *Leukemia* **16**, 433-443, doi:10.1038/sj.leu.2402417 (2002).

195 Dou, Q. P. & Zonder, J. A. Overview of proteasome inhibitor-based anti-cancer therapies: perspective on bortezomib and second generation proteasome inhibitors versus future generation inhibitors of ubiquitin-proteasome system. *Current cancer drug targets* **14**, 517-536 (2014).

196 Mellman, I., Coukos, G. & Dranoff, G. Cancer immunotherapy comes of age. *Nature* **480**, 480-489, doi:10.1038/nature10673 (2011).

197 Green, D. R., Ferguson, T., Zitvogel, L. & Kroemer, G. Immunogenic and tolerogenic cell death. *Nat Rev Immunol* **9**, 353-363, doi:10.1038/nri2545 (2009).

198 Michaud, M. *et al.* Autophagy-dependent anticancer immune responses induced by chemotherapeutic agents in mice. *Science* **334**, 1573-1577, doi:334/6062/1573 [pii]

10.1126/science.1208347 [doi] (2011).

199 Beignon, A. S., Skoberne, M. & Bhardwaj, N. Type I interferons promote cross-priming: more functions for old cytokines. *Nat Immunol* **4**, 939-941, doi:10.1038/ni1003-939 (2003).

200 Sistigu, A. *et al.* Cancer cell-autonomous contribution of type I interferon signaling to the efficacy of chemotherapy. *Nat Med* **20**, 1301-1309, doi:10.1038/nm.3708 (2014).

201 Guo, Z. S., Liu, Z. & Bartlett, D. L. Oncolytic Immunotherapy: Dying the Right Way is a Key to Eliciting Potent Antitumor Immunity. *Frontiers in oncology* **4**, 74, doi:10.3389/fonc.2014.00074 (2014).

202 Kaufman, H. L., Kohlhapp, F. J. & Zloza, A. Oncolytic viruses: a new class of immunotherapy drugs. *Nature reviews. Drug discovery* **14**, 642-662, doi:10.1038/nrd4663 (2015).

203 Lu, C. & King, R. D. An investigation into the population abundance distribution of mRNAs, proteins, and metabolites in biological systems. *Bioinformatics* **25**, 2020-2027, doi:10.1093/bioinformatics/btp360 (2009).

204 Rasch, D. A. M. K., Teuscher, F. & Guiard, V. How robust are tests for two independent samples? *Journal of Statistical Planning and Inference* **137**, 2706–2720 (2007).

MANUSCRIPTS

Manuscript 1

The impact of macroautophagy on CD8$^+$ T-cell-mediated antiviral immunity.

Perot BP, Ingersoll MA, Albert ML

Published in *Immunological Reviews*, 2013 Sep;255(1):40-56

Manuscript 2

Bystander hyperactivation of preimmune CD8+ T cells in chronic HCV patients.

Alanio C, Nicoli F, Sultanik P, Flecken T, Perot B, Duffy D, Bianchi E, Lim A, Clave E, van Buuren MM, Schnuriger A, Johnsson K, Boussier J, Garbarg-Chenon A, Bousquet L, Mottez E, Schumacher TN, Toubert A, Appay V, Heshmati F, Thimme R, Pol S, Mallet V, Albert ML.

Published in *ELife*, 2015 Nov 14;4. pii: e07916

Manuscript 3

Autophagy represses the early interferon-β response to influenza A virus resulting in differential expression of interferon stimulated genes.

Brieuc P. Perot, Jeremy Boussier, Nader Yatim, Jeremy S. Rossman, Molly A. Ingersoll, Matthew L. Albert.

Submitted to *Autophagy*, August 11th 2016.